Università degli Studi dell'Insubria
Dipartimento di Scienze Chimiche e Ambientali

Dottorato di Ricerca in Scienze Chimiche

INTEGRATED EXPERIMENTAL AND THEORETICAL STUDY OF SURFACE PROPERTIES OF TiO_2 NANOPARTICLES

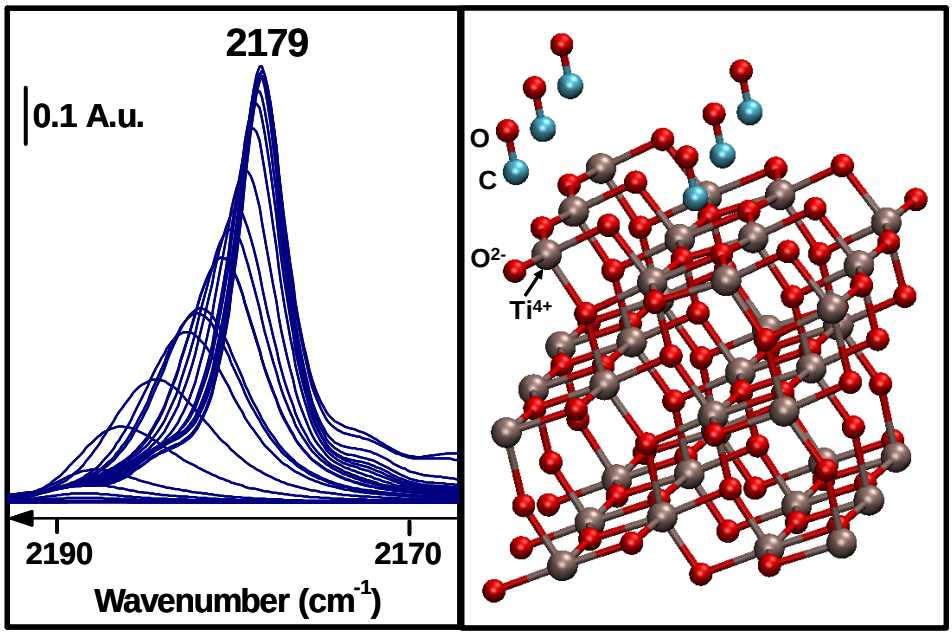

PhD Thesis

PhD Student: **Chiara Deiana**

Tutors: **Prof. Ettore Fois; Prof. Gianmario Martra**

Coordinatore: **Prof. Giovanni Palmisano**

XXIV Ciclo, 2008-2011

Università degli Studi dell'Insubria
Dipartimento di Scienze Chimiche e Ambientali

Dottorato di Ricerca in Scienze Chimiche

INTEGRATED EXPERIMENTAL AND THEORETICAL STUDY OF SURFACE PROPERTIES OF TiO_2 NANOPARTICLES

PhD Thesis

PhD Student: **Chiara Deiana**

Tutors: **Prof. Ettore Fois; Prof. Gianmario Martra**

Coordinatore: **Prof. Giovanni Palmisano**

Settore Scientifico-disciplinare: CHIM/02

XXIV Ciclo, 2008-2011

Contents

Abstract

Questa tesi di dottorato è stata dedicata allo studio delle proprietà di superficie di nanoparticelle di TiO_2 mediante l'uso combinato della spettroscopia infrarossa e del calcolo teorico.
Lo studio della struttura dei siti esposti alla superficie di TiO_2, con un ruolo rilevante per la chimica di superficie, è stato condotto attraverso una prima analisi della morfologia delle nanoparticelle, mediante microscopia elettronica in trasmissione ad alta risoluzione, seguita dall'analisi vibrazionale di molecole/gruppi sonda (OH/H_2O, CO) in interazione con i siti superficiali. Questo studio sperimentale ha permesso l'individuazione di alcune delle bande vibrazionali dovute ai siti difettivi esposti alla superficie del biossido di titanio P25 (Degussa), considerato un materiale di riferimento per le applicazioni fotocatalitiche della titania.

L'utilizzo di questo materiale, costituito da particelle dai bordi irregolari, comporta la presenza di un'ampia eterogeneità di siti di superficie, rendendo complessa l'assegnazione delle bande vibrazionali di molecole sonda adsorbite e quindi anche l'individuazione della struttura dei siti.
Di conseguenza, è stato studiato un campione di biossido di titanio, costituito da nanoparticelle con forma regolare e superfici definite. La conoscenza a priori della struttura dei siti esposti ha quindi consentito l'assegnazione univoca di alcune delle bande vibrazionali dello spettro infrarosso di molecole adsorbite. Questi dati sono stati utilizzati come riferimento per la simulazione degli spettri IR di CO adsorbito, che hanno permesso l'assegnazione di altri segnali di cui non era possibile una attribuzione certa sulla base dei soli dati sperimentali.

Il ruolo della superficie del biossido di titanio è stato poi studiato attraverso l'interazione TiO_2-biomolecole, attraverso cui è stato possibile individuare lo

specifico ruolo catalitico della superficie di TiO_2 nel promuovere la formazione di legami ammidici tra biomolecole adsorbite.
Si ritiene importante sottolineare che quanto ottenuto costituisce il primo caso di osservazione della formazione di oligopeptidi contenenti fino a 17 termini per interazione alla superficie di un solido tra amminoacidi non pre-attivati per via chimica e della loro auto-aggregazione per successiva idratazione del sistema.

E’ stato infine condotto un breve studio della variazione delle proprietà elettroniche del biossido di titanio in seguito al drogaggio con fluoro e boro.

Chapter 1

Scientific background and aim of the work

1.1. Introduction and aim of the work

The commercial production of titanium dioxide (TiO_2) started in early twentieth century, on the basis of a demand for different employments in several applications/products, like in pigments, toothpaste, sunscreens.[1] The discover made by Fujishima and Honda in 1972, of the photocatalytic water spitting on TiO_2 electrodes,[2] marked the beginning of a new and rising interest in the research studies of TiO_2 materials. In addition, the increasing energetic demand, the consequent necessity to find an energetic source economic and environmentally sustainable and the increasing environmental pollution, led to the development of new applications of TiO_2 in (i) heterogeneous photocatalysis for environmental cleanup, by the photo-oxidation of organic pollutants,[3,4] and (ii) in electrical energy production, with Grätzel solar cells.[5,6] Moreover, the TiO_2 material has been studied and employed also for its photo-induced hydrophilicity[7] and its possible role as part of biomaterials, typically in the form of oxide layer on the Ti-based implants.[8]

Owing to these numerous applications, many efforts have been done to characterize the properties of titanium dioxide, in order to improve its performances, particularly in the photocatalytic applications.[3,9,10] Despite that, in

the majority of degradation processes, the photonic efficiency of titanium dioxide does not overtake the 10%.[11] Therefore, it is necessary to improve the photocatalytic system by reaching a better knowledge of the material properties and the reaction mechanisms and, subsequently, to optimize the system by modulating the synthetic conditions.

The first way to accomplish this goal and to obtain improved photocatalytic performances, is the **doping** of TiO_2 semiconductor.[9,10] One of the limit in the employ of TiO_2 in environmental cleanup is that this semiconductor absorbs in UV range (at 3.0 eV / 410 nm for TiO_2 rutile phase and 3.2 eV / 384 nm for the anatase [11,12]), hence it is necessary to modify the system to shift the absorption in the visible region. The presence of dopants in the TiO_2 photocatalytic systems can improve the light-absorption capability mainly by inducing a batho-chromic shift or generating new photocatalytically active centers.[9,10]

Another way to optimize the catalytic performances of TiO_2 is through its **structural and morphological modifications**.[11] The photocatalytic activity depends on the availability of active sites,[13] hence parameters like crystal structure, particle size, surface hydroxylation and acidity/basicity can play a relevant role in determining the photocatalytic efficiency.[14]

The *particle size* and the *specific surface area (SSA)* are two of the parameters to take in consideration. Indeed, research works reported in literature[15-17] highlight that particle size influences the electron-hole recombination. Also a proper specific surface area has to be selected for each particular reaction, because, if a high SSA results in an increase of the amount of adsorbed molecules and, consequently, of the probability of their photodegradation, it must be considered that powders with high SSA could present a large amount of crystalline defects, responsible for electron-hole recombination, leading to a decrease in the efficiency of the process.[17]

The *surface characteristics* play a central role in determining the performances of TiO_2. For instance, the hydroxylation influences the photocatalytic activity

because surface OH groups are directly involved in the reaction mechanism.[18] The surface hydroxylation can be enhanced if the synthesized nanoparticles expose those surfaces that promote the water dissociation.

Despite the efforts that have been done to improve the photocatalytic performances of TiO_2, [3,9,11] further optimizations can be achieved by a deeper knowledge of the TiO_2 properties. For instance, on one hand, the model system TiO_2 rutile (110) single crystal has been extensively studied,[19-21] however the surface reactivity of this simple system is not completely understood, yet.[3] On the other hand, significant progresses have been achieved in understanding the relationships between the structure of coordinative defects located on steps of (101) TiO_2 anatase surfaces and their reactivity towards various molecules,[22,23] but the possibility to recognize precisely such structures at the surface of actual TiO_2 nanoparticles is still lacking. Hence, the investigation of the TiO_2 materials, used in different applications, is still an open research field, especially considering that it is possible to deeply modify the surface properties of titania nanoparticles and, consequently their reactivity by using different synthetic routes.[1]

On such a basis, the main target of this work was the elucidation (or at least the beginning of a research pathway toward the elucidation) of the surface features of TiO_2 nanoparticles as revealed by the IR spectra of both intrinsic (surface hydroxy groups) and extrinsic (CO adsorbed as probe molecule) surface oscillators. This method offers some unique characteristics resulting from the combination of (i) a high sensitivity of the frequency of the indicated oscillators even to fine differences in the local structure of the surface sites they are in interaction with, (ii) a satisfactory quantitative sensitivity, (iii) the possibility to collect the experimental data on materials conditioned and kept in controlled atmosphere, as well as to control the (relative) amount of adsorbed species[24] (Chapter 2).

1.1.1. The material

Titanium dioxide is a transition metal oxide that crystallizes in nature in different polymorphs: rutile (tetragonal), anatase (tetragonal), brookite (rhombohedrical).

Among them, rutile and anatase are those of actual interest in many applications, including catalysis and solar cells.[11,19]

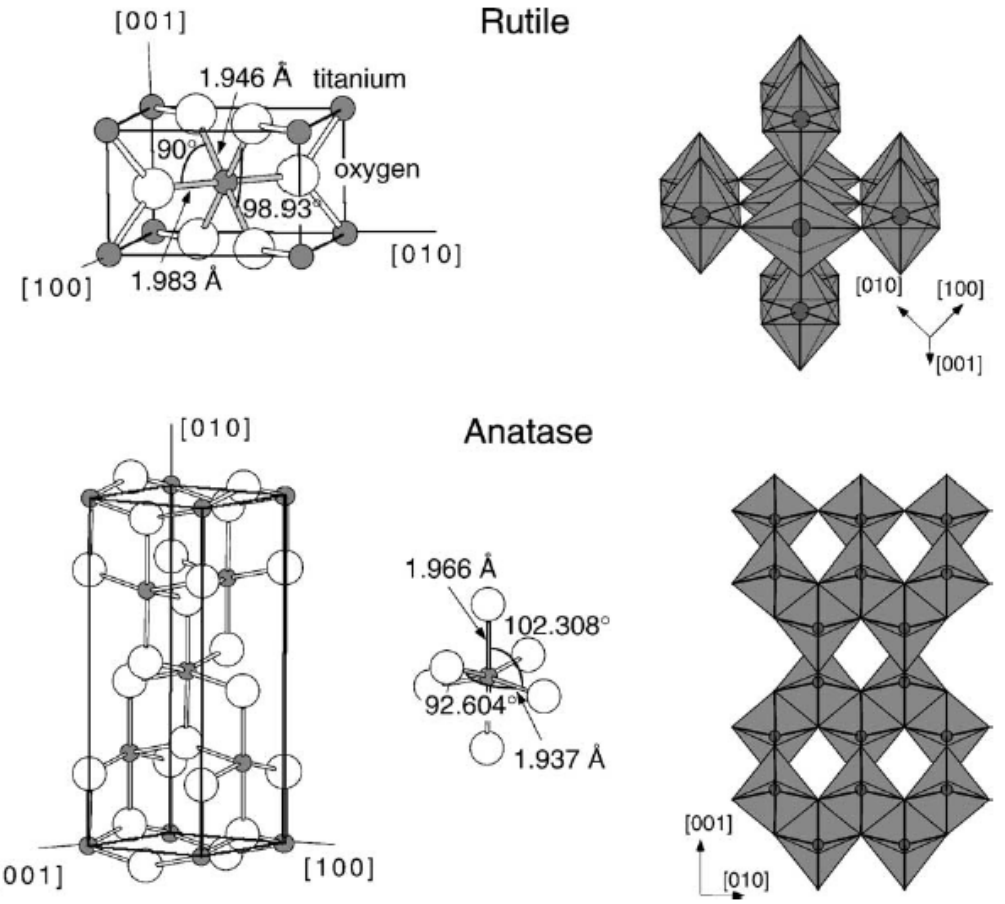

Figure 1.1. Crystal structures of rutile and anatase.[19]

The basic building block of these two structures is a distorted octahedral, where a titanium atom is surrounded by six oxygen atoms.[19]

The rutile phase is more stable than anatase at normal pressure and temperature, even if a size dependence of crystalline stability has been reported, suggesting that anatase can be more stable than rutile when the crystals have a dimension of only few nanometers in diameter.[25]

In the present work, materials with different crystalline phases have been investigated:

- TiO_2 P25 (by Degussa) nanoparticles, constituted by a mixed phase of anatase and rutile (Chapter 3 and 5);
- TiO_2-HT anatase nanoparticles prepared via hydrothermal synthesis, exposing defined surfaces (Chapter 4);
- TiO_2 rutile microparticles, B and F co-doped (Chapter 6).

1.1.2. Surface structure

As already mentioned, a complete knowledge of the surface properties of TiO_2 is still missing. In particular, the use of nanocrystals implies the presence of a wide heterogeneity of sites that can play different roles in the surface reactivity.

In the present case, the attention will be first focused on the surface hydroxylation of the commercial TiO_2 Degussa P25 (Chapter 3).

The radical reactions in which surface OH groups are involved[26,27] are still subject of investigation, because of the complex reaction pathway. An additional source of complexity is coming from the heterogeneity of sites exposed at the surface; moreover the roughness of borders implies the presence of surface defective sites, that behave differently both in terms of molecules adsorption and reactivity.[28,29]

In literature, some theoretical investigation on anatase surface defects have been carried out,[22,23] but no vibrational analysis of the OH formed by dissociation of water on such sites has been reported. In other studies, the vibrational analysis of hydroxy groups has been taken into account, but only extended surfaces were considered.[30,31]

Hence, one of the purposes of this investigation is the vibrational characterization of the OH groups belonging to the surface defective sites.

1.1.3. Study of defined surfaces

The infrared spectroscopic detection of defective sites was the initial step of this research work. However, in order to have more insights on the surface structure

of sites, it has been necessary to study simpler model systems. Therefore, the investigation of nanocrystals with well defined exposed surfaces, allowed to experimentally assign the surface sites structure, giving the chance to establish reference data to be compared with results of theoretical studies and, additionally, to provide information on the more complex TiO_2 P25 system (Chapter 4).

1.1.4. Insights on surface reactivity

Other than for the role in chemistry of pollutants photodegradation,[3] the TiO_2 surface is of interest for the interaction with biomolecules. In this case, a way to study, at a molecular level, the surface-biomolecule interaction has been developed, and the catalytic role of TiO_2 in promoting the oligomerization of glycine has been established (Chapter 5).

1.1.5. TiO_2 doping

Finally a brief investigation of the electronic properties of modified TiO_2 material have been carried out, providing information on the effect of the B- and F- co-doping of titanium dioxide (Chapter 6).

References

(1) Chen, X.; Mao, S. S. *Chemical Reviews* **2007**, *107*, 2891.
(2) Fujishima, A.; Honda, K. *Nature* **1972**, *37*, 238.
(3) Fujishima, A.; Zhang, X. T.; Tryk, D. A. *Surface Science Reports* **2008**, *63*, 515.
(4) Fujishima, A.; Rao, T. N. *Proceedings of the Indian Academy of Sciences-Chemical Sciences* **1997**, *109*, 471.
(5) Grätzel, M. *Nature* **2001**, *414*, 338.
(6) Grätzel, M. *Journal of Photochemistry and Photobiology C-Photochemistry Reviews* **2003**, *4*, 145.
(7) Taga, K.; Sowa, M. G.; Wang, J.; Etori, H.; Yoshida, T.; Okabayashi, H.; Mantsch, H. H. *Vibrational Spectroscopy* **1997**, *14*, 143.
(8) Sittig, C.; Textor, M.; Spencer, N. D.; Wieland, M.; Vallotton, P. H. *Journal of Materials Science-Materials in Medicine* **1999**, *10*, 35.
(9) Anpo, M.; Takeuchi, M. *Journal of Catalysis* **2003**, *216*, 505.
(10) Ji, P. F.; Takeuchi, M.; Cuong, T. M.; Zhang, J. L.; Matsuoka, M.; Anpo, M. *Research on Chemical Intermediates* **2010**, *36*, 327.

(11) Carp, O.; Huisman, C. L.; Reller, A. *Progress in Solid State Chemistry* **2004**, *32*, 33.

(12) Kavan, L.; Grätzel, M.; Gilbert, S. E.; Klemenz, C.; Scheel, H. J. *Journal of the American Chemical Society* **1996**, *118*, 6716.

(13) Sclafani, A.; Herrmann, J. M. *Journal of Physical Chemistry* **1996**, *100*, 13655.

(14) Serpone, N. *Journal of Photochemistry and Photobiology a-Chemistry* **1997**, *104*, 1.

(15) Zhang, Z. B.; Wang, C. C.; Zakaria, R.; Ying, J. Y. *Journal of Physical Chemistry B* **1998**, *102*, 10871.

(16) Chen, Y. X.; Wang, K.; Lou, L. P. *Journal of Photochemistry and Photobiology A: Chemistry* **2004**, *163*, 281.

(17) Tanaka, K.; Capule, M. F. V.; Hisanaga, T. *Chemical Physics Letters* **1991**, *187*, 73.

(18) Hoffmann, M. R.; Martin, S. T.; Choi, W. Y.; Bahnemann, D. W. *Chemical Reviews* **1995**, *95*, 69.

(19) Diebold, U. *Surface Science Reports* **2003**, *48*, 53.

(20) Henderson, M. A. *Surface Science Reports* **2011**, *66*, 185.

(21) Henderson, M. A. *Surface Science Reports* **2002**, *46*, 5.

(22) Gong, X. Q.; Selloni, A.; Batzill, M.; Diebold, U. *Nature Materials* **2006**, *5*, 665.

(23) Gong, X. Q.; Selloni, A. *Journal of Catalysis* **2007**, *249*, 134.

(24) Sheppard, N.; De La Cruz, C. *Catalysis Today* **2001**, *70*, 3.

(25) Zhang, H. Z.; Banfield, J. F. *Journal of Materials Chemistry* **1998**, *8*, 2073.

(26) Serpone, N.; Pelizzetti, E.; Eds. *Photocatalysis: Fundamental and Applications*; Wiley-Interscience: New York, NY, U.S., 1989.

(27) Linsebigler, A. L.; Lu, G. Q.; Yates, J. T. *Chemical Reviews* **1995**, *95*, 735.

(28) Hadjiivanov, K. I.; Klissurski, D. G. *Chemical Society Reviews* **1996**, *25*, 61.

(29) Zecchina, A.; Scarano, D.; Bordiga, S.; Spoto, G.; Lamberti, C. *Advances in Catalysis, Vol 46* **2001**, *46*, 265.

(30) Arrouvel, C.; Digne, M.; Breysse, M.; Toulhoat, H.; Raybaud, P. *Journal of Catalysis* **2004**, *222*, 152.

(31) Dzwigaj, S.; Arrouvel, C.; Breysse, M.; Geantet, C.; Inoue, S.; Toulhoat, H.; Raybaud, P. *Journal of Catalysis* **2005**, *236*, 245.

Chapter 2

Infrared spectroscopy of adsorbed probe molecules

2.1. Infrared spectroscopy of metal oxides

The infrared spectroscopy (IR) provides information on the chemical nature of the surface and on the structure of powder samples,[1-3] like metal oxides; if the sample is properly pre-treated, IR spectroscopy can also be used to study the species present on the surface, like hydroxy groups.

However, the simple IR spectrum of the sample cannot afford in the characterization of the ions exposed at the surface. Conversely, as the coordination of the surface sites is lower than for the bulk ones, they are available for the interaction with probe molecules.[4]

Therefore the IR spectroscopy of adsorbed probe molecules allows the surface sites characterization, because, as consequence of the adsorption, the probe molecules spectral features change and indirectly provide information on the surface sites.[4]

The molecules chosen for probing the surface, must be small (to avoid sterical hindrance), does not have to chemically modify the surface and their spectral feature must be sensitive to the surface state.[5] Carbon monoxide possesses all these characteristics and, indeed is the most frequently used molecule for probing the surface Lewis acid sites of oxides.[4,6]

2.1.1. Carbon monoxide as extrinsic probe molecule for surface Lewis acid sites

In order to understand how the CO molecules can interact with the surface Lewis acid sites, a brief description of the CO electronic properties is reported.
In Figure 2.1, a schematic representation of CO molecular orbitals is shown.

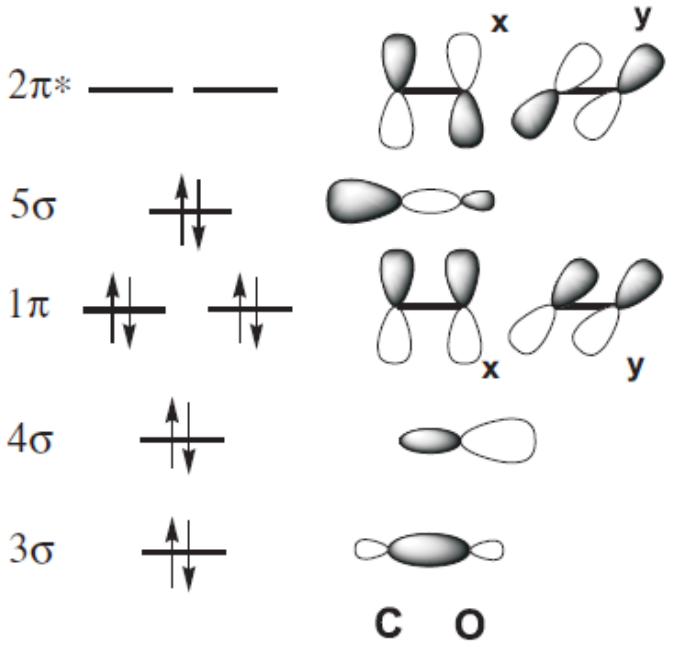

Figure 2.1. Schematic representation of CO molecular orbitals.[4]

The 3σ, 4σ and 1π are occupied bonding orbitals; the 5σ is a slightly anti-bonding occupied orbital that is also the highest occupied molecular orbital (HOMO). Because of this anti-bonding character, if its electronic occupation decreases because of the interaction with surface sites, the entire CO molecule is stabilized, hence the C-O bond is strengthened and the CO stretching (νCO) frequency increased in respect with the CO gas frequency.

The other important molecular orbital is the lowest unoccupied one (LUMO), that is the $2\pi^*$; if the electronic density is added to these anti-bonding orbitals, the C-O bond is weakened and the νCO frequency decreases.[4]

When the CO molecules linearly coordinate to surface cations via C atom, three different interactions can be established.

Electrostatic, that does not imply an electron transfer and that can be described as interaction among the CO charge distribution and the cation field.

σ bond, when an interaction between the HOMO (5σ) of CO and LUMO of metal ion is established. This interaction is favored for metal ions with unoccupied *d* orbitals (Figure 2.2).

π bond is formed when the LUMO ($2\pi^*$) of CO interacts with the HOMO (d_{xy}, d_{xz}) of metal ion. The electron density is transferred from the metal ion to the CO ligand, and therefore is called π back-donation (Figure 2.2).

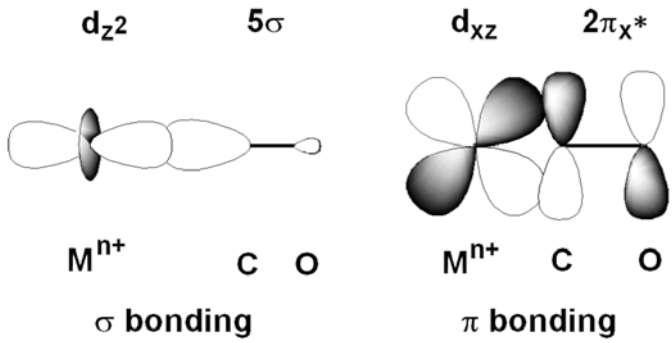

Figure 2.2. Schematic representation of σ and π bonding.[4]

In case of TiO_2 material that has been considered in this work, all the samples analyzed with IR spectroscopy of adsorbed CO, will be previously pre-activated at high temperature, in presence of oxygen, hence, only Ti^{4+} metal ions will be available for the interaction with CO. Since their electronic configuration is d^0, only the electrostatic interaction and the σ bond formation would be possible.

As already mentioned, the σ bonding decreases the C-O bond strength, consequently affecting the CO stretching frequency.

In particular, the stretching frequency of CO in the gas phase[4] is 2143.16 cm^{-1} and the electrostatic interaction and the σ bond formation causes a shift to higher frequency.

However, the kind and the strength of the interaction established among CO adsorbed molecules and surface sites, is not the only factor influencing the CO stretching frequency. Indeed, also the adsorbate-adsorbate interactions contribute to the frequency shift, and they can be of two types: dynamic or static.

The dynamic shift is due to coupling among vibrating dipoles of identical adsorbed molecules (same frequency, so also same isotopes), that are parallel one to the other. In respect with the isolated adsorbed probe molecule (singleton), this coupling, in case of only electrostatic and σ bond interaction, causes a shift towards higher frequency and depends on the coverage (θ).[7]

The static shift is due to two kinds of contributions: through space and through solid; both depend on the type of solid, the coverage and the distance among the adsorbed molecules.

The first one, through space, is related to the dipole interactions among static dipoles, and its effect on the frequency is analogous to the one of dynamic shift; the second type, through solid, affects a site by the adsorbing influence transmitted, through the solid, from another site. This effect lowers the CO stretching frequency in respect with the singleton one.[7]

The shift extent can be established by using proper isotopic mixture of ^{12}CO and ^{13}CO. [8,9]

2.1.2. Low frequency modes of adsorbed CO

When CO is used as vibrational probe of surface sites, the main source of information is the perturbation of the internal C-O stretching mode.

However, the physisorption of CO on a surface results also in other five low-frequency vibrational modes for the CO-surface bond, schematically represented in Figure 2.3.

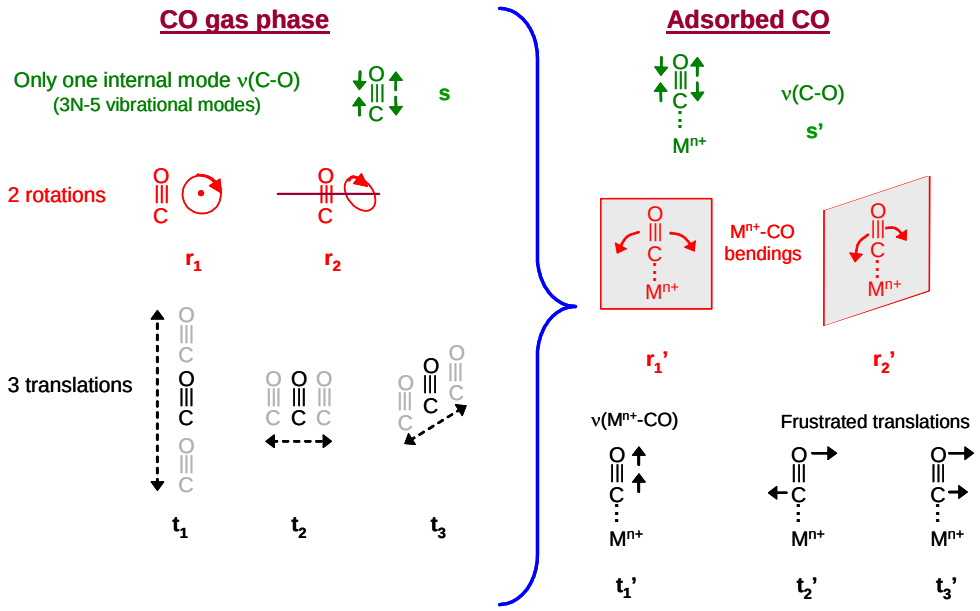

Figure 2.3. Schematic representation of CO modes for molecules in gas phase (left) and for adsorbed molecules (right). s: stretching; r: rotation; t=translation.

- The two rotations of CO in the gas phase (Figure 2.3, r_1 and r_2), become metal-CO bendings (r_1' and r_2') for the adsorbed CO on the metal oxide surface.
- The t_1 translation of the CO molecule in the gas phase becomes the metal-CO stretching (t_1'), while the other two translational modes become frustrated translations (t_2 and t_3) of CO adsorbed on the surface sites (t_2' and t_3') .[10]

Direct evidence of (some of) these modes can be recorded on single crystals by inelastic atom-beam scattering (IABS) .[11] In principle, the same can occur for IR, provided the availability of sources bright enough in the Far-IR region, as synchrotron radiation is.[12] Conventional black-body sources are strong enough relative to thermal fluctuation of the systems only in the spectral region above ca. 400 cm^{-1}, and this make allowance to observe the metal-carbon stretch vibration of CO on metals, by infrared-reflection absorption spectroscopy (IRRAS).[13]

However, frustrated rotations and translations occur at lower frequency, as well as the surface-carbon stretch for CO adsorbed on oxides or halides. Information on such modes are then extracted from their combination with the stretching internal mode of adsorbed CO (Figure 2.4). In this way, data on cation-carbon stretching of CO adsorbed on microcrystalline oxides[14,15] or zeolites,[16] frustrated rotation of CO on microcrystalline MgO [15] and on NaCl films[17] were observed.

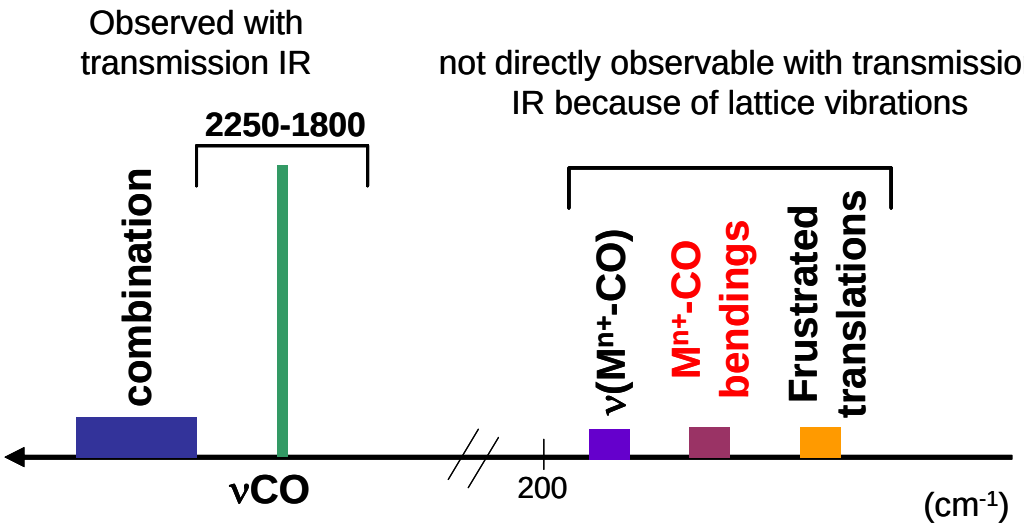

Figure 2.4. Diagram of wavenumbers range for CO modes.

In the next chapters, the presence of a combination of νCO and frustrated translational mode of CO adsorbed on TiO_2 surface, will be reported.

2.1.3. Hydroxy groups as intrinsic probes

The other probes considered in the present work are the hydroxy groups.

It is known that the spectral features of isolated surface hydroxy groups depend on the chemical structure of oxides and their assignment allows to draw conclusions on the surface structure of oxides and on their active sites.

The vibrational pattern of OH groups present on the surface of oxides is generally quite complex. This can be explained by considering that the oxygen atoms of the surface OH groups can be in contact with several immediate neighboring metal atoms (Figure 2.5), influencing the vibrational frequency (νOH).

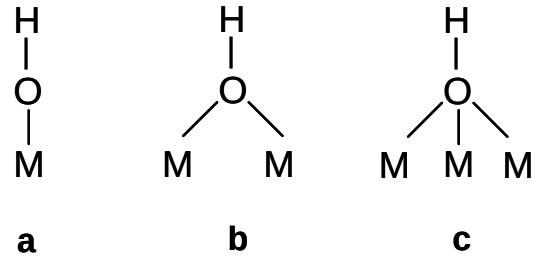

Figure 2.5. Hydroxy groups bonded to (a) one, (b) two, (c) three metal atoms.

As result of the coordinate bond formation, the stretching frequency of “free” OH groups is downshifted as the number of coordinate bonds increases, while the instauration of hydrogen-bonding between adjacent OH groups, causes a frequency lowering.[18,19]

The presence of surface hydroxy groups derives from water dissociation on the oxide surface, resulting in the bond of OH group of water to surface metal atom, and in the link of surface oxygen to hydrogen atom of water.

In the specific case of TiO_2, two types of OH groups are present (Figure 2.6), but the heterogeneity of surfaces exposed on nanoparticles makes difficult the interpretation of the νOH pattern.

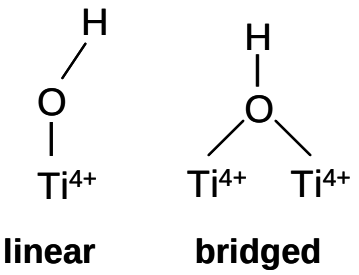

Figure 2.6. Schematic representation of linear and bridged OH groups on TiO_2 surface.

The assignment of the complex IR spectra of OH and CO adsorbed on titanium dioxide, will be presented in the following chapters.

References

(1) Busca, G. *Catalysis Today* **1996**, *27*, 323.
(2) Busca, G. *Catalysis Today* **1998**, *41*, 191.
(3) Busca, G. The Use of Infrared Spectroscopic Methods in the Field of Heterogeneous Catalysis by Metal Oxides In *Metal Oxide Catalysis*; Jackson, D., Hargreaves, J. S. J., Eds.; Wiley-VCH: Weinhein, Germany, 2009; Vol. 1; pp 95.
(4) Hadjiivanov, K. I.; Vayssilov, G. N. *Advances in Catalysis, Vol 47* **2002**, *47*, 307.
(5) Kustov, L. M. *Topics in Catalysis* **1997**, *4*, 131.
(6) Yates, J. T. *Surface Science* **1994**, *299*, 731.
(7) Platero, E. E.; Scarano, D.; Zecchina, A.; Meneghini, G.; DeFranceschi, R. *Surface Science* **1996**, *350*, 113.
(8) Spoto, G.; Morterra, C.; Marchese, L.; Orio, L.; Zecchina, A. *Vacuum* **1990**, *41*, 37.
(9) Morterra, C.; Bolis, V.; Fubini, B.; Orio, L.; Williams, T. B. *Surface Science* **1991**, *251*, 540.
(10) Abe, H.; Manzel, K.; Schulze, W.; Moskovits, M.; DiLella, D. P. *Journal of Chemical Physics* **1981**, *74*, 792.
(11) Lahee, A. M.; Toenniesa, J. P.; Wölla, C. *Surface Science* **1986**, *177*, 371.
(12) Hirschmugl, C. J.; Williams, G. P.; Hoffmann, F. M.; Chabal, Y. J. *Physical Review Letters* **1990**, *65*, 480.
(13) Hoge, D.; Tüshaus, M.; Schweizer, E.; Bradshaw, A. M. *Chemical Physics Letters* **1988**, *151*, 230.
(14) Scarano, D.; Spoto, G.; Bordiga, S.; Zecchina, A.; Lamberti, C. *Surface Science* **1992**, *276*, 281.

(15) Spoto, G.; Gribov, E. N.; Ricchiardi, G.; Damin, A.; Scarano, D.; Bordiga, S.; Lamberti, C.; Zecchina, A. *Progress in Surface Science* **2004**, *76*, 71.

(16) Otero Areán, C.; Palomino, G. T.; Zecchina, A.; Spoto, G.; Bordiga, S.; Roy, P. *Physical Chemistry Chemical Physics* **1999**, *1*, 4139.

(17) Richardson, H. H.; Baumann, C.; Ewing, G. E. *Surface Science* **1987**, *185*, 15.

(18) Tsyganenko, A. A.; Filimonov, V. N. *Journal of Molecular Structure* **1973**, *19*.

(19) Davydov, A. *Molecular spectroscopy of oxide catalyst surfaces*; John Wiley &Sons Ltd: Chichester, England, 2003.

Chapter 3

Surface structure of TiO_2 P25 nanoparticles

3.1. Introduction

This first part of the thesis has been devoted to the investigation of surface sites of TiO_2 Degussa P25. The interest towards the disclosure of surface properties of titanium dioxide, derives from the possibility to identify the active centers that rule the photocatalytic performances of this semiconductor. Such functional behavior depends on the separation and diffusion at the surface of the photogenerated e^-/h^+, but a significant role is also played by surface centers that control the interfacial transfer of such charges.[1,2] In particular, surface hydroxylated centers have been proposed to act as trapping sites for both electrons and holes migrated to the surface, as in the following reactions:[1,2]

$$e^- + Ti_{IV}(O\text{-}H)^- \rightarrow Ti_{III}(O\text{-}H)^-$$
$$h^+ + Ti_{IV}(O\text{-}H)^- \rightarrow Ti_{IV}(O\text{-}H)^{\cdot}$$

Evidence for the hydroxy species resulting from these processes has been obtained,[3] as well as for the actual influence of the surface hydroxylation on the photo-oxidation of phenol[4] and the degradation of methylene blue.[5] Furthermore, surface hydroxy groups are exploitable for the modification of the titania surface, as in the case of fluorination by OH^-/F^- exchange.[6,7]

The increased interest toward titania stimulated the development of a variety of preparation methods to obtain materials with better performance than commercial titania powders.[8-11] Nevertheless, TiO_2 P25 (Degussa) represents a kind of landmark among these materials for photocatalytic applications and, in many instances, exhibits unsurpassed photocatalytic activity, as recently reported in a comparative work on 10 different TiO_2 powders.[12]

IR spectroscopy is widely employed for the investigation of surface hydroxy groups of catalysts and photocatalysts.[13] The investigation of the IR features of surface -OH on titania powders has been the subject of many papers[3,5,14-22] that have based the assignment of various OH groups stretching (νOH) bands on the pioneering work of Primet et al.[14] and Tsyganenko et al.[15] Using these reports, νOH bands at frequencies higher than 3680 cm^{-1} were assigned to linear hydroxy groups, while bands at lower frequencies were related to bridged -OH, the two species resulting from the dissociation of H_2O on pairs of coordinatively unsaturated Ti^{4+} and O^{2-} surface sites. However, more recent theoretical works have proposed that the dissociation of water on Ti^{4+}-O^{2-} pairs exposed on the reactive anatase TiO_2 faces (001) results in the breaking of the Ti-O bond,[23,24] with the production of two linear Ti-OH groups. These investigations also highlighted the dependence of the molecular and dissociative effects on the adsorption of H_2O on TiO_2 surfaces with different types of surface planes and amounts of water coverage. Furthermore, both experimental[17,25] and theoretical[26,27] investigations have pointed out the dissociative character of the adsorption of H_2O on coordinative defect sites as steps and corners, the amount of which should increase as the size of the TiO_2 particles decreases. However, depending on the local configuration, steps can be less reactive than flat surfaces.[26] Despite such a rich panorama of research, a detailed study of the multicomponent νOH pattern exhibited by some types of TiO_2 nanoparticles, including TiO_2 P25,[17,19,28] is still missing. A general assignment was proposed by Busca et al. for TiO_2 P25,[20] and experimental data and theoretical calculations from Dzwigaj et al. explored the dependence of the νOH pattern on the morphology of two types of anatase TiO_2 particles, focusing on regular faces.[29]

Furthermore, in those experiments water molecules were present on the surfaces, and most of the observed νOH bands were attributed to adsorbed H_2O. Notably, the investigation of structure-reactivity relationships of steps on anatase TiO_2 single crystals has been the subject of a combined experimental and theoretical study.[26] Unfortunately no vibrational analyses were performed as part of such modeling. To contribute to the elucidation of such stimulating matter, even more complex for nanoparticles exposing a variety of surface terminations, a selective approach has been adopted, targeting the recognition of νOH bands that should be due to hydroxy species on coordinative defect sites and/or on poorly extended faces exposing Ti^{4+} in low coordination. To assess the actual morphology of the borders of the TiO_2 particles, high resolution transmission electron microscopy was employed. Although sites of these kinds represent a minor fraction of the surface centers, they belong to the category of surface defects that are responsible for much of the surface chemistry of oxides.[30,31] Moreover, OH groups on coordinative defect sites are expected to be removed at a higher temperature than those of regular planes and water molecules, allowing a selective observation of their IR stretching absorption bands. Conversely, water molecules, which are strongly adsorbed on Ti^{4+} cations through a coordinative interaction, and hydroxy groups on regular planes share a range of outgassing temperatures,[17] preventing an unequivocal observation of the stretching bands due to such OH groups only. Furthermore, to assess the actual location of hydroxy groups on sites with different local structures, IR spectroscopy of adsorbed CO was employed to probe the Lewis acidity of Ti^{4+} sites originally occupied by OH species and H_2O molecules.

3.2. Materials and methods

3.2.1. Materials

The material investigated was TiO_2 P25 (80% anatase and 20% rutile), obtained from Degussa and produced by pyrolysis of $TiCl_4$. As received, it exhibited a SSA_{BET} of ca. 55 $m^2\ g^{-1}$, which remained essentially unchanged under

thermal treatment up to 773 K, but then decreased to ca. 40 m^2 g^{-1} when the temperature was raised to 873 K. This temperature represents the limit temperature before the anatase to rutile phase transformation occurs in vacuo.[32] For this reason, the spectroscopic study was carried out on samples treated at 873 K (in the IR cells, as reported in the next section) and then rehydrated by contact with 20 mbar of H_2O vapor for 60 min. This rehydration did not restore the initial SSA_{BET}, so changes of the intensity of the IR bands from increasing the temperature of subsequent treatments were no longer affected by changes in specific surface area.

H_2O and D_2O (99.90% D, Euriso-top) were introduced onto the samples after several freeze-pump-thaw cycles and high purity CO (Praxair) was employed after liquid nitrogen trapping.

3.2.2. Methods

High resolution transmission electron microscopy (HR-TEM) images of the materials (powder grains "dry" dispersed on lacey carbon Cu grids) were obtained using a JEOL 3010-UHR microscope with an acceleration potential of 300 kV.

X-Ray Diffraction (XRD) pattern was obtained by an Analytical X'Pert Pro equipped with an X'Celerator detector powder diffractometer using Cu-Kα radiation generated at 40 kV and 40 mA. A quartz sample holder was used. The 2θ range was from 5° to 60° with a step size (2θ) of 0.05 and a counting time of 3 s.

Specific surface area (SSA_{BET}) and porosity were evaluated by adsorption of an inert gas (N_2) at the temperature of liquid nitrogen (77K) with a Micrometrics ASAP 2020. The adsorption isotherm has been measured and the data analyzed with BET (Brunauer, Emmet and Teller) model for specific surface area determination.[33] For the adsorption measurements samples were preoutgassed at 523 K to dehydrate the sample before nitrogen adsorption.

For **IR measurements**, the TiO_2 powder samples were pressed in self-supporting pellets and placed in quartz cells designed to carry out spectroscopic

measurements at the beam temperature (b.t., ca. 323 K; cell equipped with CaF_2 windows, optical path ca. 7 mm) or at low temperature (i.e., ca. 100 K) by cooling with liquid N_2 (cell equipped with KBr windows, optical path ca. 100 mm).

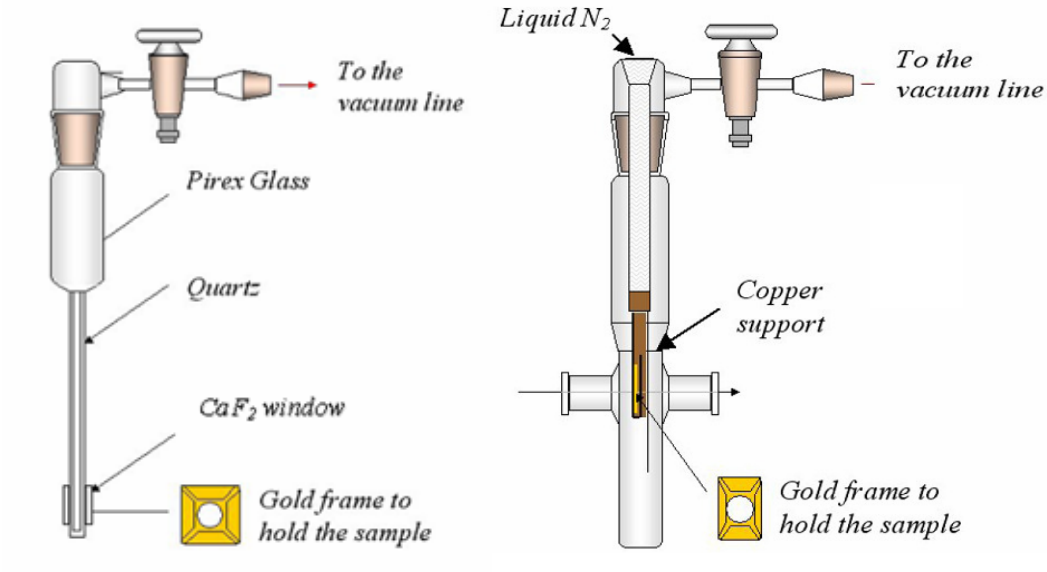

Figure 3.1. Schematic representation of cells used for infrared measurements at room temperature (on the left) and at ca. 100 K (on the right).

Because of the high intensity of the bands due to CO adsorbed at low temperature, pellets with an "optical thickness" of ca. 10-15 mg·cm^{-2} were used for this kind or measurement, whereas the "optical thickness" of the pellets used to collect spectra at b.t. was increased to 20-30 mg·cm^{-2}. The cell was connected to a conventional vacuum line (residual pressure: 1 × 10^{-5} mbar) allowing all thermal treatments and adsorption-desorption experiments to be carried out in situ. A Bruker IFS 28 spectrometer (resolution: 2 cm^{-1}; detector: MCT) was employed for the spectra collection. Depending on the case, from 150 to 500 scans were accumulated to obtain a good signal-to-noise ratio. Before IR measurements, the samples were outgassed at a temperature ranging from b.t. to 873 K for 60 min. For outgassing temperatures ≥ 573 K, samples were placed in contact with O_2 (6 mbar) at the same temperature for 60 min after initial outgassing. Then, the

pellets were cooled to 473 K in O_2 and further cooled to room temperature under outgassing. For the sake of simplicity, this multistep treatment will be simply referred to as “outgassing” or “pre-outgassing” (when followed by CO adsorption). In all cases, at the end of the procedure, the samples were white in color, as expected for stoichiometric (fully oxidized) TiO_2. To remove from the νOH and δH_2O regions the slope due to scattering, at the end of the IR measurements at room temperature, the TiO_2 pellets were retreated at 873 K, contacted with 20 mbar D_2O and outgassed at b.t., and their spectra were used as the background for data elaboration (Figure 3.2).

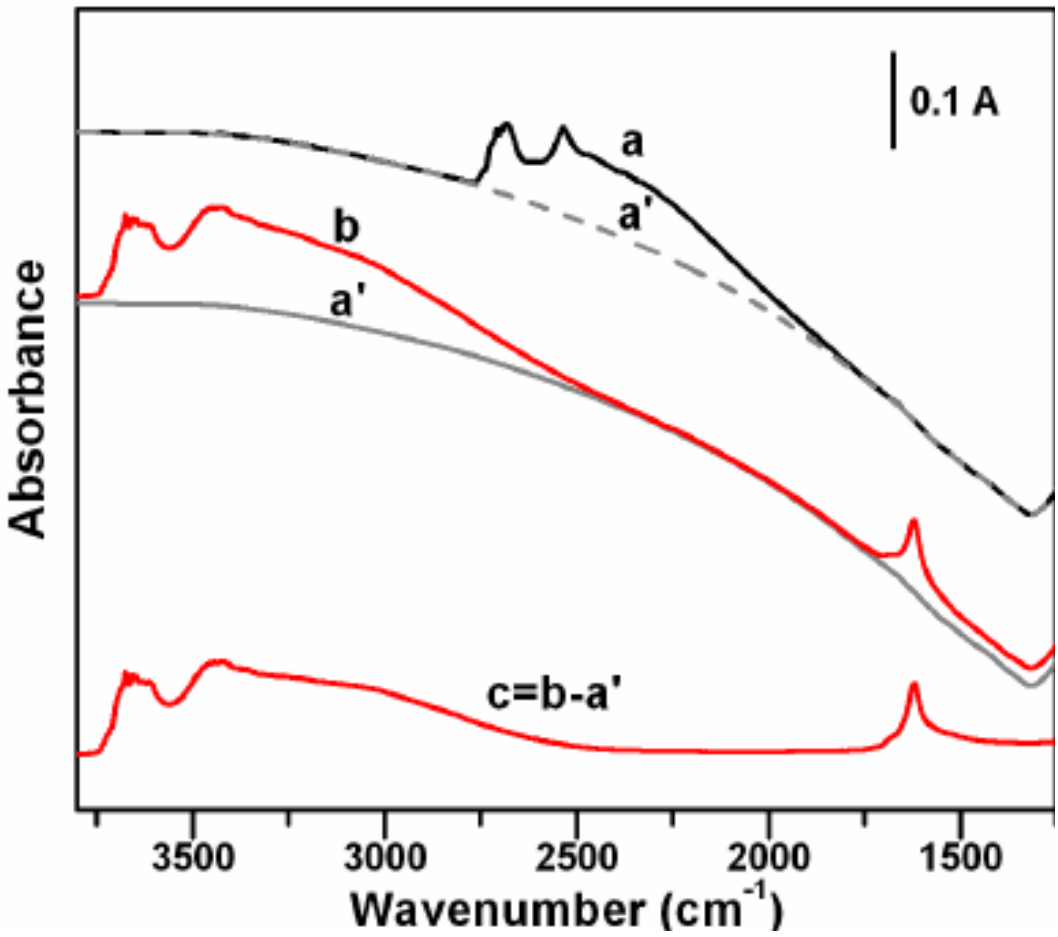

Figure 3.2. Example of data elaboration for the removal from the spectra of the contribution due to scattering: (a) original spectrum of TiO_2 P25 outgassed at 873 K, contacted with 20 mbar D_2O and then outgassed for 60 min at beam temperature; (a′) profile derived after suppression of the νOD pattern in the 2750-1800 cm^{-1} range, substituted by a reasonable baseline; (b) original spectrum of TiO_2 P25 outgassed for 60 min at b.t.; (c) "scattering corrected" spectrum of TiO_2 P25 outgassed for 60 min at b.t. resulting from the subtraction of simulated spectrum (a′) from spectrum (b). On the low frequency side, the spectra have been limited to 1250 cm^{-1}, to avoid a negative feature at 1190 cm^{-1} due to the δD_2O mode.
Resolution of subbands present in the spectra of adsorbed CO was achieved by using the "curve fit" utility of OPUS 5.0 (Bruker Optic Gmbh). The fits were optimized by using a local least squared method.

3.3. Surface morphological features

TEM inspections evidenced a wide heterogeneity in the size of the titania particles, ranging from ca. 10 to 50 nm (Figure 3.3A), in agreement with data previously reported by Ohno et al.[34]

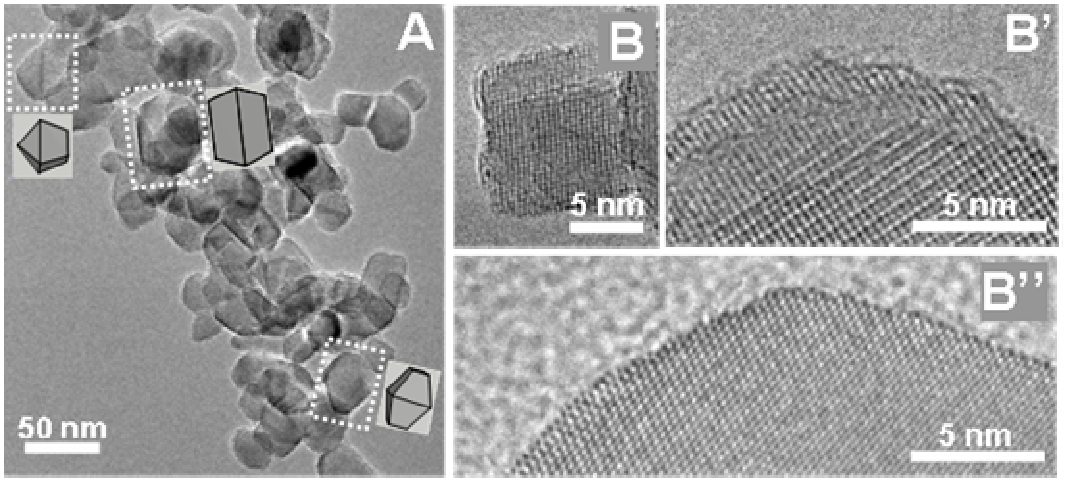

Figure 3.3. TEM images representative of size and morphology of TiO_2 P25. Panel A: overall view (original magnification: ×80k). Panels B, B′, B″: zoomed view of some rough border regions (original magnification: ×500k). (Reprinted with permission from Deiana et al.[35] Copyright 2010 American Chemical Society.)

As for the shapes, some of the observed profiles were easily recognized as bidimensional projections of truncated bipyramids with the main axis (almost) parallel to the image plane, as displayed by 3D schemes. For most of the shapes, however, the contours of the projections could be due to more isometric particles. A different possibility was that such contours resulted from the projection of bipyramids (or capped prisms) with the main axis perpendicular to the image plane. However, all these morphologies were in agreement with those proposed in theoretical and experimental reports dealing with pure anatase powders.[23,29,36] At high magnification, fringes due to diffraction contrast appeared resolved (Figure 3.3B), supporting the crystalline nature of TiO_2 particles. In previous investigations,[28,37] the exposure of planes of the (101) and (001) type was

proposed for the extended surfaces. Focusing on the roughness, at the level of a few reticular steps, of part of the borders of the particles (Figure 3.3B,B′,B″), it indicated the presence of a variety of local terminations rich in corners, steps and edges, where the coordinative unsaturation of exposed lattice atoms should be higher than on more regular and flat surfaces.

3.4. Dehydration, dehydroxylation and probing of coordinatively unsaturated surface cations by CO adsorption

3.4.1. Evolution of bands due to hydroxy groups and adsorbed water

Figure 3.4 shows the spectra of TiO_2 outgassed up to 773 K in the νOH (section A) and δH_2O (section B) ranges, which exhibited a general trend quite similar to that reported by Morterra in his seminal work on an anatase sample prepared via the chloride.[17]

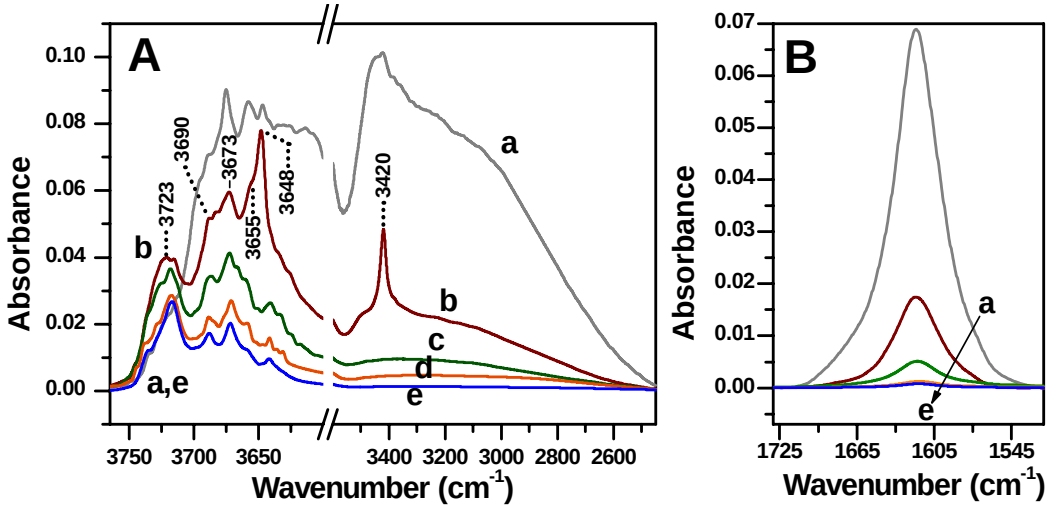

Figure 3.4. IR spectra in the νOH and δH_2O regions (sections A and B, respectively) of TiO_2 P25 outgassed for 60 min at: (a) beam temperature, i.e., ca. 323 K, (b) 473, (c) 573, (d) 673, and (e) 773 K. On the *X* axis, the scale has been changed at 3600 cm^{-1}, to zoom the region at higher frequency. The gap on the axis is just of 1 cm^{-1}. (Adapted from Deiana et al.[35] Copyright 2010 American Chemical Society.)

After degassing at beam temperature (curve a), the region at high frequencies was dominated by a broad and complex absorption spread over a range from 3600 to 2500 cm^{-1}, due to -OH oscillators involved in H-bonds, and accompanied by a series of narrow and partly resolved peaks/subbands in the 3750-3600 cm^{-1} range, related to -OH groups experiencing weaker intermolecular interactions (Figure 3.4A). In experimental studies, bands in the latter range have been mostly assigned to hydroxy groups, whereas undissociated water molecules, coordinatively adsorbed on surface Ti^{4+} ions, mainly contributed to the 3600-2500 cm^{-1} absorption,[17] other than produce the δH_2O band at ca. 1620 cm^{-1} (Figure 3.4B). However, more recent theoretical investigations proposed that H_2O adsorbed at high coverage, apparently not involved in H-bonds, should absorb in the 3750-3600 cm^{-1} range.[23] Nevertheless, the number of components in this range (at least 9, considering maxima and shoulders) indicated the presence of several types of surface sites bearing hydroxyl groups and adsorbed H_2O molecules. The decrease in integrated intensity of the δH_2O band after outgassing at 473 K (Figure 3.4B, b) monitored the removal of approximately 75% of the adsorbed H_2O molecules. Water desorption and condensation of hydroxy groups were also responsible for the decrease in intensity of the νOH pattern that occurred to a much higher extent for the broad 3600-2500 cm^{-1} band than for the set of sharp 3750-3600 cm^{-1} peaks. This latter now exhibits a main peak at 3648 cm^{-1}, asymmetric toward the lower frequency side and with a shoulder at 3655 cm^{-1}. Additionally, another component at 3673 cm^{-1} with subbands at 3690 cm^{-1}, and a new band with a maximum at 3723 cm^{-1}, resulting from the overlap of several components, appeared. This complex signal was assigned to O-H oscillators initially involved in H-bonding (and then absorbing at lower frequencies) with hydroxyl groups/water molecules that were removed by outgassing. Noticeably, a quite narrow band was now observed at 3420 cm^{-1}, still superimposed on a broad absorption. This band was supposed to be characteristic of the rutile phase present in the TiO_2 P25 [3] but was also observed for a pure anatase sample.[17] In this last case, it was assigned to coordinated water species on the basis of the similar evolution in dependence on the

outgassing temperature with respect to the δH_2O band. Conversely, in a more recent paper, this component was supposed to be due to hydroxy groups playing a special role in the photocatalytic behavior of the TiO_2 P25, but unfortunately, the δH_2O spectral range was not reported.[5] In the present case, outgassing at 573 K (Figure 3.4A,B, curves c) resulted in the depletion of the 3420 cm^{-1} band and in a decrease in intensity of the broad feature below, while the δH_2O band appeared significantly weaker. This behavior might support the assignment of the 3420 cm^{-1} signal to water molecules. However, it must be considered that two νOH absorptions were expected for H_2O molecules and that a partner signal must be identified. In addition, the location of the considered band was in the range typical for OH oscillators involved in H-bonds, and such interactions usually produce a significant broadening of the absorption profile (increasing as the frequency of the maximum is decreased). Furthermore, none of the frequencies calculated by Arrouvel et al.[23] for adsorbed H_2O fit with the band at 3420 cm^{-1}. The assignment of this component remains a matter of debate for future experimental and theoretical investigations. As for the set of signals at higher frequencies, the main effect of outgassing at 573 K was the depletion of the 3648 cm^{-1} peak, accompanied by an overall decrease in intensity of the other components. Subsequent outgassing at increasing temperatures up to 773 K left only traces of the broad absorption in the 3600-2600 cm^{-1} region and resulted in a progressive decrease in intensity of the 3750-3600 cm^{-1} pattern (Figure 3.4A). As for molecular water, it must be considered that outgassing at $T \geq 673$ K should result in a complete desorption of H_2O molecules. Nevertheless, a very weak δH_2O was still observed.

The presence of H_2O molecules should be ascribed to readsorption of trace amounts of water released from the inner walls of the cell (that were not fully heated during outgassing) once the sample was cooled to beam temperature. Noticeably, despite the presence of adsorbed H_2O, no signal was present in the 3600-2600 cm^{-1} range for the sample outgassed at 773 K (Figure 3.4B, e). This feature will be commented on in the section 3.4.3., devoted to the spectra collected after outgassing at higher temperatures.

Focusing on the 3750-3600 cm^{-1} pattern (Figure 3.4A), no significant changes in the relative intensity of the various components occurred by outgassing at 773 K, except for the more severe suppression of the subband at $\nu \geq 3725$ cm^{-1} (Figure 3.4A, d). To assess the actual level of coordinative unsaturation of surface Ti^{4+} centers that were initially occupied by water and hydroxyl groups, IR spectra of CO adsorbed on TiO_2 outgassed at increasing temperatures were then collected. The results obtained are reported and commented in the next section.

3.4.2. IR spectra of CO adsorbed at 100 K on samples preoutgassed up to 773 K

The adsorption of CO at 100 K on TiO_2 preoutgassed at increasing temperatures from 473 to 773 K resulted in the appearance of a dominant peak at 2179 cm^{-1} in the IR spectra, which exhibited some increase in intensity as the preoutgassing temperature was increased (Figure 3.5).

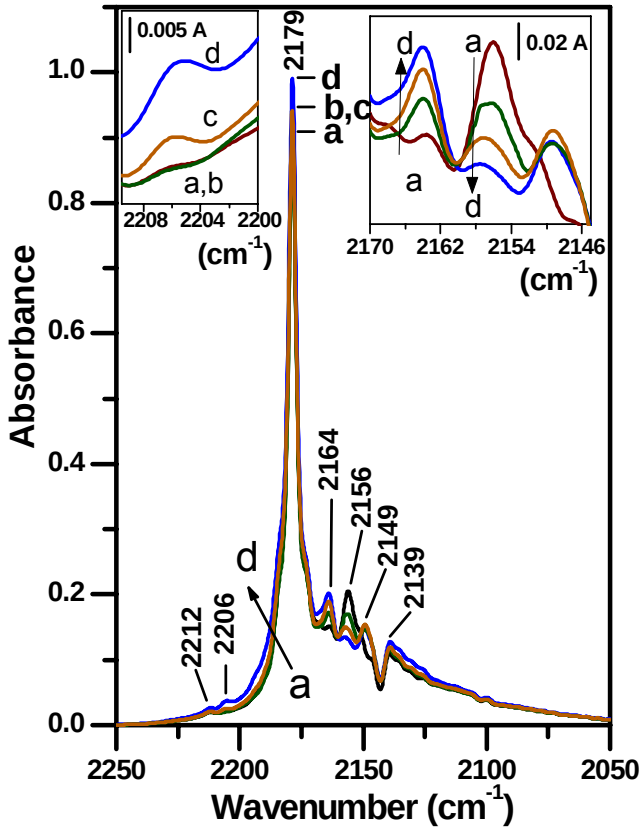

Figure 3.5. IR spectra of CO adsorbed at ca. 100 K on TiO_2 P25 outgassed at (a) 473, (b) 573, (c) 673, and (d) 773 K. Insets: zoomed views of the 2210-2000 and 2170-2145 cm^{-1} ranges. (Reprinted with permission from Deiana et al.[35] Copyright 2010 American Chemical Society.)

Furthermore, by decreasing the CO coverage, the maximum shifted to ca. 2190 cm^{-1} (Figure 3.6), which usually resulted from the weakening of interactions among parallel and close oscillators, as described in Chapter 2.[38,39]

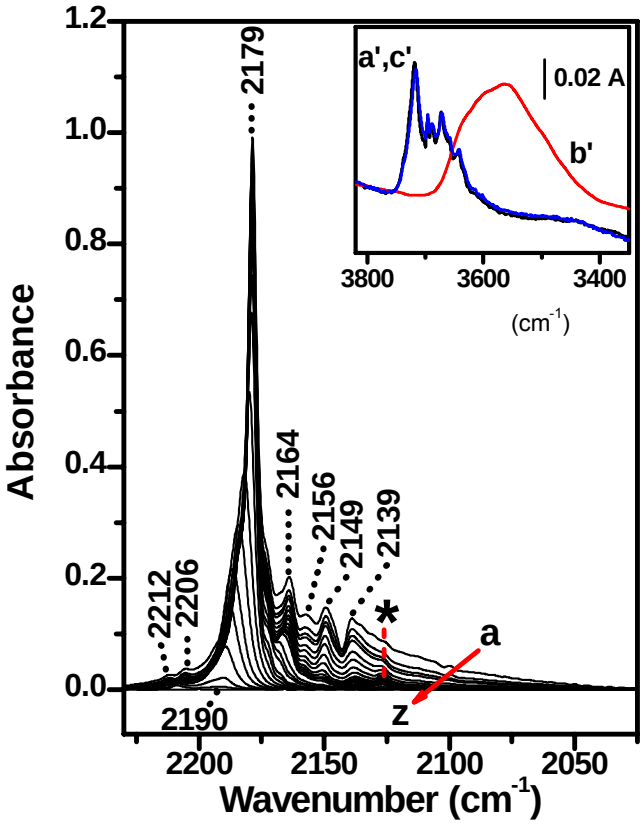

Figure 3.6. IR spectra of CO adsorbed at ca. 100 K on TiO_2 P25 outgassed at 773 K. Lettering is in the sense of decreasing coverages, from (a) 40 mbar CO to (z) outgassing for 10 min at ca. 100 K. Inset: spectra in the νOH region: (a') before contact with CO; (b') in the presence of 40 mbar CO; (c') after decreasing of CO pressure to 0.5 mbar. In the main panel, the weak band labeled with the asterisk is due to ^{13}CO present in natural abundance, adsorbed on β cationic sites. The data reported in the figure are representative of similar spectral behaviors observed for CO adsorbed at 100 K at decreasing coverages on TiO_2 samples outgassed at 473, 573 and 673 K.

All these features were typical of CO molecules adsorbed on penta-coordinated Ti^{4+} ions (hereafter β sites, following the nomenclature proposed by Hadjiivanov et al.[40]) exposed on (010) [isostructural with (100)] or (101) [isostructural with (011)].[29,37,40] By considering that

(i) preoutgassing at 473 K removed ca. 75% of the initially adsorbed water while affecting the hydroxy groups to a significantly lesser extent (Figure 2) and

(ii) the peak due to CO adsorbed on β sites exhibited only a limited increase in intensity from increasing preoutgassing temperatures over 473 K,

it can be concluded that an overwhelming portion of the β sites were initially occupied by H_2O molecules (the local structure of β sites will be discussed in detail in Chapter 4). Conversely, the weaker band at 2164 cm^{-1}, due to CO on penta-coordinated Ti^{4+} ions on (001) planes (γ sites),[40] increased progressively in intensity as the preoutgassing temperature was increased (Figure 3.5, right inset), indicating that such sites should have been originally occupied also by hydroxy groups. This feature is in agreement with the calculations performed by Arrouvel et al.,[23] that indicated a dissociative character for the adsorption of H_2O on (001) anatase surfaces. Moreover, hydroxy groups resulting from the dissociation on such surfaces were expected to contribute to the high frequency part of the νOH pattern, and in the present case subbands at $\nu > 3730$ cm^{-1}, decreasing in intensity by outgassing at 473-773 K, were present (Figure 3.4A). Also hydroxy groups remaining on the surface acted as sites for CO adsorption, producing the weak νCO band at ca. 2156 cm^{-1}, which decreased in intensity as the preoutgassing temperature increased (Figure 3.5, right inset). Accordingly, the perturbation of the νOH pattern in the 3750-3600 cm^{-1} range occurred (Figure 3.6, inset). Two other νCO components appeared at 2149 and 2139 cm^{-1} (Figure 3.5). The former one was not observed in previous studies. Here, it is tentatively assigned to CO in interaction with surface Ti^{4+} ions with a very weak Lewis acid character, also on the basis of the results obtained dosing CO on samples outgassed at higher temperature (vide infra). Conversely, the band at 2139 cm^{-1} is the typical feature due to physically adsorbed CO (this is the only signal increasing in intensity by increasing the pressure of CO over 40 mbar).[37,40]

Another band, not previously reported in literature, is observed at 2212 cm^{-1} at frequency and with reversibility higher that α sites, hence it is assigned to sites

with Lewis acidity lower that α ones. The origin of this particular component will be discussed in detail in section 3.5.

Preoutgassing at 673 and 773 K resulted in a slight increase of the main peak at 2179 cm^{-1}, monitoring the exposure to CO of additional β sites. Moreover, a weak component at 2206 cm^{-1} was noticeable, due to CO adsorbed on α sites, i.e., surface coordinative defect sites.[40] These surfaces, when hydrated, have been proposed to carry OH groups rather than undissociated water molecules.[23] On the basis of the calculations by Arrouvel et al.,[23] OH on (110) surfaces should be responsible for a component around 3725 cm^{-1} in the spectra in Figure 3.4A. However, the variety of surface terminations on the rough parts of the particle terminations suggested the possible presence of several types of local structures that could expose Ti^{4+} and O^{2-} acid-base pairs able to dissociate H_2O molecules, producing a multicomponent νOH pattern. To elucidate this question, the outgassing temperature was increased stepwise to 873 K, the maximum temperature attainable without a significant occurrence of the anatase to rutile phase transformation, and the Ti^{4+} sites rendered coordinatively unsaturated by dehydroxylation were probed with CO.

3.4.3. TiO_2 samples outgassed up to 873 K

TiO_2 was outgassed at 823 and 873 K and the related spectra in the νOH (sample in vacuo) and νCO ranges [dealing with CO (150 mbar) adsorbed at beam temperature] are reported in Figure 3.7 (sections A and B, respectively); a scheme of the experimental procedure is reported in Figure 3.8.

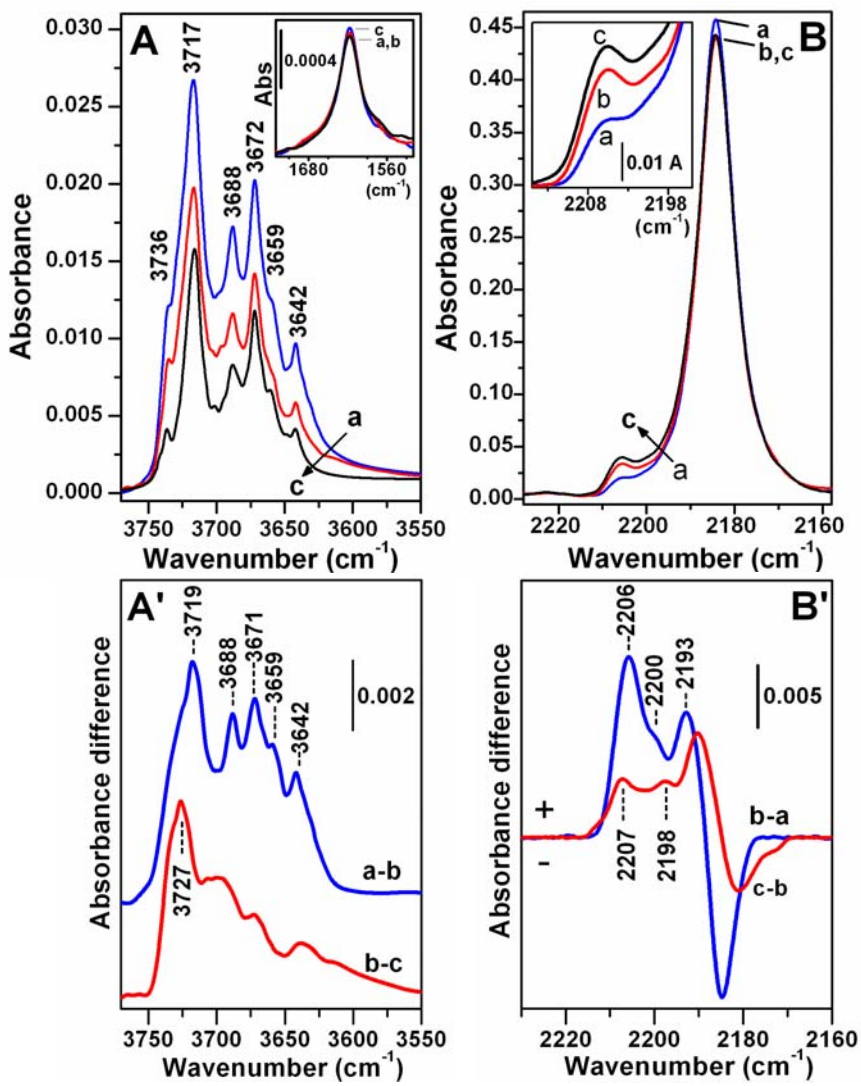

Figure 3.7. Upper panels: IR spectra in the νOH (section A) and νCO (section B) regions of TiO_2 P25 stepwise outgassed at $T \geq 773$ K and contacted at beam temperature with 150 mbar of CO. In both sections, lettering is as follows: (a) T_{outg} 773 K; (b) T_{outg} 823 K; (c) T_{outg} 873 K. Insets: zoomed views of the δH_2O (section A) and 2215-2195 cm^{-1} (section B) ranges. Lower panels: results of the subtraction between spectra in upper panels. In sections A′ (νOH region) lettering is as follows: (a-b) difference between spectra of the sample outgassed at 773 K (a) and at 823 K (b); (b-c) difference between spectra of the sample outgassed at 823 K (b) and at 873 K (c). In section B′ (νCO region) lettering is as follows: (b-a) difference between spectra of CO (150 mbar) adsorbed on the sample outgassed at 823 K (b) and at 773 K (a); (c-b) difference between spectra of CO (150 mbar) adsorbed on the sample outgassed at 873 K (c) and at 823 K (b). (Reprinted with permission from Deiana et al.[35] Copyright 2010 American Chemical Society.)

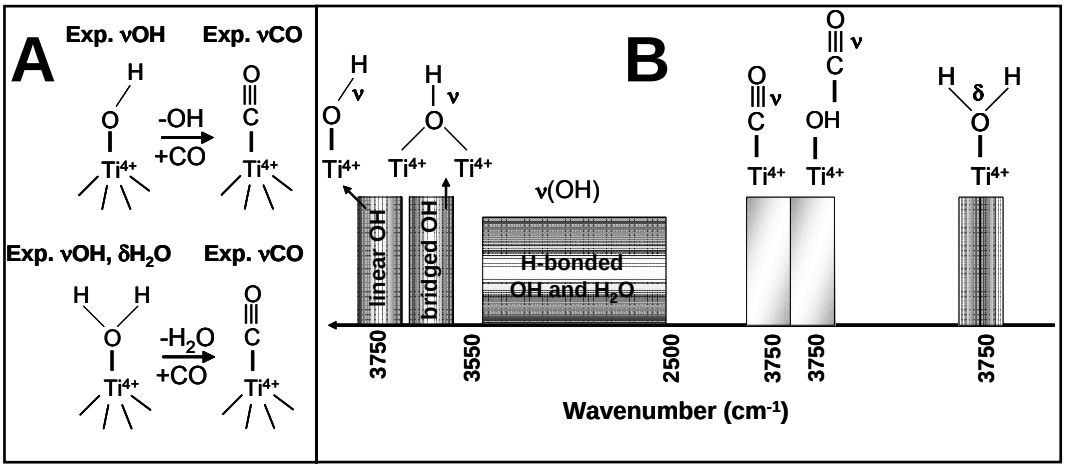

Figure 3.8. Panel A. Schematic representation of the experimental procedure: (i) acquisition of νOH vibrational pattern, (ii) then removal of OH with thermal treatment and (iii) subsequent acquisition of adsorbed CO infrared spectra. Panel B. Schematic diagram of wavenumbers range for vibrational frequencies of νOH and νCO.

The spectra obtained for TiO_2 outgassed at 773 K are also shown, for the sake of completeness. As reported above, trace amounts of water molecules were reabsorbed on the sample after outgassing, as proved by the presence of an extremely weak δH_2O signal (Figure 3.7A, inset). Conversely, no signals were detected in the 3600-2600 cm^{-1} region, so it was concluded that the observed νOH absorptions due to water molecules should fall in the 3750-3600 cm^{-1} range. In actuality, calculation for high water coverage produced stretching frequencies at 3710 cm^{-1} for H_2O on (100) faces (8.2 $H_2O \cdot nm^{-2}$) and at 3665 and 3646 cm^{-1} for H_2O on (101) faces (10.1 $H_2O \cdot nm^{-2}$).[23] Such values, much higher than expected for adsorbed water molecules, were explained on the basis of intermolecular repulsions that hindered H-bonding. Dipole-dipole repulsions were also proposed to be an origin for the νOH upward shift observed in the HREELS spectrum by increasing H_2O coverage on (110) rutile single crystals.[25] In the present case, however, the amount of adsorbed H_2O was rather small (the integrated intensity of the δH_2O bands in the inset of Figure 3.7A was ca. 0.5% of the band originally observed after outgassing at b.t., see Figure 3.4B, curve a). Therefore, the

hypothesis of interactions between adsorbed H_2O molecules could only hold considering a highly heterogeneous distribution of adsorbed water molecules, for instance, forming patches on the external surface/first layers of the TiO_2 pellet first encountered during their adsorption. In support of this claim, a limited diffusion for a gaseous probe dosed at low pressure within a pelletized powder was previously reported for CO.[41] A different possibility for this phenomenon is the adsorption of H_2O on sites with local structure that oriented the molecules with their two OH bonds pointing out from the surface and caused them to experience a very weak interaction with neighboring surface O^{2-} or OH sites.

However, two points must be stressed:

(i) the amount of water appeared to be essentially the same after all treatments in the range 773-873 K (Figure 3.7A, inset), and then also the bands due to their stretching modes should contribute to the same extent to the three νOH spectra in Figure 3.7A. Hence, the decrease in intensity of such patterns by increasing the outgassing temperature should have been due to the removal of hydroxy groups;

(ii) the δH_2O exhibited a very weak intensity, and then also the partner stretching modes, the protons not being involved in strong H-bonding, should exhibit an intensity of the same order of magnitude.[42] Hence, they contributed to a very minor extent to the νOH absorptions. It can be then concluded that the signals at 3736, 3717, 3688, 3672, 3659, and 3642 cm^{-1} present after outgassing at 773 K are essentially due to hydroxy groups. Furthermore, the multiplicity of components due to both linear (νOH > 3680 cm^{-1}) and bridged (νOH < 3680 cm^{-1}) OH indicates the presence of more than one local structure for each type of hydroxyl species.

The overall pattern obtained in the present case appeared quite similar to that found by Dzwigaj et al.[29] after dehydration at 693 K of another type of pure anatase commercial TiO_2, where, conversely, most of the signal was assigned to the presence of water. Unfortunately, an estimation of the amount of H_2O molecules is rather difficult, as the δH_2O spectral range was not reported.

Outgassing at T > 773 K resulted in a decrease in intensity of the pattern, indicating the removal of part of these hydroxy groups.

The resulting coordinative unsaturation of Ti^{4+} sites deprived of such ligands was then tested by IR spectroscopy of adsorbed CO. As reported in the Section 3.2.2, CO was adsorbed at beam temperature (ca. 323 K) to optimize the observation of the weak νCO components at frequencies ≥ 2190 cm^{-1}. Under such experimental conditions, CO was able to probe all α sites, but only a part of the β ones, termed by Hadjiivanov as β'.[40] The difference in the adsorption capacity of CO on β' and the other β sites (termed as β'') was proposed to have an induced character, i.e., the occurrence of a decrease in Lewis acidity of still unoccupied Ti^{4+} ions (the β'' sites) once CO was adsorbed on surface cations (the β' sites).[40]

Focusing on CO adsorbed at beam temperature, a progressive increase in intensity of the 2206 cm^{-1} band due to CO adsorbed on α sites occurred by increasing the preoutgassing temperature, as well as a slight broadening of the peak due to CO on the β' sites. This signal also exhibited some decrease in intensity for preoutgassing temperatures ≥ 823 K (Figure 3.7B). Therefore, the combination of spectral data in Figure 3.7A,B indicated that the νOH pattern in the 3750-3600 cm^{-1} range was due to -OH groups sitting on sites not located on extended, regular faces exposing penta-coordinated Ti^{4+} ions of the β type. Furthermore, the decrease in integrated intensity of only ca. 50% by increasing the outgassing temperature from 773 to 873 K indicated that these OH groups are bound quite strongly to the surface. The observed decrease in intensity of the νOH pattern was accompanied by some change in the relative intensity of the various components. To extract the pattern due to hydroxyl groups removed by raising the outgassing temperature (T_{outg}) from 773 to 823 K and then to 873 K, the difference between the spectra recorded after consecutive outgassing temperatures was calculated (Figure 3.7A′). The spectral profile due to OH removed by increasing T_{outg} at 823 K (curve “a-b”) appeared rather similar to the pattern observed after outgassing at 773 K (Figure 3.7A, a), indicating that the

removal of hydroxy groups occurred via a classical condensation between linear and bridged OH. Conversely, outgassing at 873 K seemed to remove OH groups responsible for the band at 3726 cm^{-1}, likely terminal OH groups, to a large extent. It is proposed that such groups could have originated through a dissociation mechanism similar to that proposed for H_2O on an (001) anatase face,[23,24] resulting in the breaking of the Ti-O bond. If this mechanism can occur for some type of Ti^{4+}-O^{2-} in coordinative defective positions, neighboring linear Ti-OH groups might be produced, which will condense, restoring the Ti-O bond, at a due temperature. A different possibility was proton migration, as proposed for the last stages of dehydroxylation of MgO.[44] Furthermore, minor components at lower frequency appeared quite broad and ill defined, suggesting the presence, in low amounts, of families of hydroxy groups, each constituted by OH oscillators located in slightly different local structures. This feature could be another consequence of the roughness of the borders of the TiO_2 particles observed, on a larger scale, by TEM.

The subtraction between spectra of CO adsorbed on TiO_2 outgassed at two subsequent steps was also carried out. In this case, the signal increased in intensity by increasing the preoutgassing temperature, and then, for each pair of selected spectra, the spectrum due to CO adsorbed on the sample outgassed at higher temperature was considered as minuend, and the other one as subtrahend. The results are reported in Figure 3.7B′ and show the νCO signals due to probe molecules adsorbed on Ti^{4+} ions deprived of -OH ligands by increasing the outgassing temperature from 773 to 823 K (curve “b-a”) and from 823 to 873 K (curve “c-b”). As expected, a component at 2006-2007 cm^{-1} was present (the largest signal by far in the case of the sample outgassed at 823 K, curve a), due to CO adsorbed on α cationic sites, but additional ones were also observed at 2200-2198 and 2193-2190 cm^{-1}. However, this last signal appeared partly superimposed on a negative band at 2184-2181 cm^{-1}, which may have affected its actual position. The negative part of the signal indicated the disappearance of some β' sites that could have resulted from inward relaxation or

from conversion in cationic centers with a higher degree of coordinative unsaturation by removal of an hydroxy group.

Other than from the difference spectra, evidence of the presence of more than one νCO component in the 2210-2185 cm^{-1} range was provided by the spectra collected over decreasing CO coverage (Figure 3.9).

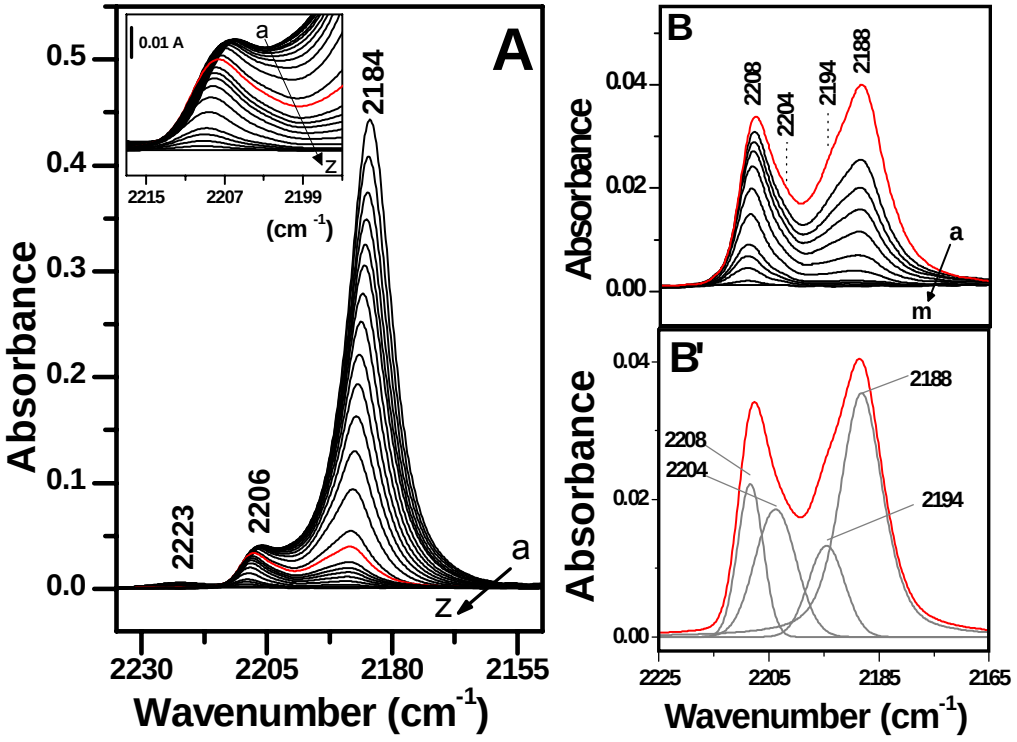

Figure 3.9. IR spectra of CO adsorbed at beam temperature on TiO_2 P25 outgassed at 873 K for 60 min. Section A: progressively decreasing coverages from (a) 150 mbar CO to (z) outgassing for 5 min at beam temperature. In red is the spectrum taken in the presence of 3 mbar of CO. Inset: zoomed view of the 2217-2195 cm^{-1} range. Section B: zoomed view of the spectra taken at progressively decreasing CO coverages from (a) 3 mbar of CO (red line) to (m) outgassing for 5 min at beam temperature. Section B′: components (solid gray lines) and simulated total profile (dashed gray line) resulting from the fitting of the spectrum taken in the presence of 3 mbar CO (red line, upshifted for the sake of clarity). (Reprinted with permission from Deiana et al.[35] Copyright 2010 American Chemical Society.)

The complete set of data is shown for TiO_2 preoutgassed at 873 K in Figure 3.9, whereas a comparison among selected spectra collected for TiO_2 preoutgassed at increasing temperatures is reported in Figure 3.10.

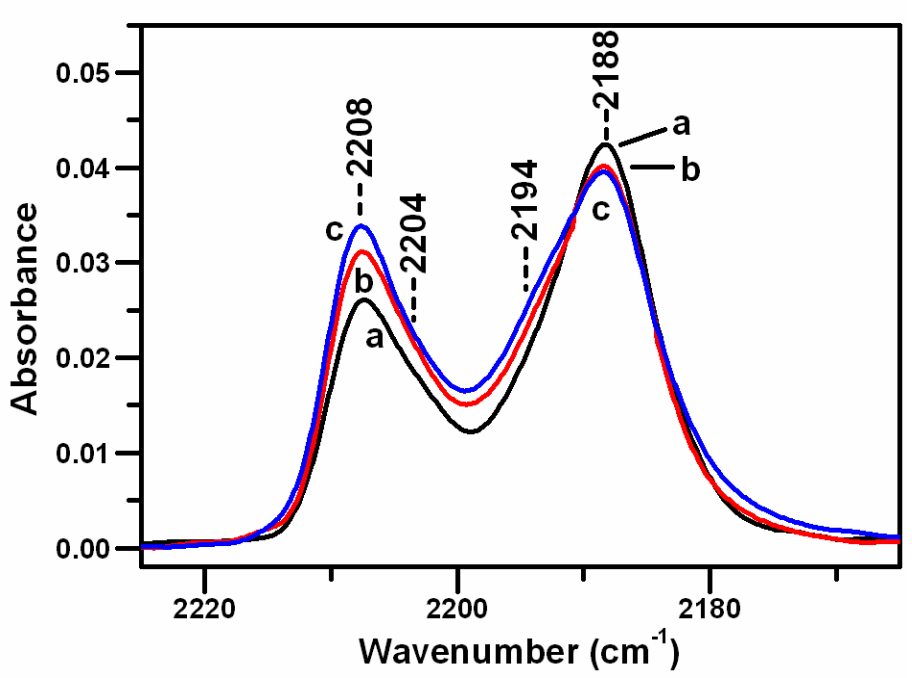

Figure 3.10. IR spectra of CO (P_{CO}= 3 mbar) adsorbed at beam temperature on TiO_2 P25 outgassed at: (a) 773, (b) 823 and (c) 873 K.

Focusing on Figure 3.9A, the progressive removal of CO produced a preferential decrease in intensity of the main band at 2184 cm^{-1} with respect to the components at higher frequencies, reflecting the weaker interaction of CO with β' sites than other surface cationic sites active toward CO adsorption at beam temperature. The main band also up-shifted from 2184 to 2188 cm^{-1} as a consequence of the decrease in adsorbate-adsorbate interactions. Such interactions (limited to the static type) also involved CO on α sites (Figure 3.9A, inset), as the related component slightly upshifted. This signal then started to decrease in intensity and moved to 2208 cm^{-1} as CO outgassing progressed.

In the case of CO adsorbed ad b.t. it is also possible to observe a band at ca. 2223 cm^{-1} that is due to the same component reported at 2212 cm^{-1} for CO at

100 K on TiO_2 P25 but at lower coverage and it will be discussed in detail in the next section 3.5.

Starting from an equilibrium pressure of 3 mbar of CO, other than the remaining part of the 2188 and 2208 cm^{-1} bands, two shoulders at ca. 2204 and 2194 cm^{-1} can be observed (Figure 3.9B). Indeed, a minimum of four components was necessary to fit the experimental spectra. As an example, the fitting of the spectrum collected in the presence of 3 mbar of CO is reported in Figure 3.9B′.

The component at 2194 cm^{-1} appeared quite close to the location indicated for the singletone of CO adsorbed on β sites[37,40] but was distinct from the signal at 2188 cm^{-1} that resulted from the evolution of the band due to such species. Furthermore, the 2194 cm^{-1} component was even less defined with respect to the 2188 cm^{-1} peak in the spectrum of CO adsorbed on TiO_2 outgassed at 773 K (Figure 3.10), indicating that these signals are due to CO on sites that retained hydroxy groups more strongly than the β sites. The entire collection of data presented here indicated that two other types of cationic centers, one with a Lewis acidity slightly lower than α sites, and the other with a Lewis acidity slightly higher than β sites, are present on the surface of the TiO_2 P25. Moreover, the differences in the profiles of the differential spectra (Figure 3.7B) and the broadness of the 2204 and 2194 cm^{-1} components of the fit of the direct spectra (Figure 3.7B′) suggested the presence of some structural heterogeneity among such cationic sites.

Assuming that the molar extinction coefficient of adsorbed CO species is independent of frequency changes in the 2220-2180 cm^{-1} interval,[45,46] the ratio among integrated intensities indicated that the amount of these cationic sites is of the same order as the α sites.

In conclusion, the data obtained for outgassing temperatures ≤ 773 K put in evidence that the overwhelming majority of the surface of TiO_2 P25 with exposed β cationic sites adsorbed H_2O molecules undissociatively. Moreover, confirmative evidence of the presence of hydroxy groups on γ sites on (001) faces was

obtained. As for the main target of the investigation, the νOH pattern related to hydroxy species on surface sites under low coordination conditions was recognized. The number of observed components well accounted for the heterogeneity seen for the defective surface terminations suggested by the TEM images. Notably, evidence for the presence of two types of surface Ti^{4+} ions with Lewis acid strength intermediate between the already known α and β cationic sites was also obtained.

3.5. Translational modes of CO adsorbed on TiO_2

In Chapter 3 it was put in evidence the presence of a band of adsorbed CO located at 2212 cm^{-1} and at 2223 cm^{-1} when CO is adsorbed at 100 K and at beam temperature, respectively. For the sake of clarity, the CO adsorption isotherms are shown again in the following Figures 3.11 and 3.12.

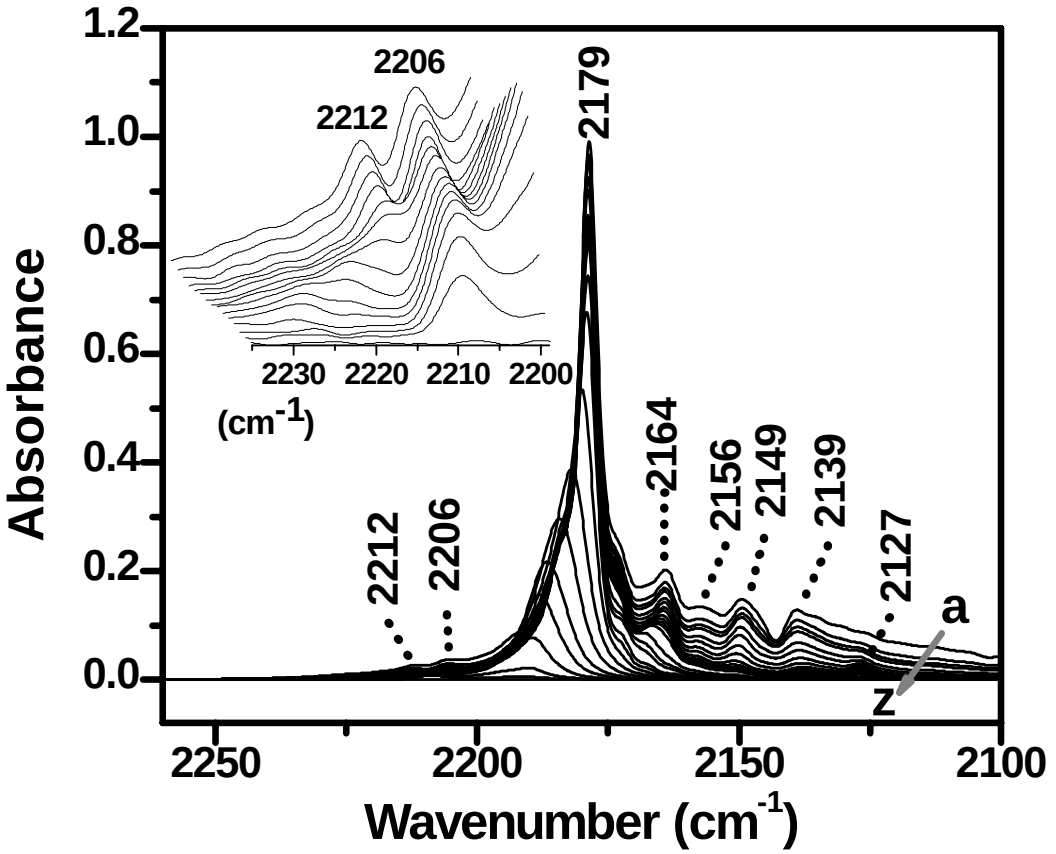

Figure 3.11. IR spectra of CO adsorbed at ca. 100 K on TiO_2 P25 outgassed at 873 K, from 40 mbar of CO (a) to 10 minutes outgassing at ca. 100 K (z). Inset: zoomed view of 2235-2200 cm^{-1} range.

Clear evidence of the connection of the weak, highly reversible feature with the band due to the main peak related to the internal mode of CO adsorbed on β sites

was provided by the measurements carried out at 100 K, where the CO coverage on such faces is strongly increased, as well as on other minor surface terminations and on few hydroxy groups that resisted outgassing at 873 K (Figure 3.11).

In these conditions, components at ν > 2000 cm^{-1} seem almost negligible with respect to the others (Figure 3.11).

However, by a proper zooming (Figure 3.11, inset) it is possible to clearly observe that the band at 2206 cm^{-1} of CO on α sites in now accompanied by a component of similar intensity, with maximum initially located at 2212 cm^{-1}. Thus, this component exhibited a significant increase in intensity by increasing the CO coverage passing from beam temperature down to 100 K, as the band due to CO on β sites did. The component at higher frequency than the band due to CO on α sites, appeared more sensitive to CO desorption than the band at 2206 cm^{-1}, that then remained the only one present in such range. Furthermore, by decreasing the CO coverage the 2212 cm^{-1} band exhibited progressive (but not regular) upshift and broadening (Figure 3.11, inset), with a trend similar to the main component of CO on β sites, initially located at 2179 cm^{-1}, due to the progressive fading away of adsorbate-adsorbate interactions (Figure 3.11, main frame).

The same component can be observed also at lower coverages, when CO is adsorbed at b.t. (Figure 3.12).

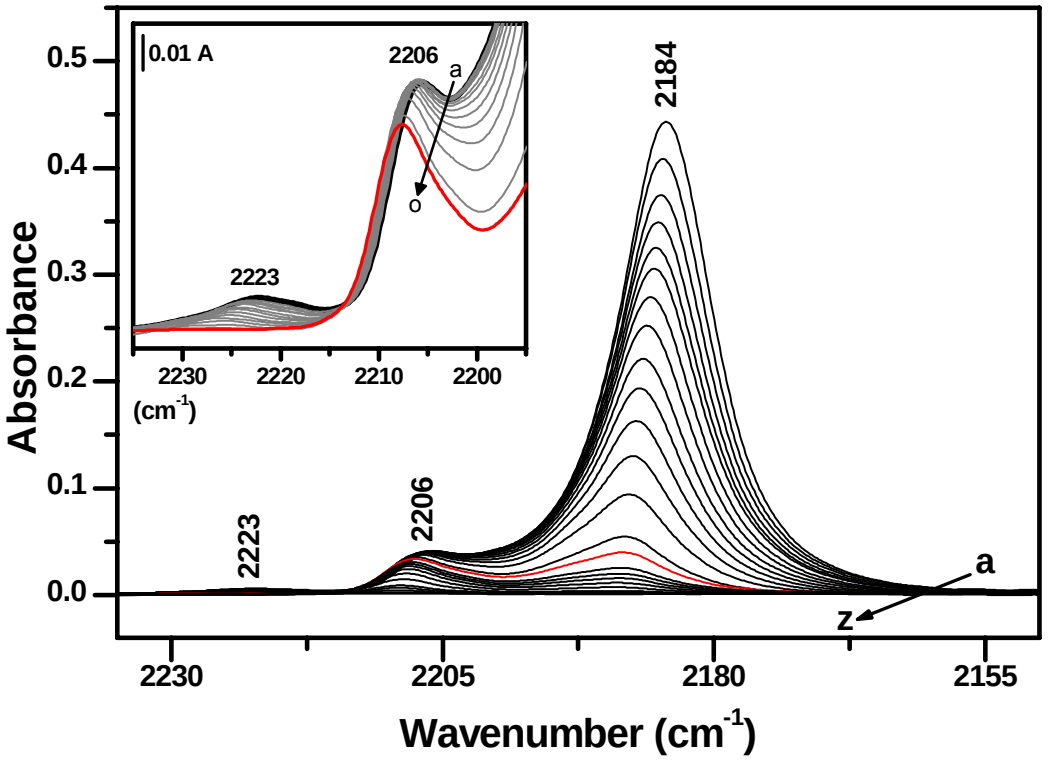

Figure 3.12. IR spectra of CO adsorbed at beam temperature on TiO_2 P25 outgassed at 873 K from (a) 150 mbar of CO to (z) 5 minutes outgassing at b.t. Inset: zoomed view of 2235-2195 cm^{-1} range from 150 mbar of CO (a) to 1 mbar (o). In red it is shown the spectrum at 1 mbar of CO.

As can be observed in the inset of Figure 3.12, the band at 2223 cm^{-1} is more reversible that the one of α sites, meaning that the sites responsible for that signal of adsorbed CO, have a lower Lewis acidity.

As the presence of the component at 2206 cm^{-1} interfered in some extent with the observation of that at higher frequency, CO was dosed also on a TiO_2 P25 sample outgassed at 673 K, where most part of α sites are still occupied by hydroxy groups, and then inactive toward the absorption of CO. For the sake of effectiveness, in Figure 3.13 only the evolution of the 2212 cm^{-1} (section A) and 2179 cm^{-1} (section B) bands are depicted, by properly adjusting the scale of the

two sections in order to have apparent similar intensity for the two components. (The series of full spectra is reported in Figure 3.14).

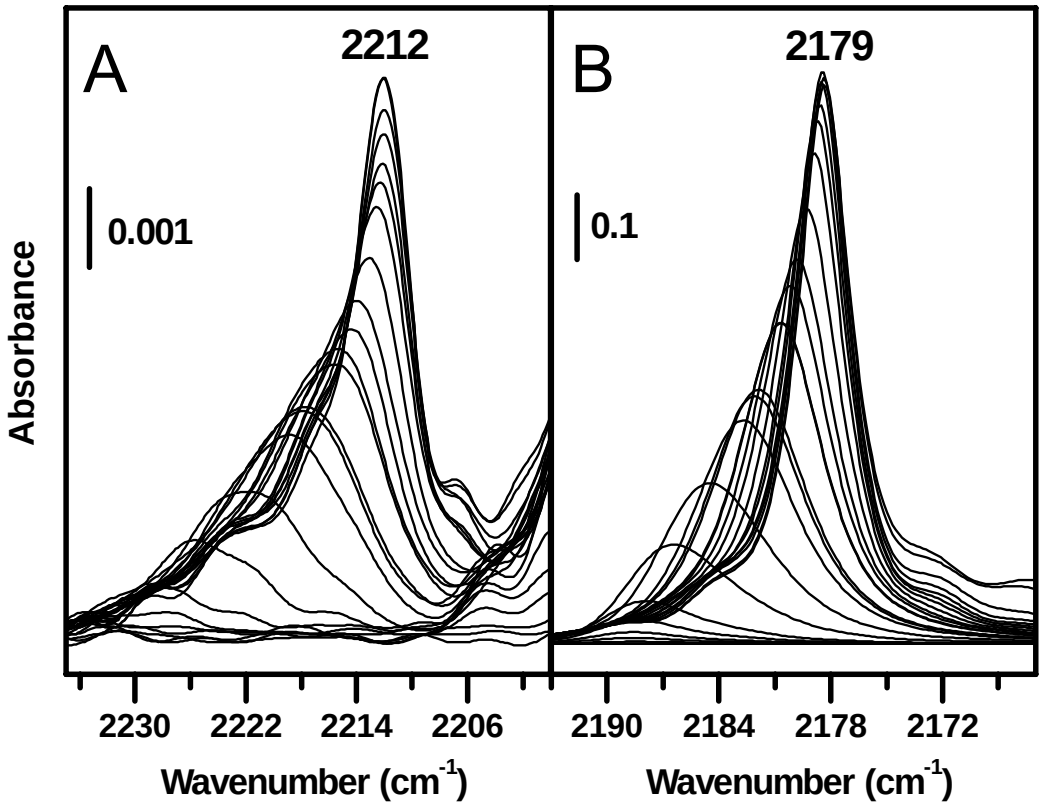

Figure 3.13. IR spectra of CO adsorbed at ca. 100 K on TiO_2 P25 outgassed at 673 K. Panel A: zoomed view of 2235-2200 cm^{-1} range; Panel B: zoomed view of 2193-2167 cm^{-1} range.

The similarity of the behavior of the two bands is unequivocal, witnessing for the connection of the 2212 cm^{-1} one with the main peak at 2179 cm^{-1} (initial positions).

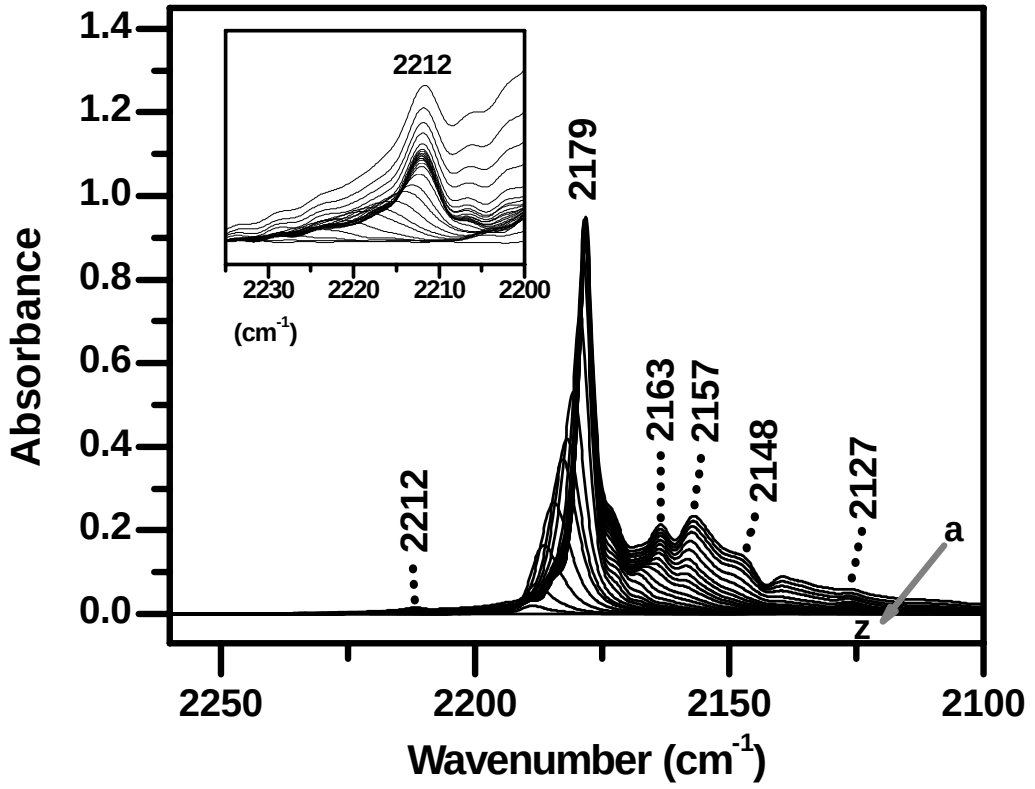

Figure 3.14. IR spectra of CO adsorbed at ca. 100 K on TiO_2 P25 outgassed at 673 K, from 40 mbar of CO (a) to 10 minutes outgassing at ca. 100 K (z).

A further, and last, proof of this connection is the spectrum in Figure 3.15, due to CO remaining adsorbed on a sample pre-outgassed at 673 K after (i) admission of 100 mbar CO at 263 K, (ii) cooling down to 60 K, and (iii) outgassing at such temperature until invariance of the spectra until equilibrium; (iv) increase the temperature to 77 K, and (v) outgassing at such temperature until invariance of the spectra until equilibrium. The full series of spectra collected during steps (i) to (iii) is reported in Figure 3.15B.

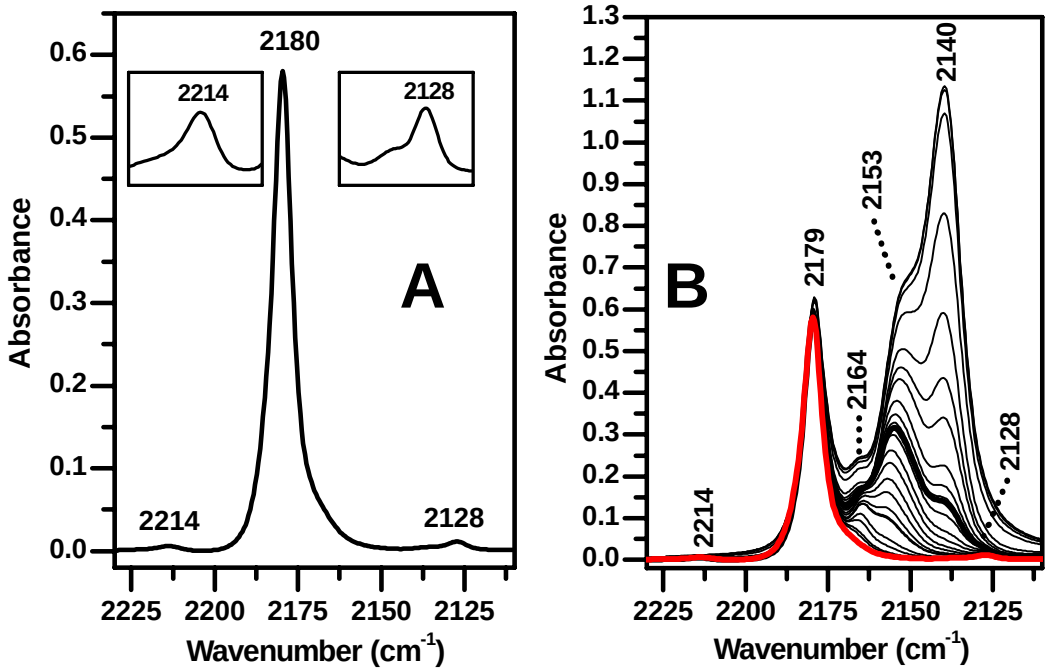

Figure 3.15. Panel A: IR spectrum of CO irreversibly adsorbed at ca. 77 K on TiO_2 P25 outgassed at 673 K. Panel B: IR spectra of CO adsorbed at ca. 60 K and 77 K on TiO_2 P25 outgassed at 673 K. The thick black line represents the spectrum of irreversible fraction of CO adsorbed at ca. 60 K; in red the CO irreversibly adsorbed at ca. 77 K (spectrum reported in Panel A).

Focusing on the spectral pattern in Figure 3.15, it can be observed that it is simply composed by a main νCO band at 2180 cm^{-1}, the partner weak signal at 2128 cm^{-1} related to ^{13}CO present in natural abundance (ca. 1%) , and the similarly weak component at 2214 cm^{-1}.

Summarizing, the collection of data presented make allowance to establish that this last feature, present in the spectra of CO adsorbed on TiO_2, should results from the combination of the main band due to the internal stretching of CO in interaction with Ti(IV) exposed on β sites exposed at (010) or (101) faces[40] and a low frequency mode, that, on the basis of the difference in position between the two signals, should have a frequency ranging from 2212-2179= 33 cm^{-1} at high CO coverage and 2188-2230= 42 cm^{-1} at low CO coverage. Such values are too

low for a surface-CO stretching vibration. For instance, CO experiencing a weaker interaction (on the basis of the νCO stretching) with surface sites, like alkali cations in zeolites[47] or sodium cations[48] at the surface of NaCl exhibited a surface-C stretching frequency ranging from 88 to 141 cm^{-1} and at ca. 90 cm^{-1}, respectively. As for librational modes, they were estimated to occur at ca. 140 cm^{-1} for CO on NaCl film.[48] Conversely, still for CO on NaCl, thermodynamic measurements provided an estimate of 30 cm^{-1} for the frustrated translation frequency,[48] and the evaluation of the Boltzmann factor associated with the temperature dependence on the position and shape of the νCO band made allowance to determine that such mode should have a frequency of 40 cm^{-1}. [49] Thus, it seems reasonable to assign the weak band at 2212 – 2130 cm^{-1} to a frustrated translational mode of CO adsorbed on the β sites of surface of TiO_2.

Conclusions

The collection of results obtained by the combined analysis of vibrational frequencies of intrinsic (i.e., hydroxy groups) and extrinsic (i.e., CO) probes allowed the recognition and the assignment of signals related to TiO_2 surface sites located in coordinatively defective positions. Additionally, the IR spectroscopy of adsorbed CO resulted in the first observation, for an oxide, of a combination mode involving internal stretching and frustrated translational modes of CO. These results represent a further extension of the knowledge of the rich, highly informative spectroscopy of CO adsorbed on titania nanopowders.

Moreover, these results could then represent a database that should significantly help in selecting/refining theoretical models in the elucidation of the local structures of sites.

References

(1) Linsebigler, A. L.; Lu, G. Q.; Yates, J. T. *Chemical Reviews* **1995**, *95*, 735.

(2) Serpone, N.; Pelizzetti, E.; Eds. *Photocatalysis: Fundamental and Applications*; Wiley-Interscience: New York, NY, U.S., 1989.

(3) Szczepankiewicz, S. H.; Colussi, A. J.; Hoffmann, M. R. *Journal of Physical Chemistry B* **2000**, *104*, 9842.

(4) Palmisano, L.; Schiavello, M.; Sclafani, A.; Martra, G.; Borello, E.; Coluccia, S. *Applied Catalysis B-Environmental* **1994**, *3*, 117.

(5) Du, P.; Bueno-López, A.; Verbaas, M.; Almeida, A. R.; Makkee, M.; Moulijn, J. A.; Mul, G. *Journal of Catalysis* **2008**, *260*, 75.

(6) Maurino, V.; Minero, C.; Mariella, G.; Pelizzetti, E. *Chemical Communications* **2005**, 2627.

(7) Minella, M.; Faga, M. G.; Maurino, V.; Minero, C.; Pelizzetti, E.; Coluccia, S.; Martra, G. *Langmuir* **2010**, *26*, 2521.

(8) Kondo, J. N.; Yamashita, T.; Nakajima, K.; Lu, D. L.; Hara, M.; Domen, K. *Journal of Materials Chemistry* **2005**, *15*, 2035.

(9) Buonsanti, R.; Grillo, V.; Carlino, E.; Giannini, C.; Curri, M. L.; Innocenti, C.; Sangregorio, C.; Achterhold, K.; Parak, F. G.; Agostiano, A.; Cozzoli, P. D. *Journal of the American Chemical Society* **2006**, *128*, 16953.

(10) Kitano, M.; Matsuoka, M.; Ueshima, M.; Anpo, M. *Applied Catalysis A: General* **2007**, *325*, 1.

(11) Centi, G.; Passalacqua, R.; Perathoner, S.; Su, D. S.; Weinberg, G.; Schlögl, R. *Physical Chemistry Chemical Physics* **2007**, *9*, 4930.

(12) Ryu, J.; Choi, W. *Environmental Science & Technology* **2008**, *42*, 294.

(13) Busca, G. The Use of Infrared Spectroscopic Methods in the Field of Heterogeneous Catalysis by Metal Oxides In *Metal Oxide Catalysis*; Jackson, D., Hargreaves, J. S. J., Eds.; Wiley-VCH: Weinhein, Germany, 2009; Vol. 1; pp 95–175.

(14) Primet, M; Pichat P.; Mathieu M. V. *The Journal of Physical Chemistry* **1971**, *75*, 1216.

(15) Tsyganenko, A. A.; Filimonov, V. N. *Journal of Molecular Structure* **1973**, *19*, 579.

(16) Hadjiivanov, K. I.; Klissurski, D. G. *Chemical Society Reviews* **1996**, *25*, 61.

(17) Morterra, C. *Journal of the Chemical Society, Faraday Transaction 1* **1988**, *84*, 1617.

(18) Erdem, B.; Hunsicker, R. A.; Simmons, G. W.; Sudol, E. D.; Dimonie, V. L.; El-Aasser, M. S. *Langmuir* **2001**, *17*, 2664.

(19) Morterra, C.; Chiorino, A.; Boccuzzi, F.; Fisicaro, E. *Z. Phys. Chem. Neue Folge* **1981**, *124*, 211–222.

(20) Busca, G.; Saussey, H.; Saur, O.; Lavalley, J. C.; Lorenzelli, V. *Appl. Catal.* **1985**, *14*, 245.

(21) Finnie, K. S.; Cassidy, D. J.; Bartlett, J. R.; Woolfrey, J. L. *Langmuir* **2001**, *17*, 816.

(22) Hadjiivanov, K. I.; Davydov, A. A.; Klissurski, D. G. *Kinetic Catalysis* **1988**, *29*, 161.

(23) Arrouvel, C.; Digne, M.; Breysse, M.; Toulhoat, H.; Raybaud, P. *Journal of Catalysis* **2004**, *222*, 152.

(24) Vittadini, A.; Selloni, A.; Rotzinger, F. P.; Gratzel, M. *Physical Review Letters* **1998**, *81*, 2954.

(25) Henderson, M. A. *Langmuir* **1996**, *12*, 5093.

(26) Gong, X. Q.; Selloni, A.; Batzill, M.; Diebold, U. *Nature Materials* **2006**, *5*, 665.
(27) Gong, X. Q.; Selloni, A. *Journal of Catalysis* **2007**, *249*, 134.
(28) Martra, G. *Applied Catalysis A-General* **2000**, *200*, 275.
(29) Dzwigaj, S.; Arrouvel, C.; Breysse, M.; Geantet, C.; Inoue, S.; Toulhoat, H.; Raybaud, P. *Journal of Catalysis* **2005**, *236*, 245.
(30) Henrich, V. E.; Cox, P. A. *The Surface Science of Metal Oxides*, Cambridge University Press: Cambridge, U.K. ed., 1994.
(31) Freund, H. J. *Faraday Discussions* **1999**, *114*, 1.
(32) Cerrato, G.; Marchese, L.; Morterra, C. *Applied Surface Science* **1993**, *70-1*, 200.
(33) Brunauer, S.; Emmett, P. H.; Teller, E. J. *J. Amer. Ceram. Soc.* **1938**, *60*, 309–319.
(34) Ohno, T.; Sarukawa, K.; Tokieda, K.; Matsumura, M. *Journal of Catalysis* **2001**, *203*, 82.
(35) Deiana, C.; Fois, E.; Coluccia, S.; Martra, G. *Journal of Physical Chemistry C* **2010**, *114*, 21531.
(36) Oliver, P. M.; Watson, G. W.; Kelsey, E. T.; Parker, S. C. *Journal of Materials Chemistry* **1997**, *7*, 563.
(37) Spoto, G.; Morterra, C.; Marchese, L.; Orio, L.; Zecchina, A. *Vacuum* **1990**, *41*, 37.
(38) Platero, E. E.; Scarano, D.; Zecchina, A.; Meneghini, G.; DeFranceschi, R. *Surface Science* **1996**, *350*, 113.
(39) Hadjiivanov, K. I.; Vayssilov, G. N. *Advances in Catalysis, Vol 47* **2002**, *47*, 307.
(40) Hadjiivanov, K.; Lamotte, J.; Lavalley, J. C. *Langmuir* **1997**, *13*, 3374.
(41) Marchese, L.; Boccuti, M. R.; Coluccia, S.; Lavagnino, S.; Zecchina, A.; Bonneviot, L.; Che, M. The Pt/Al_2O_3 System: Infrared Studies. In *Structure and Reactivity of Surfaces*; Morterra, C., Zecchina, A., Costa,, G., Eds.; Elsevier: Amsterdam, The Netherlands, 1989; pp 653.
(42) Eisenberg, D.; Kauzmann, W. *The structure and properties of water*; Oxford University Press: London, U.K., 1969.
(43) Barnard, A. S.; Zapol, P.; Curtiss, L. A. *Surface Science* **2005**, *582*, 173.
(44) Coluccia, S.; Lavagnino, S.; Marchese, L. *Mater. Chem. Phys.* **1988**, *18*, 445.
(45) Platero, E. E.; Scarano, D.; Spoto, G.; Zecchina, A. *Faraday Discuss. Chem. Soc.* **1985**, *80*, 183.
(46) Hush, N. S.; Williams, M. L. *J. Mol. Spectrosc.* **1974**, *50*, 349.
(47) Otero Areán, C.; Palomino, G. T.; Zecchina, A.; Spoto, G.; Bordiga, S.; Roy, P. *Physical Chemistry Chemical Physics* **1999**, *1*, 4139.
(48) Richardson, H. H.; Baumann, C.; Ewing, G. E. *Surface Science* **1987**, *185*, 15.
(49) Noda, C.; Richardson, H. H.; Ewing, G. E. *Journal of Chemical Physics* **1990**, *92*, 2099.

Chapter 4

Elucidation of the correspondence between the local structure of surface cations of TiO_2 and IR features of adsorbed CO: study of titania nanoparticles with defined surfaces

Many efforts have been done to study the surface properties of TiO_2, [1-4] but the employ of nanoparticles represents a source of complexity in this kind of investigation, since the roughness of nanocrystals borders causes the presence of a wide heterogeneity of surface sites with different local structures, as shown in the previous chapter for the IR study of CO adsorbed on TiO_2 Degussa P25.

Nevertheless, this vibrational characterization could represent a sort of database in the study of sites exposed at the TiO_2 surface: indeed, the investigation of simplified/model nanoparticles would result in an unambiguous association of vibrational signals to CO in interaction with cationic centers sitting in previously defined local structure of sites. For instance, if successful, such an approach should allow to distinguish between penta-coordinated Ti^{4+} centers exposed at the surface of (101) or (100) facets that, at present, are both comprised in the "β sites" family (see previous chapter).

Furthermore, the reproduction by theoretical calculations of the experimental data dealing with unambiguously recognized surfaces (typically, by HRTEM), would result in a validation of models of regular surfaces. Such surfaces could then be used as a starting point for the modeling of sites resulting from their intersections, i.e. edges or corners. The calculated frequencies of adsorbed CO could be compared with those present in the experimental spectra of CO on TiO_2 nanoparticles exposing coordinatively defective sites, allowing the recognition of the defective termination actually present.

Furthermore, once attained the correspondence between experimental and calculated spectra of adsorbed CO, the models of the surface sites, including the defective ones, could be employed for the study of the interaction with water and the calculation of the related νOH (and δH_2O, in the case of molecular adsorption) frequencies. As in the case of CO, the calculated values will then be used for the recognition in the experimental spectra of the components, monitoring the presence of specific types of hydroxylated surface sites.

Such an approach has been adopted for the part of this research devoted to the investigation of TiO_2 nanoparticles with regular shape, that became available in the last period of this Ph.D. work. For the sake of comparison with the experimental data obtained for TiO_2 P25 and the modeling of the TiO_2-CO interaction, priority was given to the analysis of HRTEM images and of IR spectra of adsorbed CO. Conversely, only preliminary data dealing with surface hydration and hydroxylation have been obtained.

SECTION A. Experimental studies of TiO_2 nanocrystals with defined shape

The interest in synthesizing TiO_2 nanoparticles with controlled morphology, rises from the differences in physico-chemical properties and reactivity exhibited from the different crystal surfaces.[5,6] In this respect, nanoparticles with truncated bipyramid shape (Figure 4.1) have been considered in this thesis.

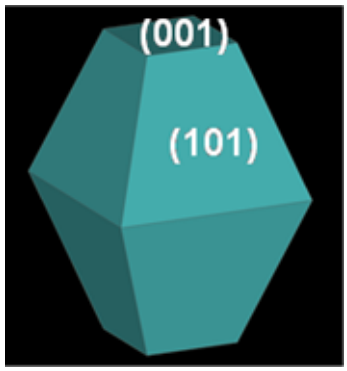

Figure 4.1. 3D model of TiO_2-HT nanocrystals.

Many works devoted to different preparation methods of TiO_2 anatase nanoparticles with this shape or exposing preferentially (001) surfaces are present in literature.[7-14] The aim of these studies was to find a synthetic route making allowance to prepare not only nanoparticles with controlled shape and size, but also with a defined ratio between the exposed surfaces (101) and (001): (001) facets have higher energy and, therefore, are considered to be more reactive, while (101) surfaces are thermodynamically stable.[1,15]

Despite the increasing interest towards such TiO_2 nanomaterials, a complete characterization of surface sites is still missing. In the present case anatase nanocrystals with controlled shape and exposing defined surfaces have been taken in consideration as model systems, in order to associate the vibrational signals of adsorbed CO to defined facets.

4.1. Material and methods

The TiO_2 nanocrystals with truncated bipyramid shape have been prepared by the group of Prof. Minero of University of Torino. The synthetic methodology is a hydrothermal preparation and it has been developed starting from the works of Sugimoto et al.[16-19] Because of the hydrothermal preparation method, this titanium dioxide will be hereafter indicated as TiO_2-HT.

The material exhibited as received a SSA_{BET} of 43 m^2/g, that decreased to 37 m^2/g after treatment at 873 K (see below). The crystalline form was anatase, that remained unaffected by the thermal treatment.

In order to be studied by IR spectroscopy of adsorbed CO, the material underwent to same treatment (in the IR cell) reported in Chapter 3, section 3.2, for TiO_2 P25 Degussa. Furthermore, TiO_2 particles were observed by HR-TEM both as received and after the thermal treatment.

Preliminary hydrogen peroxide photodegradation tests were carried out on 5 ml of aqueous suspension containing the desired amount of the photocatalyst powder (0.5 g dm^{-3}) and 1 mM hydrogen peroxide. The irradiation was made by fluorescent lamps characterized by an emission band centered at 360 nm. The H_2O_2 concentration as a function of the irradiation time was monitored spectrophotometrically by the heptamolibdate catalyzed iodide oxidation method (λ = 350 nm).[20]

4.2. Morphological features and surface planes

The shape and size of TiO_2-HT nanocrystals have been characterized by HR-TEM. In Figure 4.2, a TEM image representative of their morphology is reported.

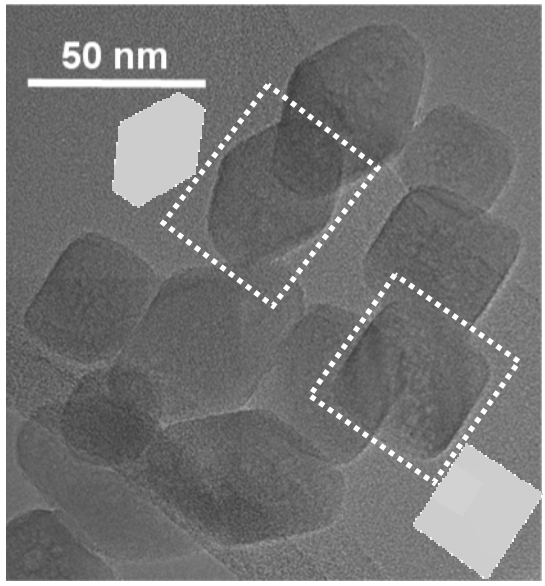

Figure 4.2. TEM image of TiO_2-HT sample (original magnification x 120 k).

Essentially 2D images with rhombic or square shape are present.

However, such different shape cannot correspond to an heterogeneity of actual 3D shapes of TiO_2 nanoparticles, but more simply to the “projection” on the image plane of nanoparticles with the same 3D shape and differently oriented along the electron beam. For instance, rhombic like shape are straightforwardly due to truncated bipyramids (Figure 4.3).

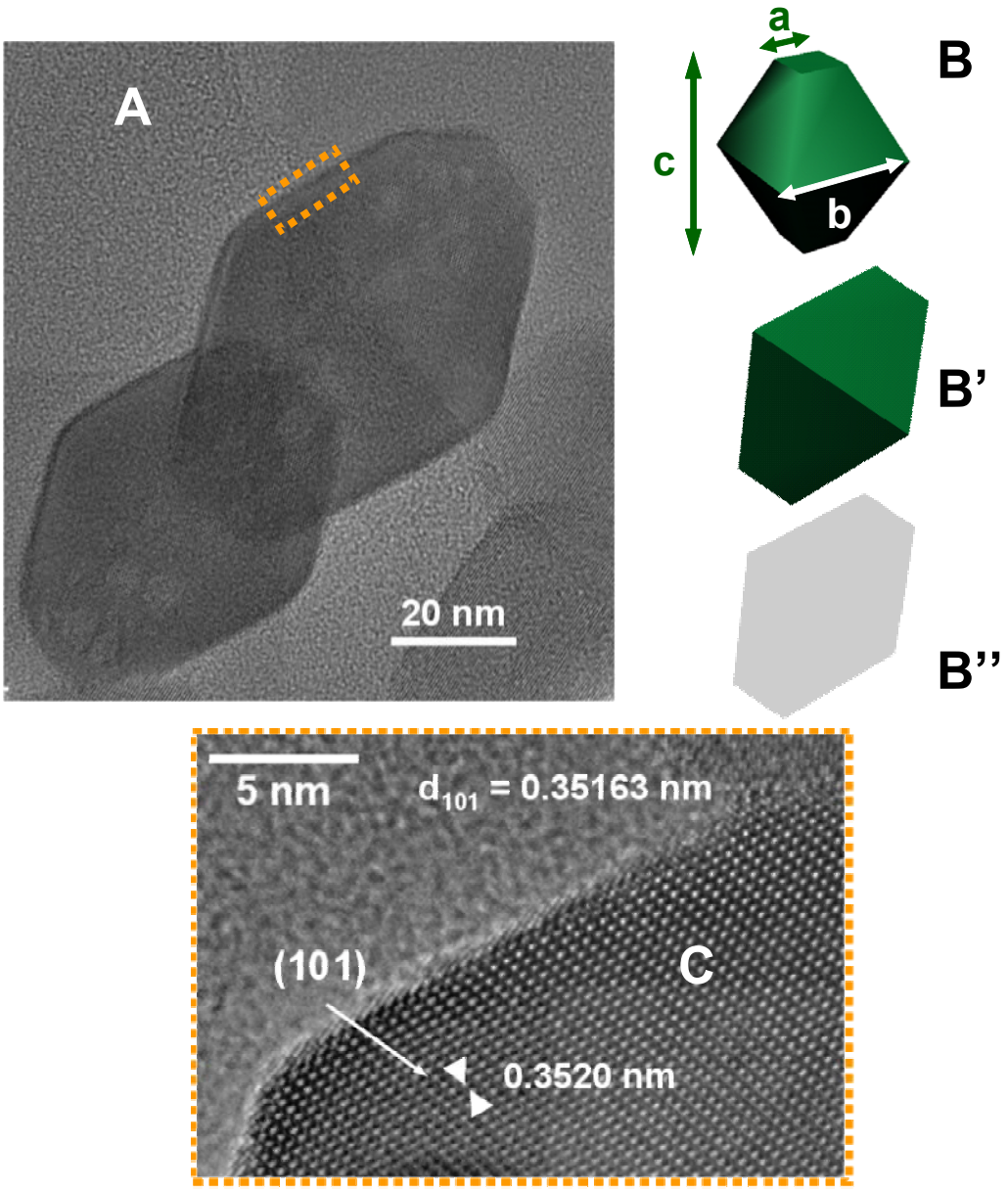

Figure 4.3. TEM image (original magnification x 300 k) of TiO_2-HT (A) and related models of nanoparticles: (B) 3D model; (B') 2D projection, with a different contrast for the two (101) facets exposed to the line sight; (B'') the same 2D projection, but with the same contrast (grayscale) of the two (101) facets; (C) zoomed view of (A) (original magnification x 800 k). d_{hkl} reference value from JCPDS.[21]

The origin of this projection can be derived from the models reported in Figure 4.3B,B',B'', where it can be noticed that the 2D shape is the result of the orientation of nanocrystals along the "c" axis, almost perpendicularly to the electron beam.

At high magnification (panel C), lattice fringes due to phase contrast appeared, running parallel to one of the main borders. Their spacing, 0.3520 nm, corresponds to the d_{101} distance for TiO_2 anatase[21], confirming that the more extended facets that enclose the TiO_2-HT particles belong to the {101} family.

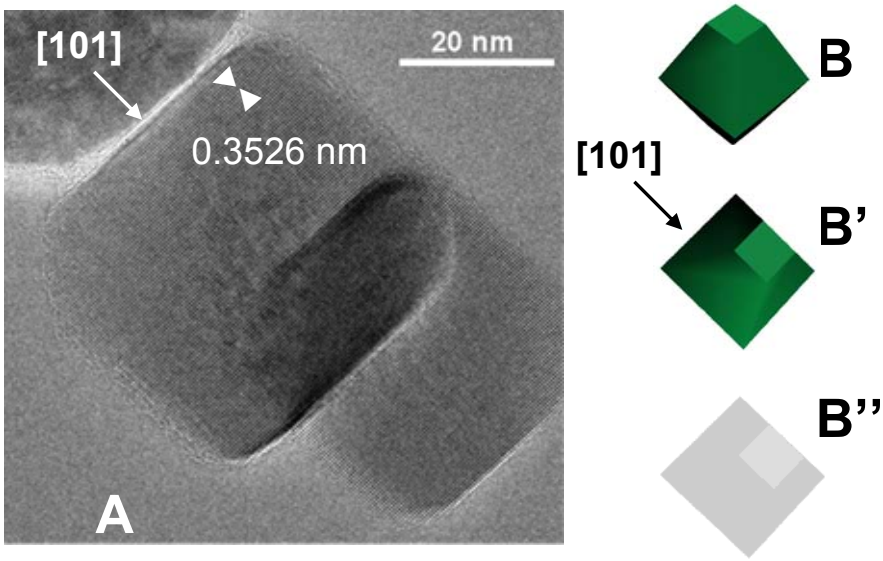

Figure 4.4. (A) TEM image of TiO_2-HT sample (original magnification x 300 k); (B) 3D model; (B') 2D projection; (B'') the same 2D projection, but in grayscale.

As for the square-like shapes, it was observed that the length of their sides appeared essentially equivalent to the minor axis of the rhombic-like shapes (labeled as "b" in Figure 4.3B).

Insights on the origin of such shapes were provided by HR-TEM images exhibiting lattice fringes (Figure 4.4A), that, on the basis of the measured spacing, appeared again to be due to (101) planes, running parallel to two opposite borders of the particle image. Hence, by using a 3D model (Figure 4.4B,B',B''), it is possible to appreciate that the square-like shape can be actually produced by a truncated

bipyramid particle with (101) facets parallel to the line-of-sight (corresponding to the direction of the impinging electron beam).

4.3. IR spectra of TiO_2-HT

Another feature showed by the TEM images, is the presence of some cavities inside the nanoparticles.

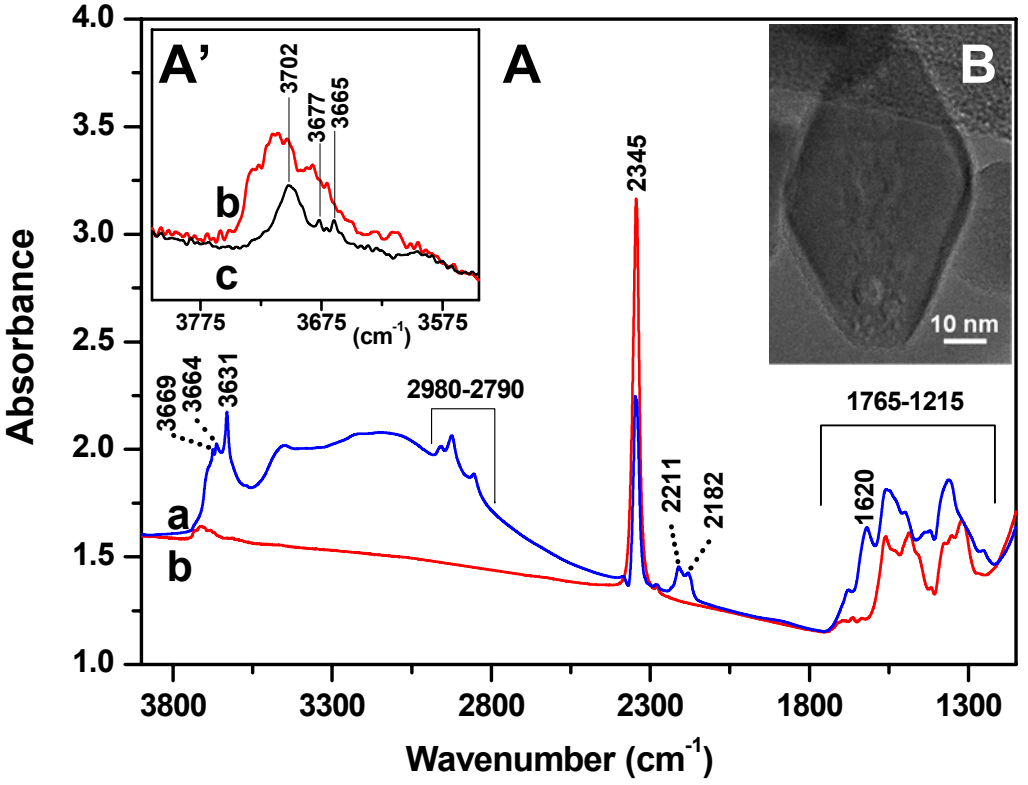

Figure 4.5. Panel A: IR spectra of TiO_2-HT (a) as received, (b) after treatment at 873 K. Inset A': zoomed view of the 3815-3545 cm^{-1} range (b) after treatment at 873 K, (c) after H/D isotopic exchange with D_2O. Panel B: TEM image of TiO_2-HT (original magnification x 200 k).

In Figure 4.5A, curve a, the spectrum of the as received material outgassed for 30 minutes at room temperature is reported. As in the case of TiO_2 P25, in the

region around 3600 cm^{-1} some bands due to some vibrationally free νOH are present, while the broad band in the 3600-2600 cm^{-1} range is assigned to νOH interacting through H-bond.[2,3,22] The signals around 2980-2790 cm^{-1} are assigned to ν(CH) of hydrocarbons adsorbed on the surface.

At lower frequency, the spectrum exhibits at 2345 cm^{-1}, an intense peak due to CO_2 [3,23] and two signals at 2211 and 2182 cm^{-1}, assigned to cyanide groups adsorbed on the surface,[24] likely deriving from dehydrogenation of the amino precursor used in the preparation of the material. Finally a complex pattern is present in the 1765-1215 cm^{-1} region: the δH_2O mode is responsible for the band at 1620 cm^{-1}, while the other signals are due to residual carboxylates/carbonates groups resulting from the calcination of organic moieties of the Ti compound used for the synthesis. The material was then activated at 873 K, and its IR spectrum is shown as curve b. Only a small fraction of the signal due to hydroxy groups is still present and the δH_2O at 1620 cm^{-1} is not longer observed, this latter feature indicating the complete removal of molecularly adsorbed water. Also the signals at 2211 and 2182 cm^{-1} disappeared, monitoring the decomposition of cyanide groups initially present. Conversely, the peak due linearly adsorbed CO_2 (2345 cm^{-1}) and the complex pattern at 1765-1215 cm^{-1} due to carboxylates/carbonates are still present, indicating that all these species are entrapped in the material, likely in the voids observed in TEM images (Figure 4.5 inset B).

Finally, in the inset A' in Figure 4.5, the IR spectra in the νOH region of TiO_2-HT after activation at 873 K (red, curve b), its evolution after contact and subsequent outgassing of D_2O (black, curve c) are reported. Noticeably, some signals at 3702, 3677 and 3665 cm^{-1} resisted isotopic exchange, supporting that some hydroxy groups should be present at the inner surface of the voids in the bulk of nanoparticles.

4.4. Surface structure of TiO_2-HT nanoparticles and comparison with TiO_2 P25

4.4.1. Surface hydration and hydroxylation

The surface structure of TiO_2-HT nanoparticles has been investigated with infrared spectroscopy and the vibrational spectra have been compared with those collected for TiO_2 P25.

Preliminary results have been obtained for the study of surface hydration and hydroxylation and are reported in Figure 4.6.

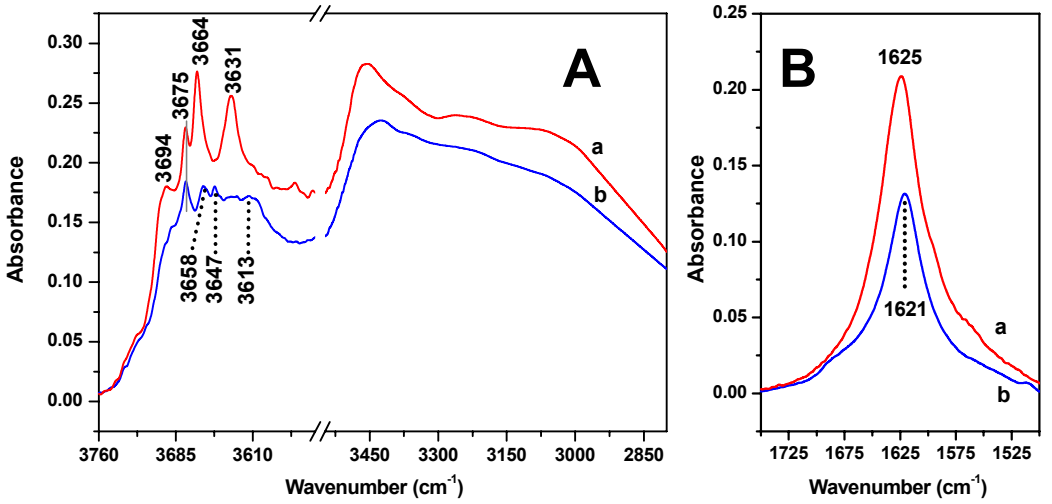

Figure 4.6. IR spectra of TiO_2-HT (a) and TiO_2 P25 (b), normalized for the "optical thickness" of the pellets and SSA_{BET}, in the (A) νOH and (B) δH_2O range. On the *X* axis, the scale has been changed at 3549 cm^{-1}, to zoom the region at higher frequency; the gap on the axis is just of 1 cm^{-1}.

In Figure 4.6 the IR spectra of TiO_2-HT (a) and TiO_2 P25 (b) are reported. The data have been acquired after (i) pre-outgassing at 873 K, (ii) subsequent rehydration with water vapor pressure, (iii) final outgassing at room temperature for ca. 30 minutes. After normalization of the data for the "optical thickness" of the pellets and SSA_{BET}, it can be noticed that the hydration extent is higher for

TiO_2-HT than for TiO_2-P25. An interesting information on the hydration condition can be obtained from the region of H_2O bending mode around 1620 cm^{-1} and reported in panel B. The calculation of the area of the δH_2O peak of the two materials provided information on the different amount of water molecularly adsorbed on the surface: in particular, the area of the peak is 40% higher in case of TiO_2-HT than for TiO_2 P25, making allowance to suggest that (101) surfaces, where water does not adsorb dissociatively,[22] are more extended and regular in case of TiO_2-HT.

From the difference in intensity observed in panel A, it can be deduced that relative amount of hydroxy groups responsible for this complex vibrational pattern, is different in the two materials: the area of the bands related to hydroxy group increases only of 7% for TiO_2-HT. It must be taken into account that the OH groups deriving from the dissociation of water on the surface of titania, and the O-H stretching of molecular water contribute to the signal at 3800-2800 cm^{-1}, while only the water molecularly adsorbed gives rise to the component at 1620 cm^{-1} due to the bending mode of H_2O. Therefore, it can be deduced that the amount of water molecularly adsorbed is higher for TiO_2-HT, but the increase in intensity in the region of νOH is lower, because is combined with a decrease in the amount of hydroxy groups deriving from H_2O dissociation. Therefore, it seems that the sites exposed to the facets that promote water dissociation are in lower amount in TiO_2-HT if compared with the case of TiO_2 P25.

Moreover, on the basis of the calculated data reported by Arrouvel and co-workers,[22] the signals observed for TiO_2-HT at 3664 and 3631 cm^{-1} (Figure 4.6 A, curve a), are here tentatively assigned to the νOH of molecularly adsorbed water on (101) facets.

4.4.2. Surface Lewis acid sites: HR-TEM and FTIR spectroscopy of adsorbed CO

The TiO_2-HT material has been then compared with TiO_2 P25. At first, the samples have been analyzed with High Resolution Transmission Electron Microscopy and the resulting micrographs are reported in Figure 4.7.

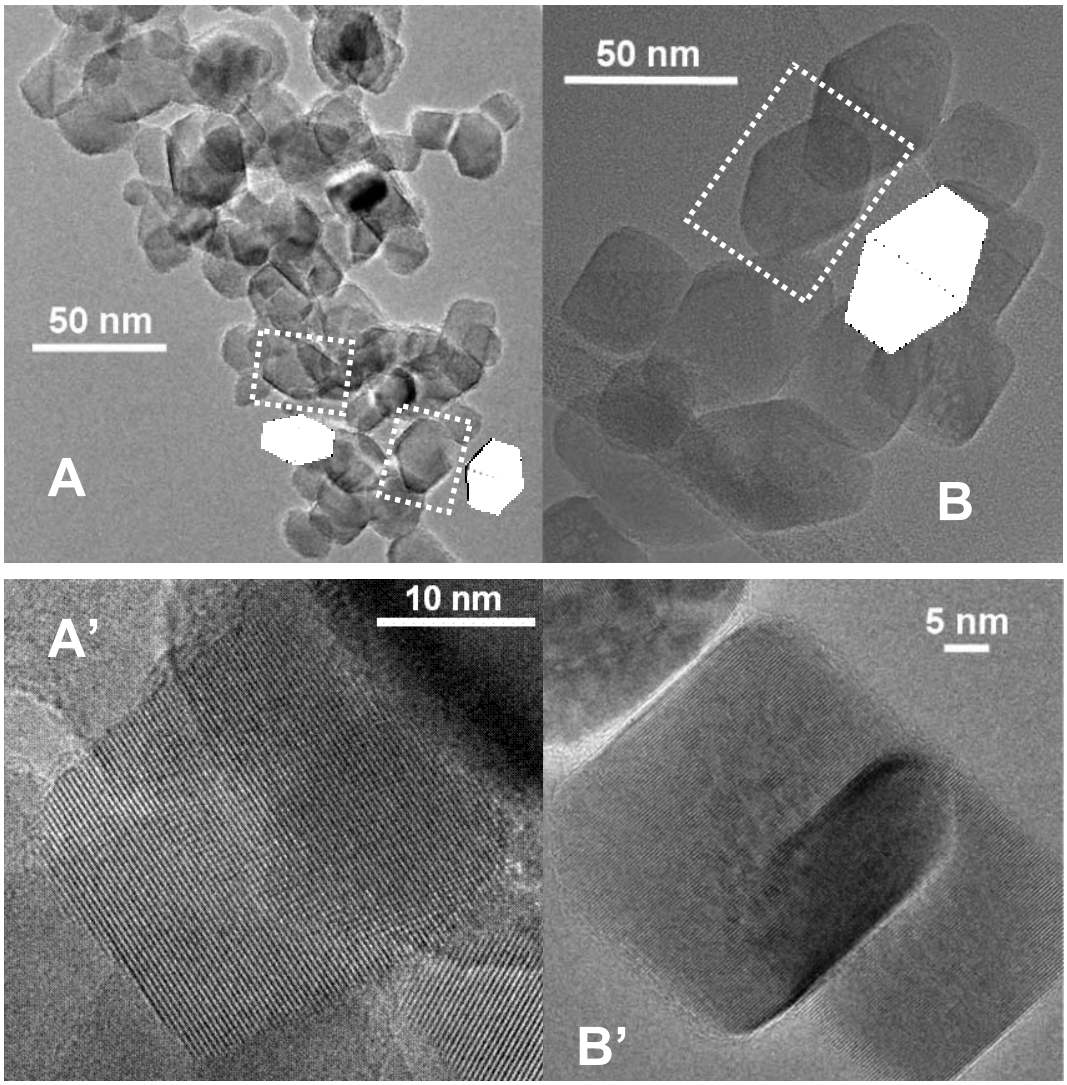

Figure 4.7. TEM images of: (A) TiO_2 P25 (original magnification x 80 k); (A') TiO_2 P25 (original magnification x 500 k); (B) TiO_2-HT (original magnification x 120 k); (B') TiO_2-HT (original magnification x 400 k).

Figure 4.7 shows low magnification TEM images representative of TiO_2 P25 (panel A) and TiO_2-HT (panel B) powders. As already reported in the previous chapter, the particles size for TiO_2 P25 sample, ranges from ca. 10 to 50 nm (Figure 4.7A) and the observed shapes can be described as 2D projections of

truncated bipyramids with the main axis (almost) parallel to the image plane, as shown by 3D schemes.

Noticeably, similar images were observed for both the materials (Figure 4.7A', B'), but exhibiting some stepping of the borders in case of TiO_2 P25 (Figure 4.7A'), witnessing for the presence of coordinatively defective surface terminations.

The surface of the two materials was then investigated at a molecular level by IR spectroscopy of CO adsorbed on samples pre-outgassed at 873 K, in order to remove H_2O molecules and OH groups from surface cations.

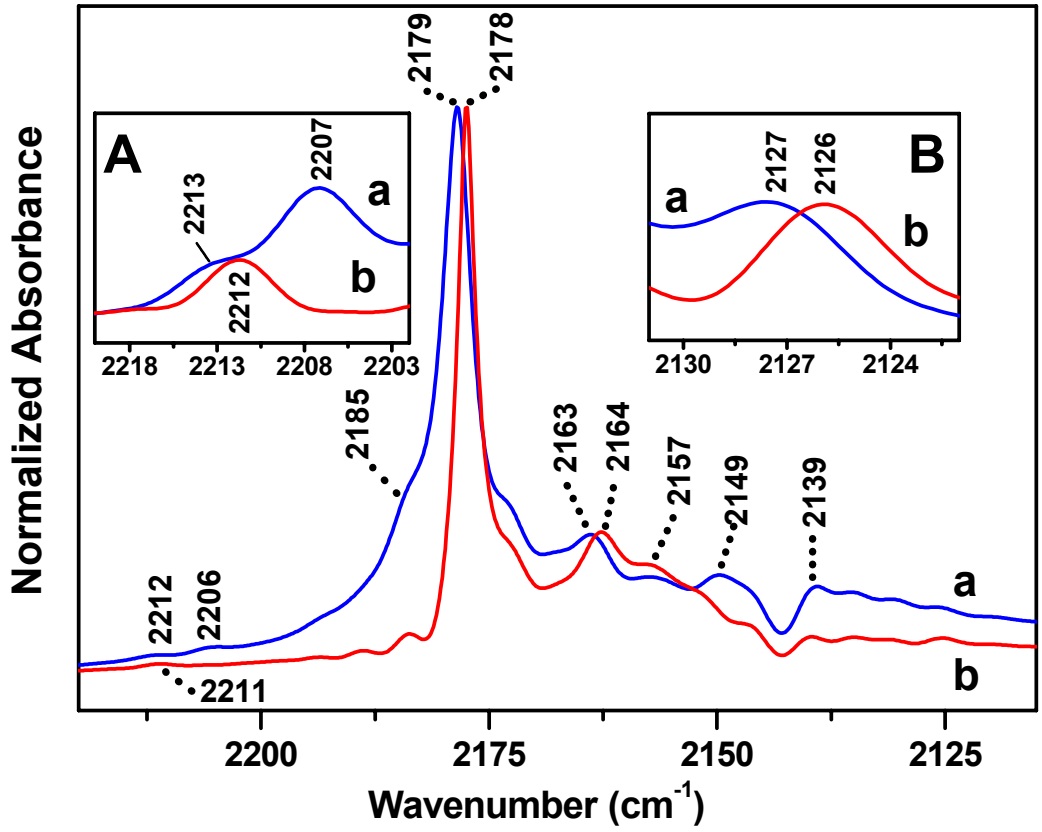

Figure 4.8. IR spectra of 60 Torr of CO adsorbed at ca. 100 K on samples outgassed at 873 K: (a) TiO_2 P25; (b) TiO_2-HT. Insets: (A) zoomed view of the 2220-2200 cm^{-1} range of the IR spectra obtained by using a "thick pellet" (ca. 30 mg/cm^2); (B) zoomed view of the 2135-2120 cm^{-1} range of the main frame.

For both types of TiO_2 particles, the spectrum collected for $\theta_{CO} \rightarrow 1$ appeared dominated by far by a narrow peak located at 2179 cm^{-1} for TiO_2 P25 and 2178 cm^{-1} for TiO_2 HT (Figure 4.8, curves a and b, respectively). This signal has been previously assigned to CO adsorbed on penta-coordinated Ti^{4+} sites exposed on (100) or (101) surfaces.[25] More recently a theoretical study[26] made allowance to propose that the main band should be due to CO probing cations on (100) faces, while CO on cationic sites exposed on (101) facets might be responsible for the shoulder at 2185 cm^{-1}. However, the evidence for an overwhelming presence of (101) surfaces in the case of TiO_2-HT nanoparticles clearly indicates that the assignment of the main peak should be revised, as it appears due to CO on cations exposed on such facets. The slight difference in position of the main peak for CO adsorbed on the two types of titania nanoparticles must be attributed to a difference in the static interaction among the adsorbed oscillators, as witnessed by the same behavior of the very weak band due to adsorbed ^{13}CO molecules in natural abundance (Figure 4.8, inset B), that, being highly diluted among ^{12}CO oscillators, are affected only by this kind of coupling, and not also from the dynamic one.[27] Moreover, the location of the singleton extrapolated by the behavior of the main peak for decreasing CO coverage (Figure 4.9) appeared almost coincident for the two materials, confirming the common origin of the peak at 2178 and 2179 cm^{-1}. It can be then inferred that (101) surfaces should be the more abundant also in the case of TiO_2 P25, confirming and extending the results of TEM observations.

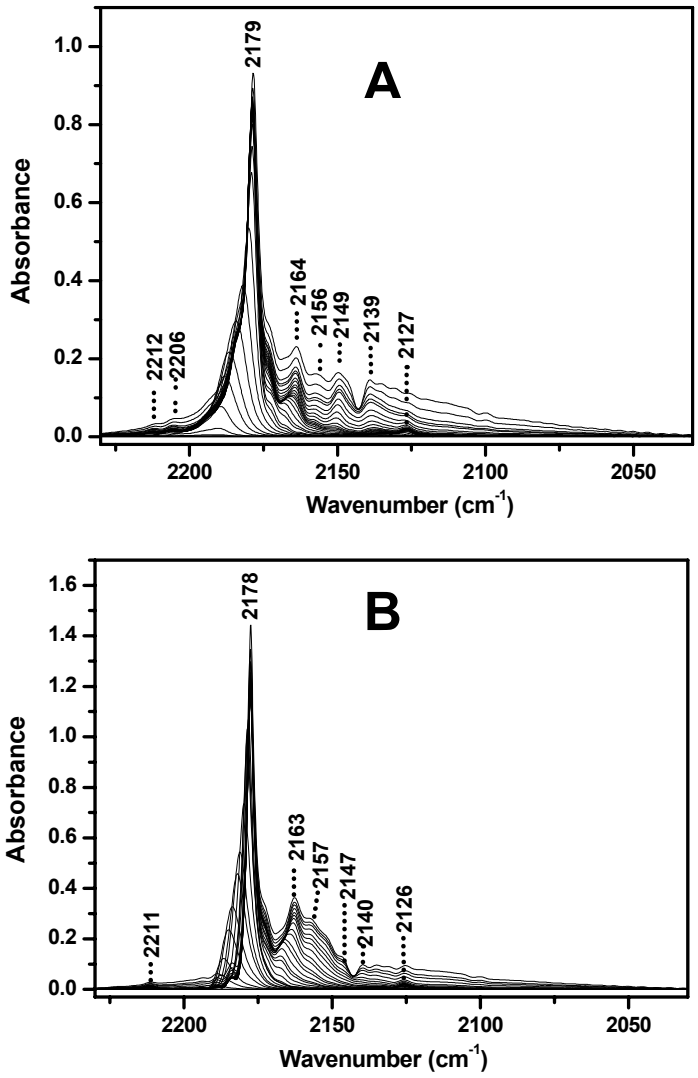

Figure 4.9. IR spectra of CO adsorbed at ca. 100 K on (A) TiO_2 P25 and (B) TiO_2-HT outgassed at 873 K. Spectra acquired at decreasing coverages, from 60 mbar CO to outgassing for 10 min at ca. 100 K.

Moreover this result allows also to assign the band at 2212/2211 cm^{-1} that, in Chapter 3.5, was attributed to a combination of a frustrated translation and a stretching mode of CO adsorbed on the same sites responsible for the peak at 2179/2178 cm^{-1}, hence to sites exposed at the (101) surfaces.

Other features with a common location for the two samples were a weaker band at 2163/2164 cm^{-1}, a minor component at 2157 cm^{-1} and the pattern at frequency lower than 2149 cm^{-1}. Conversely, the spectrum of CO adsorbed on TiO_2 P25 exhibited also a shoulder at 2185 cm^{-1} and two minor absorptions at 2149 and 2207 cm^{-1}. This latter was more clearly observed in the spectrum obtained by dosing CO on a thicker pellet (Figure 4.8, inset A).

A summary of the assignments reported in the literature for the various components listed above is reported in Table 1.

Wavenumber [cm^{-1}]		**Assignment**			
Coverage		*Site*		*Surface*	*References*
$\theta \rightarrow 1$ $\theta \rightarrow 0$	2212 2226	combination of νCO and frustrated translation on Ti^{4+}_{5c}	β	(101)	
$\theta \rightarrow 1$ $\theta \rightarrow 0$	2206 2208	νCO on coordinative detective sites	α		25
$\theta \rightarrow 1$ $\theta \rightarrow 0$	2179 2192	νCO on Ti^{4+}_{5c}	β	(101)	
$\theta \rightarrow 1$	2164	νCO on Ti^{4+}_{5c}	γ	(001)	25,26
$\theta \rightarrow 1$	2157	νCO on OH groups			25
$\theta \rightarrow 1$	2149	νCO on sites with lower Lewis acidity			
$\theta \rightarrow 1$	2139	Physisorbed CO			25,27
$\theta \rightarrow 1$ $\theta \rightarrow 0$	2127 2140	ν^{13}CO on Ti^{4+}_{5c}	β	(101)	
α, β, γ nomenclature proposed by Hadjiivanov et al. [25]					

Table 4.1. Assignment of the bands present in the spectra of CO adsorbed at ca. 100 K on TiO_2 P25 (and TiO_2-HT).

Coming back to the experimental IR spectra of adsorbed CO (Figure 4.8A), the presence/absence of the weak band at 2207 cm^{-1} for TiO_2 P25/TiO_2-HT raised a particular attention, because it monitors the possible presence of surface cationic sites in low coordination that, when hydrated, are able to dissociate water molecules, forming hydroxy groups (see Chapter 3). In a previous work devoted to the investigation of the surface fluorination of TiO_2 P25, such hydroxylated sites were supposed to be among those responsible for the decomposition of H_2O_2. [28]

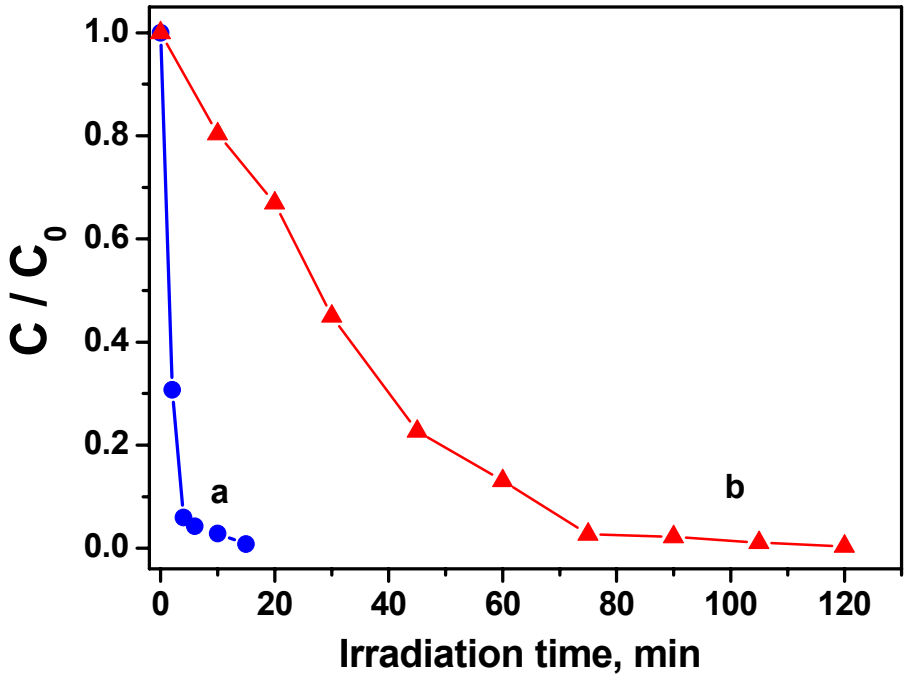

Figure 4.10. Preliminary results on photocatalytic degradation of 1 mM hydrogen peroxide on (a) -●-TiO_2 P25 and (b) -▲- TiO_2-HT.

The high reactivity of TiO_2 P25 toward the photocatalytic transformation of hydrogen peroxide (Figure 4.10) can be related to the presence of a relevant density of surface sites in low coordination condition located on edges, steps and corners, that could play a relevant role in the H_2O_2 phototransformation via an efficient direct transfer of e^-_{CB} to the hydroperoxy complexes at the surface.

Another important difference among the CO adsorption spectra of TiO_2-HT and TiO_2 P25 reported in Figure 4.8 is the width of the main peak at 2179/2178 cm^{-1}; indeed in case of TiO_2 P25 (curve a, blue), the band is broader and it isalso possible to notice the presence of a shoulder at ca. 2185 cm^{-1}, meaning that there is a wider heterogeneity of sites, already evidenced with the analysis of TEM images (Figure 4.7).

The experimental assignment of band at 2178 (2179) cm^{-1} to CO adsorbed on Ti^{4+}_{5c} sites exposed at the (101) anatase surfaces, can be used as starting reference data for theoretical modeling of surface sites local structure, as will be discussed in the SECTION B, devoted to the theoretical investigation of CO adsorption on TiO_2 anatase surfaces.

SECTION B. Theoretical modeling of surface sites local structure

The main purpose of this theoretical modeling is the elucidation of local structure of surface centers of TiO_2, and, to this aim, the results previously described on the IR spectroscopy of adsorbed CO, can represent a sort of database of vibrational frequencies, that can be used in combination with theoretical data to define the structure of sites. For this reason, the vibrational frequencies of CO adsorbed on different anatase flat surfaces and steps have been calculated and will be described in this section.

4.5. Methods

The periodic modeling of anatase surfaces and the CO adsorption with related vibrational analysis, has been performed within Density Functional Theory (DFT). The PBE approximation to DFT has been adopted along with plane waves and norm-conserving pseudopotentials for all atoms. A cutoff of 80 Ry was adopted for the plane wave expansion of the wavefunction, while a cutoff of 320 Ry was used for the density representation. Calculations were performed at the Γ point. A vacuum of 12 Å and a slab thickness of 6 (or 7) layers have been chosen, and the bottom layer has been kept fixed in the optimization. Calculations have been performed with the CPMD code.

4.6. CO adsorption on anatase surfaces

The IR spectra reported in Figure 4.8 (and 4.9), have been obtained adsorbing CO at 100K on the TiO_2 P25 and TiO_2-HT samples. At this temperature, it is possible to reach the full CO coverage of the surface (θ=1), and also multilayers of physically adsorbed CO, as demonstrated by the presence of a signal at ca. 2139 cm^{-1}. The calculated frequencies have been obtained at θ=1 and 0 K. The resulting structures of CO adsorbed on TiO_2 anatase surfaces, are reported in Figure 4.11.

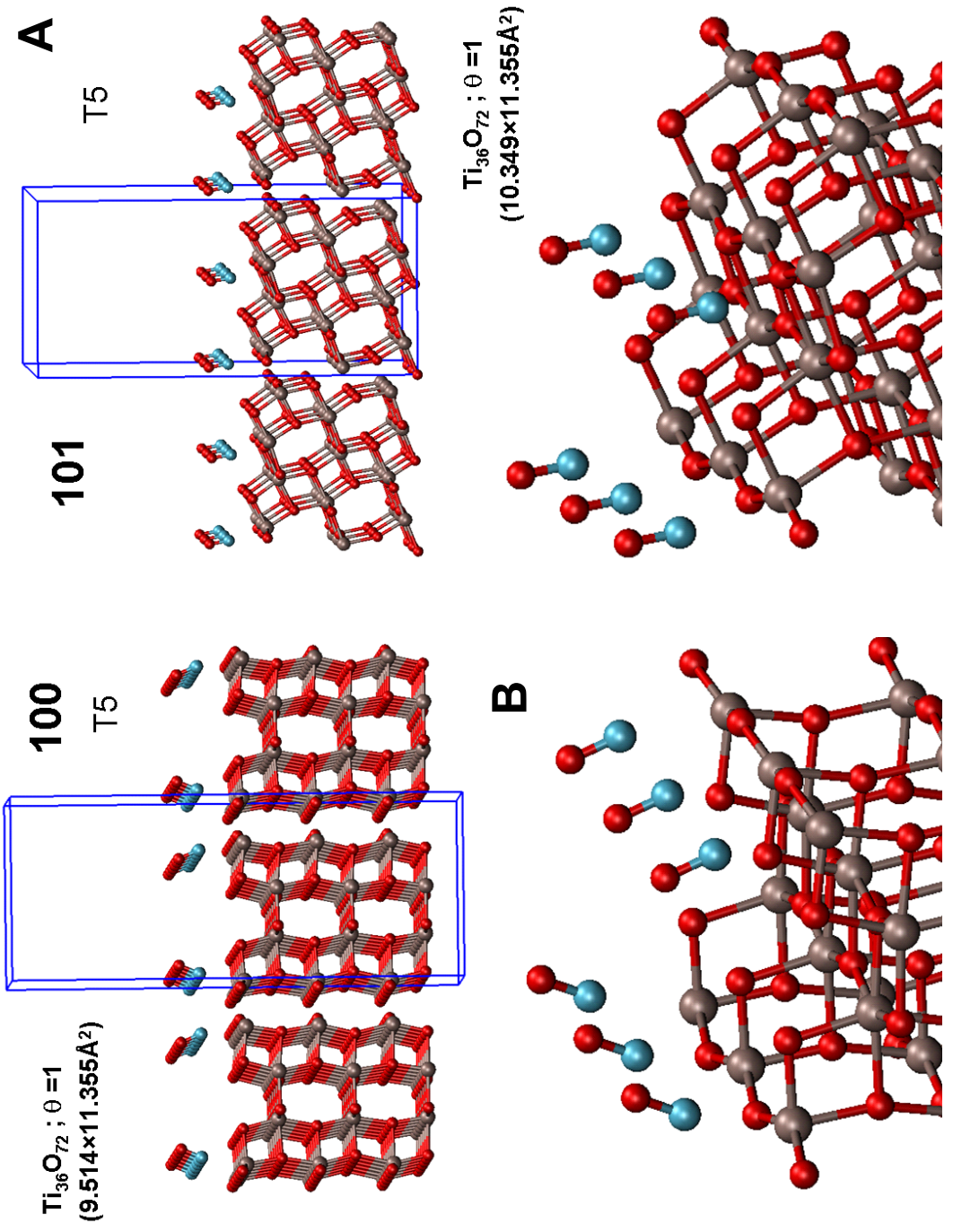
A
T5
101
$Ti_{36}O_{72}$; θ =1
(10.349×11.355Å²)
B
100
T5
$Ti_{36}O_{72}$; θ =1
(9.514×11.355Å²)

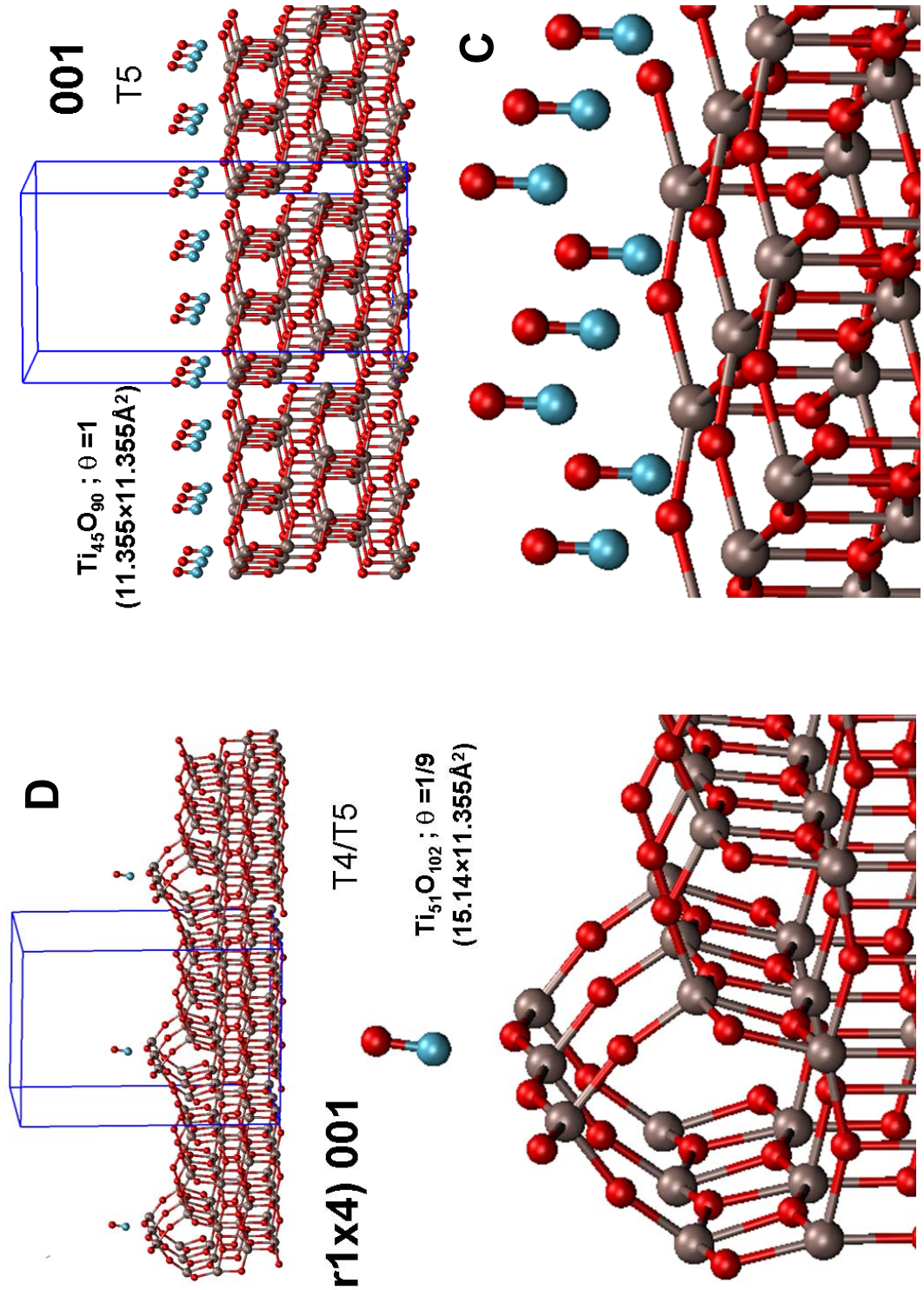
001
T5
$Ti_{45}O_{90}$; θ =1
(11.355×11.355Å²)
C
D
(r1x4) 001
T4/T5
$Ti_{51}O_{102}$; θ =1/9
(15.14×11.355Å²)

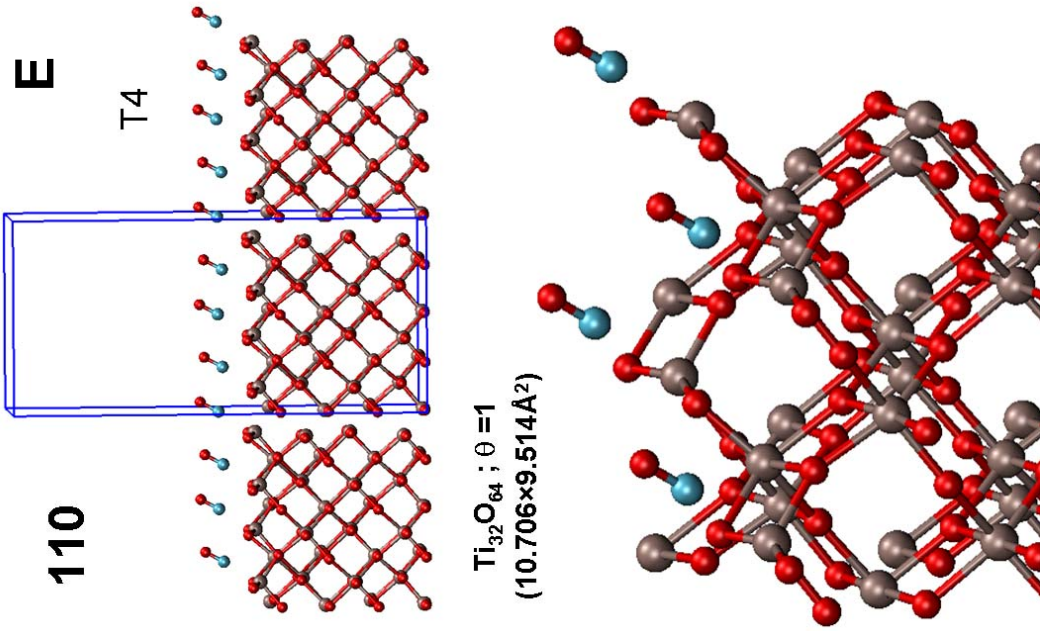

Figure 4.11. Calculated structures of CO adsorbed on A (101), B (100), C (001), D (001) reconstructed, E (110) TiO_2 anatase surfaces. Color code: Ti: gray spheres, O: red spheres, C: cyan spheres. T4 and T5: four and five-coordinated sites, respectively.

Surface	Calculated frequency [cm^{-1}] (θ=1)	Scaling factor (2178/2163 cm^{-1})	Scaled frequency [cm^{-1}]
(101)	2163	1.0070	2178
(100)	2138	1.0070	2153
(100)	2128	1.0070	2143
(001)	2127	1.0070	2142
(001) Ti 4c reconstructed	2143	1.0070	2158
(110)	2153	1.0070	2168

Table 4.2. νCO calculated frequencies at θ=1 and 0 K. The scaling factor has been obtained as result of the ratio between the experimental and the calculated value of νCO on (101) TiO_2 surface.

As previously discussed, the combination of HR-TEM and IR spectroscopy, allowed to assign the main peak of the CO adsorption spectra, located at 2178 cm^{-1}, to the penta-coordinated Ti^{4+} sites exposed at the (101) surfaces; hence, the scaling factor for the calculated frequencies have been obtained as the ratio of the experimental and calculated stretching frequencies for CO adsorbed on sites exposed at (101) surfaces (Table 4.2).

The scaled stretching frequencies of adsorbed CO are represented and compared with the experimental values in Figure 4.12.

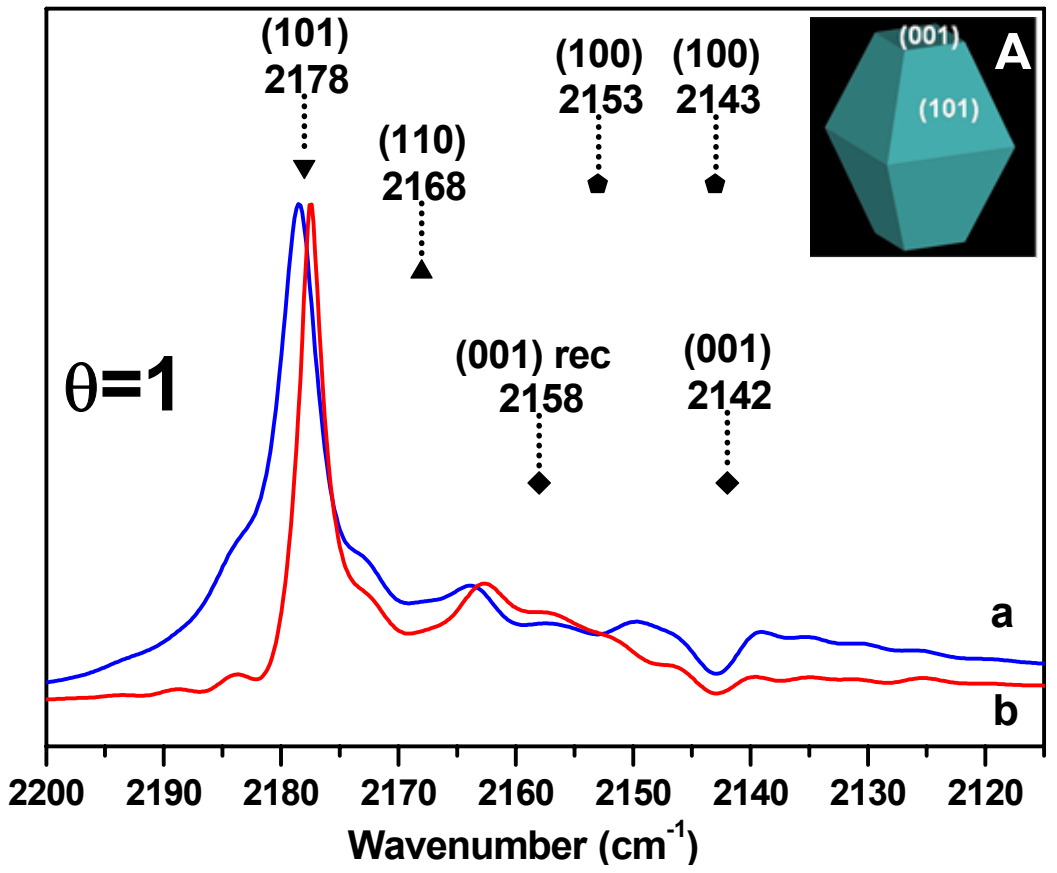

Figure 4.12. IR spectra of 60 Torr of CO adsorbed at ca. 100 K on samples outgassed at 873 K: (a) TiO_2 P25; (b) TiO_2-HT. Calculated values of νCO frequency for: -▼- (101); -▲- (110); -⬟- (100); -◆- (001) surfaces. Panel (A): 3D model of TiO_2-HT nanocrystals shape.

As it emerges from Figure 4.12, some of the calculated frequency values obtained after scaling, are very low, as in the case of the (100) surface (2143 cm^{-1}), and the (001) surface (2142 cm^{-1}). These values are too small to be assigned to the stretching of CO adsorbed on Lewis acid sites because this interaction would cause a blue shift of the frequency with respect to the one of CO in the gas phase (2143.16 cm^{-1}),[29] as described in Chapter 2.

In the data discussed so far, the model systems were considered as slabs with perfect long range symmetry. It should be noticed that in the real system ^{13}CO is present even if at low abundance. Consequently, the system is not perfectly chemically ordered and dynamic interactions among different oscillators may affect the vibrational properties of the system, in particular at high coverages.

A second source of "disorder" derives from temperature effects because calculated frequencies refer to optimized ordered structures at 0 K while experimental spectra are obtained at, e.g., 100 K, in nanocrystals, whose surfaces are generally characterized by a large number and variety of structural defects. These kinds of defects, nicknamed as "thermal", may induce splitting in the CO vibrational eigenvalues, which, in a perfectly ordered system, would be degenerate.

In order to take into account the above described effects, some isotopically different CO (^{13}CO) has been introduced in the calculations. Moreover, thermal disorder has been modeled by using the following procedure: starting from the minimum energy structure (perfectly ordered), first-principles molecular dynamics simulations at T=100 K have been performed; after such a thermalization step, geometry optimizations were performed and harmonic frequencies were calculated, as in the case of the perfectly ordered model systems, by a finite difference approach.

Table 4.3 reports the calculated frequencies obtained by keeping into account both the isotopic (chemical) disorder and the "thermal" disorder. As the ^{13}CO signal can be unambiguously assigned from the experimental data, the ratio between the calculated ^{13}CO stretching frequency on the (101) surface and the experimental ^{13}CO stretching frequency (2126 cm^{-1}, from Figure 4.8B, curve b) will be used as scaling factor.

Frequencies reported in Table 4.3 are schematically represented in Figure 4.13.

Scaling factor	
Experimental $\nu^{13}CO$/ Calculated $\nu^{13}CO$ on (101), disordered	2126/2101.3 = 1.012

Surface: (101)		
	Calculated	Scaled
Ordered ^{12}CO	2162.9	2188.3
Ordered ^{13}CO	2093.9	2118.5
Thermally (T) Disordered ^{13}CO	2101.3	2126.0
Chemically (C) Disordered ^{12}CO: 5 ^{12}CO+ 1 ^{13}CO	2138.8	2163.9
	2139.3	2164.4
	2139.9	2165.0
	2142.0	2167.1
	2148.1	2173.3
(T) and (C) Disordered ^{12}CO: 5 ^{12}CO+ 1 ^{13}CO	2146.4	2171.6
	2146.9	2172.1
	2147.2	2172.4
	2149.7	2175.0
	2154.8	2180.1
Thermally Disordered ^{12}CO	2146.3	2171.5
	2146.4	2171.6
	2147.0	2172.2
	2147.1	2172.3
	2150.3	2175.5
	2155.0	2180.3

Surface: (100)		
	Calculated	Scaled
Ordered ^{12}CO	2138.2	2163.3
Ordered ^{12}CO	2128.2	2153.2
Chemically Disordered ^{12}CO: 5 ^{12}CO+ 1 ^{13}CO	2122.5	2147.4
	2125.6	2150.5
	2126.1	2151.1

	2126.4	2151.3
	2136.3	2161.4
Surface: (001)		
	Calculated	Scaled
Ordered ^{12}CO	2127.0	2152.0
Ordered ^{12}CO:reconstructed	2143.4	2168.6
Chemically Disordered ^{12}CO: 8 ^{12}CO+ 1 ^{13}CO	2099.6	2124.3
	2099.7	2124.3
	2099.7	2124.3
	2103.1	2127.8
	2105.0	2129.7
	2108.7	2133.4
	2110.5	2135.2
	2126.1	2151.0

Surface: (110)		
	Calculated	Scaled
Ordered ^{12}CO	2153.3	2178.6
Chemically Disordered ^{12}CO: 3 ^{12}CO+ 1 ^{13}CO	2148.2	2173.5
	2149.0	2174.2
	2153.3	2178.6

Table 4.3. Calculated and scaled frequencies of $\nu^{12}CO$ and $\nu^{13}CO$ on ordered system and after introducing chemical and thermal disorder.

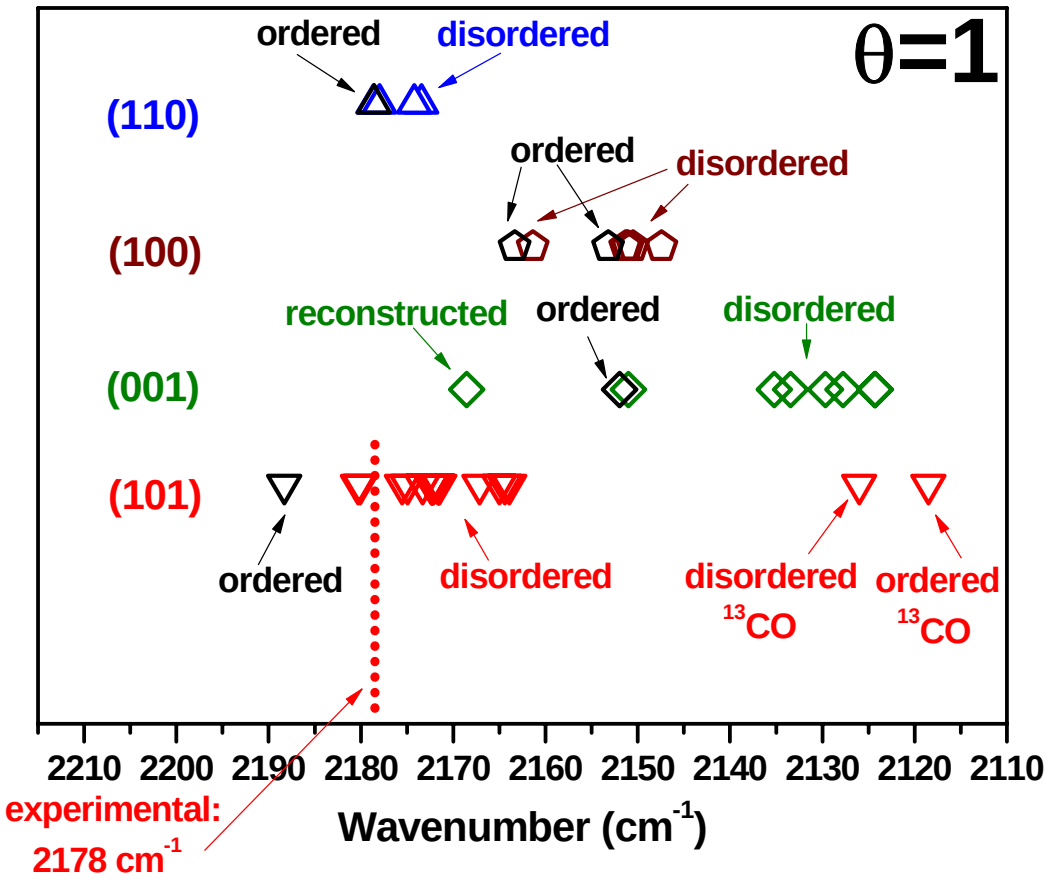

Figure 4.13. Schematic representation of data reported in Table 4.13, obtained by scaling the calculated frequencies versus the $\nu^{13}CO$ in thermal disorder value.

Figure 4.13 shows that values calculated for CO on (101) surfaces in disordered conditions are positioned around 2178 cm^{-1}, in agreement with the experimental stretching frequency of CO adsorbed on (101) facets (2178 cm^{1}).

Moreover, it can be noticed that the νCO frequencies on the most abundant (101) surfaces range from 2188 to 2164 cm^{-1}. These data may suggest that νCO on (101) contribute not only to the main peak at 2178 cm^{-1}, but also to the other signals present in the complex vibrational pattern of the CO adsorption spectrum.

Even though the (101) surfaces may contribute to more than one band in the IR spectra shown in Figure 4.8, some observations can be done on the basis of the results obtained for the other surfaces:

- **(001).** The penta-coordinated Ti^{4+} sites exposed at this surface (γ sites) have been already subject of discussion. In particular, as suggested by calculations[22] and confirmed by the combined study of vibrational spectra of internal (OH) and external (CO) probes (Chapter 3), water dissociates on these TiO_2 anatase surfaces. On these bases, the 2163 cm^{-1} νCO band may also be related to such sites (Figure 4.8). The corresponding calculated frequency is 2169 cm^{-1} (Figure 4.13) and it is due to the reconstructed (001) surface exposing four-coordinated Ti^{4+} sites.
  Indeed the (001) surfaces show a high reactivity[1] and preparation of TiO_2 nanoparticles exposing these facets is raising great interest.[6,14,15]
- **(100).** The peculiarity of the calculated stretching frequencies obtained for CO adsorbed on (100) surfaces is that two distinct values have been obtained (2138 and 2128 cm^{-1}) even for the ordered system. In fact, looking at Figure 4.11B, it emerges that there are two different orientations of adsorbed CO molecules. This phenomenon has been already reported in literature for another system, and was interpreted as being due to Davydov splitting.[30,31] Specifically, it was detected only with polarized infrared spectroscopy and for CO adsorption temperatures below 45 K. Probably these vibrational modes are not detectable in the present experimental spectra because they can be obscured by CO signals from more abundant faces. Additionally, the penta-coordinated Ti^{4+} sites exposed at the (100) surfaces contribute to the IR spectra of absorbed CO in the very complex region below 2178 cm^{-1}.
- **(110).** The (110) surface exposes four-coordinated Ti^{4+} sites. The calculated frequencies for both the ordered and disordered systems are centered at ~2175 cm^{-1}. Therefore, it may be deduced that the νCO signal related to these sites contributes to the wide band at 2179 cm^{-1} found in the TiO_2 P25 spectrum (Figure 4.8, b).

In Chapter 3 it has also been reported the first experimental evidence for a combined mode of stretching and frustrated translation of adsorbed CO at 2211 cm^{-1} (Figure 4.8). Analysis of the desorption isotherms has highlighted a correlation among the signals at 2211 cm^{-1} and the main peak at 2178 cm^{-1}, that has been assigned to CO adsorbed on sites exposed at the (101) surfaces of TiO_2. The frustrated translation has a frequency of 2211-2178 = 33 cm^{-1}. Vibrational analysis of the normal modes eigenvectors calculated for CO adsorbed on (101) surfaces evidenced a frustrated translation mode in the 65-75 cm^{-1} range (see Figure 4.14). Keeping into account that, in such a low-energy region of the spectrum, discrepancies between calculated and experimental values may be larger than for high energy modes, simulation results confirm that CO on TiO_2 has a frustrated translational mode below 100 cm^{-1}, which may combine with CO stretching modes, thus supporting the hypothesis made on the base of the experimental results.

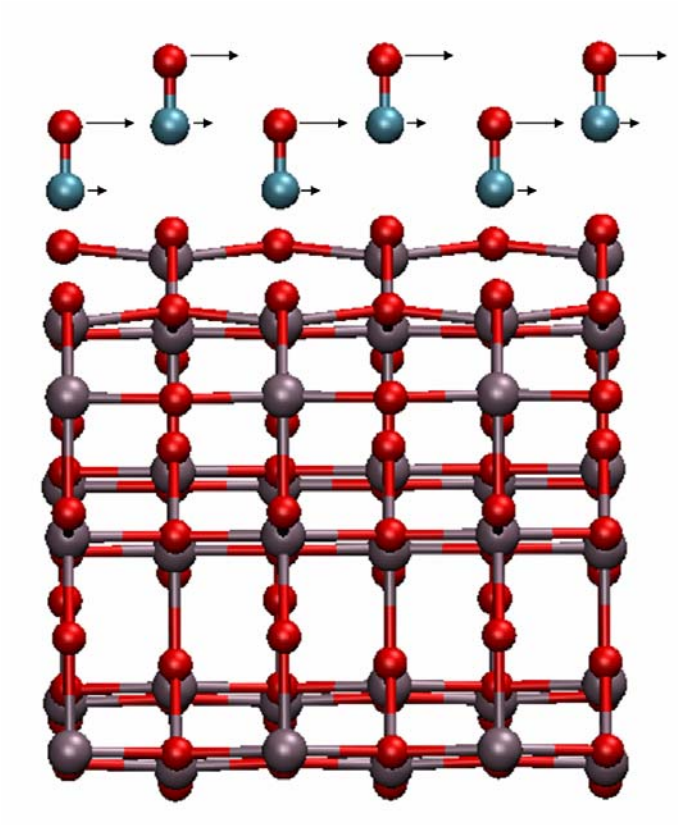

Figure 4.14. Schematic representation of frustrated translational mode of CO adsorbed on (101) TiO_2 surfaces. Color code: Ti: gray spheres, O: red spheres, C: cyan spheres.

The data presented above were dealing with CO on extended TiO_2 faces. However, defective sites that are present in the nanoparticles, due to borders roughness, should be considered as well. In particular, one of the differences in the spectra of adsorbed CO on TiO_2 P25 and TiO_2-HT is the presence only in the first case of the band at 2206 cm^{-1}, assigned to CO in interaction with sites with higher Lewis acidity. Usually such a higher Lewis acidity is associated to an increase of the coordinative unsaturation of surface cations, as for passing from planes to edges and/or corners.[25] Moreover, in Chapter 3, in case of TiO_2 P25,

the presence of two νCO signals at 2204 and 2194 cm^{-1}, assigned to sites with intermediate Lewis acidity between α and β sites, has been reported.

Therefore, as starting point for the investigation of the structure of the sites responsible for these bands, models of TiO_2 surfaces characterized by steps have been considered. In particular, the step formed by the (101) and (001) faces has been modeled and CO absorption has been simulated. The corresponding optimized structures are reported in Figure 4.15A and B, and the corresponding frequencies are listed in Table 4.4.

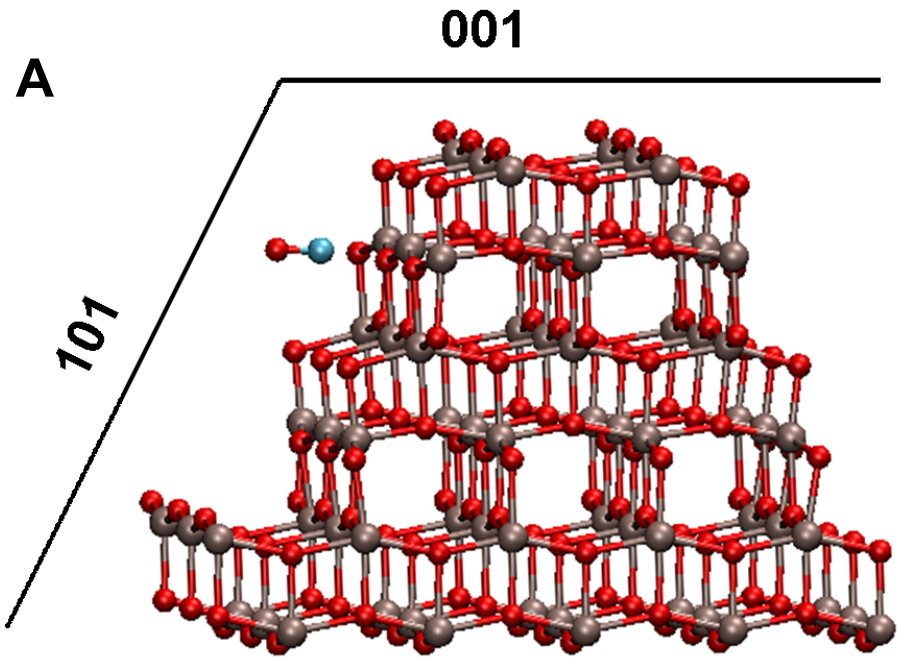

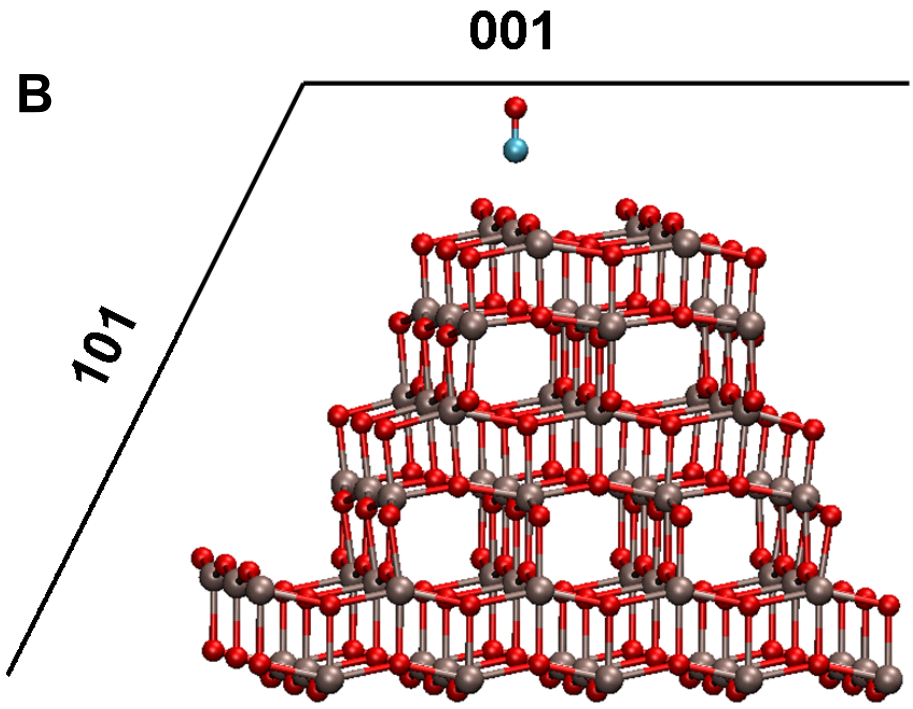

Figure 4.15. Calculated structures of CO adsorbed on A (101) and B (001) TiO_2 anatase surfaces of the step formed by the (101) and (001) faces. Color code: Ti: gray spheres, O: red spheres, C: cyan spheres.

Edge	Calculated frequency [cm^{-1}]	Scaled frequency [cm^{-1}]
(101)-(001) CO on (101)	2180	2205
(101)-(001) CO on (101) thermal disorder	2176	2201
(101)-(001) CO on (001)	2148	2173

Table 4.4. νCO calculated frequencies of CO adsorbed on TiO_2 anatase surfaces of the step formed by the (101) and (001) faces. Frequencies scaled versus the $\nu^{13}CO$ in thermal disorder value, reported in Table 4.3.

Remarkably, CO molecules on sites close to the steps are characterized by stretching frequencies higher than those found for CO adsorbed on the corresponding extended faces. Hence, not only the coordinative defective sites may contribute to νCO bands at 2206, 2204, 2194 cm^{-1} (evidenced in Chapter 3), but also the penta-coordinated Ti sites close to surface defective positions like edges.

Conclusions and perspectives

The study of defined surfaces of nanoparticles with controlled morphology, enabled to assign some of the bands of the complex CO adsorption spectra. The use of these data as references for the theoretical modeling, allowed to establish the proper thermal and chemical conditions for the computational simulation of the CO vibrational adsorption spectra of TiO_2 anatase.

The future development of this study, would provide the assignment of local structure of defective centers, that, although represent a small fraction of surface sites, they are responsible for part of the surface chemistry of oxides, as shown by preliminary results on H_2O_2 decomposition on TiO_2; hence, the combined theoretical and experimental investigation of surface hydration and hydroxylation will be an extension of the present study.

References

(1) Diebold, U. *Surface Science Reports* **2003**, *48*, 53.
(2) Morterra, C. *Journal of the Chemical Society, Faraday Transaction 1* **1988**, *84*, 1617.
(3) Martra, G. *Applied Catalysis A-General* **2000**, *200*, 275.
(4) Gong, X. Q.; Selloni, A. *Journal of Catalysis* **2007**, *249*, 134.
(5) Burda, C.; Chen, X. B.; Narayanan, R.; El-Sayed, M. A. *Chemical Reviews* **2005**, *105*, 1025.
(6) Zhou, Z. Y.; Tian, N.; Li, J. T.; Broadwell, I.; Sun, S. G. *Chemical Society Reviews* **2011**, *40*, 4167.
(7) Yang, H. G.; Sun, C. H; Qiao, S. Z; Zou, J.; Liu, G.; Smith, S. C.; Cheng, H. M; Lu, G. Q. *Nature* **2008**, *453*, 638.
(8) Alivov, Y.; Fan, Z. Y. *Journal of Physical Chemistry C* **2009**, *113*, 12954.
(9) Dai, Y.; Cobley, C. M.; Zeng, J.; Sun, Y.; Xia, Y *Nano Letters* **2009**, *9*, 2455.

(10) Ding, K. L.; Miao, Z. J.; Hu, B. J.; An, G. M.; Sun, Z. Y.; Han, B. X.; Liu, Z. M. *Langmuir* **2010**, *26*, 5129.

(11) D'Arienzo, M.; Carbajo, J.; Bahamonde, A.; Crippa, M.; Polizzi, S.; Scotti, R.; Wahba, L.; Morazzoni, F. *Journal of the American Chemical Society* **2011**, *133*, 17652.

(12) Chen, C. H., R.; Mai, K.; Ren, Z.; Wang, H.; Qian, G.; Wang, Z. *Crystal Growth & Design* **2011**, *11*, 5221.

(13) Yu, J. G.; Fan, J. J.; Lv, K. L. *Nanoscale* **2010**, *2*, 2144.

(14) Wang, Z. Y.; Lv, K. L.; Wang, G. H.; Deng, K. J.; Tang, D. G. *Applied Catalysis B-Environmental* **2010**, *100*, 378.

(15) Selloni, A. *Nature Materials* **2008**, *7*, 613.

(16) Sugimoto, T.; Zhou, X. P. *Journal of Colloid and Interface Science* **2002**, *252*, 347.

(17) Sugimoto, T.; Zhou, X. P.; Muramatsu, A. *Journal of Colloid and Interface Science* **2002**, *252*, 339.

(18) Sugimoto, T.; Zhou, X. P.; Muramatsu, A. *Journal of Colloid and Interface Science* **2003**, *259*, 43.

(19) Sugimoto, T.; Zhou, X. P.; Muramatsu, A. *Journal of Colloid and Interface Science* **2003**, *259*, 53.

(20) Frew, J. E.; Jones, P.; Scholes, G. *Analytica Chimica Acta* **1983**, *155*, 139.

(21) Powder diffraction File JCPDS 21-1272.

(22) Arrouvel, C.; Digne, M.; Breysse, M.; Toulhoat, H.; Raybaud, P. *Journal of Catalysis* **2004**, *222*, 152.

(23) Morterra, C.; Chiorino, A.; Boccuzzi, F.; Fisicaro, E. *Z. Phys. Chem. Neue Folge* **1981**, *124*, 211.

(24) Chalmers, J. M.; Griffiths, P. R. *Handbook of vibrational spectroscopy*; Wiley: London, 2002; Vol. 3.

(25) Hadjiivanov, K.; Lamotte, J.; Lavalley, J. C. *Langmuir* **1997**, *13*, 3374.

(26) Mino, L.; Ferrari, A. M.; Lacivita, V.; Spoto, G.; Bordiga, S.; Zecchina, A. *Journal of Physical Chemistry C* **2011**, *115*, 7694.

(27) Spoto, G.; Morterra, C.; Marchese, L.; Orio, L.; Zecchina, A. *Vacuum* **1990**, *41*, 37.

(28) Minella, M.; Faga, M. G.; Maurino, V.; Minero, C.; Pelizzetti, E.; Coluccia, S.; Martra, G. *Langmuir* **2010**, *26*, 2521.

(29) Hadjiivanov, K. I.; Vayssilov, G. N. *Advances in Catalysis, Vol 47* **2002**, *47*, 307.

(30) Heidberg, J.; Hustedt, M.; Kampshoff, E.; Rozenbaum, V. M. *Surface Science* **1999**, *427-28*, 431.

(31) Heidberg, J.; Kandel, M.; Meine, D.; Wildt, U. *Surface Science* **1995**, *331*, 1467.

Chapter 5

Glycine adsorption and oligomerization on TiO_2 P25

5.1. Introduction

The first part of this thesis has been devoted to study the surface properties of titanium dioxide. The results obtained, shown in previous chapters, were aimed to elucidate the structure of sites exposed at nanoparticles surface, in order to provide a description of centers with a key role in the photocatalytic applications.

For this purpose it is possible to investigate the surface terminations by studying the vibrational spectra of adsorbed probe molecules. However the same experimental procedure can be used to have insights on the interaction of TiO_2 surface with some molecules relevant for other applications of this material. In particular, titanium dioxide is not only employed in photocatalysis,[1] but also in solar cells[2] or in biomedical implants.[3]

Focusing the attention on the last application, titania has an important function in ruling the interactions occurring at the prosthesis-hosting tissue interface. Indeed titanium in implants derives its resistance to corrosion by the formation of a solid oxide layer to a depth of 10 nm. Under *in vivo* conditions the oxide (TiO_2) is the only stable reaction product. The titanium implant surface consists then of a thin oxide layer in contact with biological fluids, made of water, dissolved ions, and biomolecules (proteins with surrounding water shell) as shown in Figure 5.1.

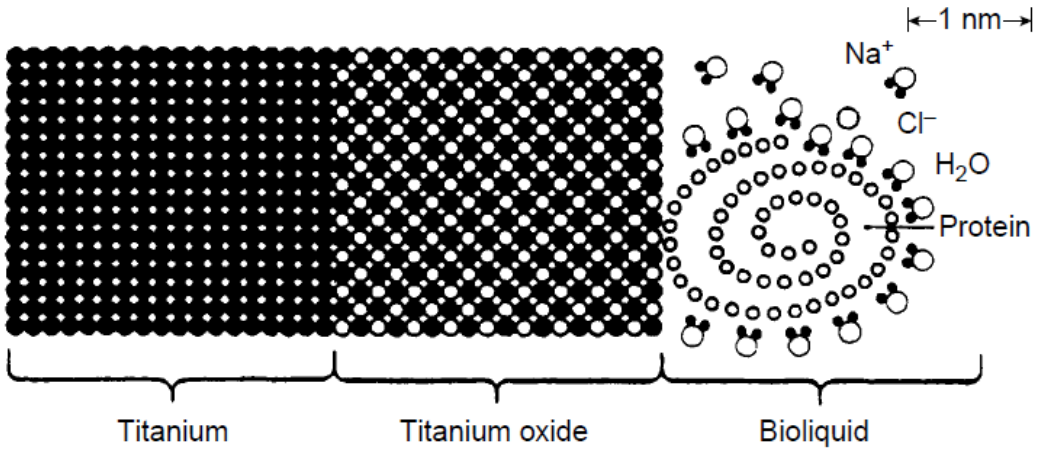

Figure 5.1. Interface between a titanium implant and bioliquid.[3]

The nature of the surface can influence the types of bonding of the biomolecules and, as a consequence, can perturb their conformation and function.[3]

Therefore the investigation of TiO_2-tissue interactions is important for understanding the processes occurring at the implant-body interface, but also for the development of new biomedical applications.[4] The complexity of the hosting tissue matrix, unfortunately prevents the possibility to directly study the interface reactions, therefore a model system is needed to have insights on biomaterial-biomolecules interactions at molecular level.

Some efforts have been already done in order to set-up model systems to investigate the surface-small molecules interaction (like in case of SiO_2),[5] with experimental and theoretical techniques. The same approach can be used to study the TiO_2 surface; in literature are reported some works on small molecules in interaction with titanium oxide surfaces,[6,7] whereas mainly well-defined single crystal surfaces are considered.

Therefore a useful contribution can come from the experimental study of biomolecules in interaction with nanostructured surfaces like in TiO_2 nanopowders by the IR spectroscopy of adsorbed molecules. In particular, in order to selectively

study the interactions occurring at the interface, it has been chosen to adsorb the biomolecules on TiO_2 from the vapor phase and not from the liquid phase, in order to avoid the presence of water and, thereby, simplify the system under investigation.

Consequently glycine (NH_2CH_2COOH) has been chosen as biomolecule because represents an ideal system for this research work. Indeed it is the simplest amino acid with only an amino and a carboxylic group.

Glycine (abbreviated as Gly or G)[8] is an organic compound with molecular weight 75.07 g/mol and structure like depicted in Figure 5.2.

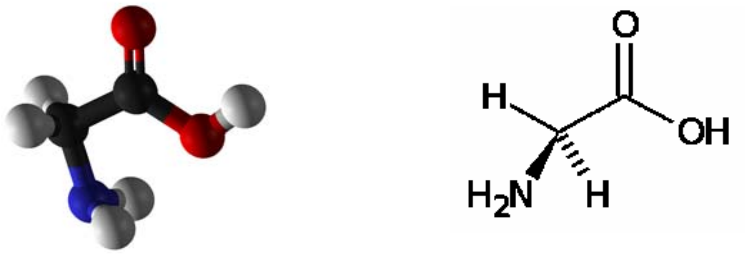

Figure 5.2. Structure of Glycine in “ball and stick” view (on the left) and Lewis formula (on the right).

Gly sublimates in vacuum at 391 K, temperature lower than the decomposition one (506-563 K).[9]

The infrared study of Gly adsorbed on TiO_2 has required the spectra acquisition of glycine in different forms (solid, in solution at different pH values), in order to constitute a reference database useful to evaluate the IR spectra of glycine adsorbed on TiO_2.

Finally the commercial TiO_2 P25 from Degussa has been selected for this study.

5.2. Materials and methods

For these investigations glycine (Gly) from Sigma-Aldrich has been used as received. Glycine has been adsorbed on TiO_2 P25 from Degussa, material already described in Chapter 3, section 3.2.1. The titania pellet has been put in a gold frame and activated in oxygen at 723 K and then rehydrated by contact with 20 mbar of H_2O vapor in the IR cell, as shown in Figure 5.3 a.

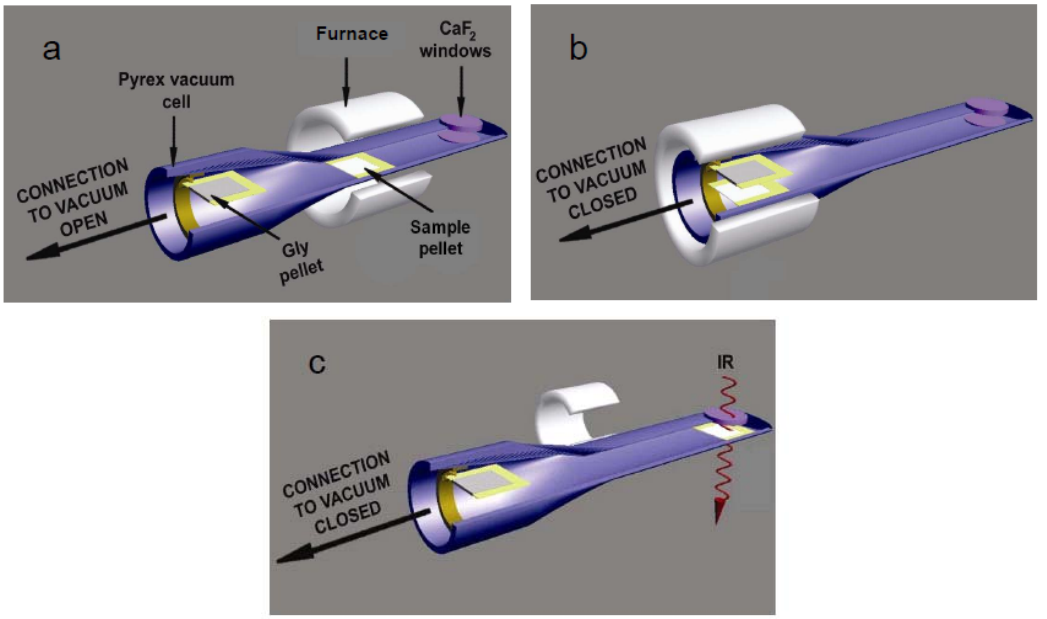

Figure 5.3. Three-dimensional representation of a cell for IR measurements during the steps of an experiment: (a) set of the tools during the pretreatment; (b) phase of sublimation, with the sample close to the glycine pellet; (c) phase of IR measurement.

Subsequently, the pellet of titania has been dehydrated at 423 K, temperature at which the Gly sublimation will be performed.

Then the TiO_2 P25 pellet has been moved in the IR cell and put as close as it is possible to a gold holder containing a glycine pellet (Figure 5.3 b): in this position the two pellets are not in contact, to avoid contaminations, but are close enough to allow the glycine vapor to be adsorbed on nanoparticles surface of titania.

Finally the TiO_2 pellet has been moved to the bottom of the cell, in order to perform the infrared investigation (Figure 5.3 c).

Another material has been used for the sake of comparison: hydoxyapatite nanocrystals (HA), that have already been the subject of previous investigations, including the combined IR and theoretical study of glycine adsorption from the vapor phase.[10]

Almost all the measurements have been carried out through IR measurements. The instrument used it is a Bruker Vector 22 Spectrometer equipped with a DTGS detector.

Different kinds of cells and sample forms have been used accordingly with the desired aim of the measurements

- *Transmission measurements*. Self-supporting pellets with optical thickness around 10-15 mg/cm^2 to analyze titania in a IR cell equipped with CaF_2 windows, as shown in Chapter 3, section 3.2.2.

- *Attenuated total reflectance (ATR)*. This technique has been used to analyze the solid glycine and its solutions.

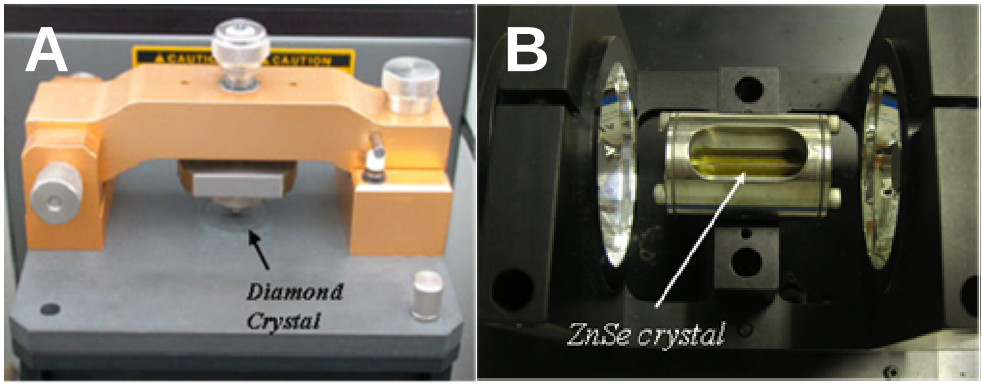

Figure 5.4. (A): picture of Micro-ATR system with Diamond crystal; (B): picture of CIR cell with ZnSe crystal, for ATR of liquid solution.

The solid glycine powder has been analyzed in a Micro-ATR cell equipped with a diamond crystal, on which the Gly has been simply deposited (Figure 5.4A); while IR measurements of the glycine solutions have been performed in a Cylindrical Internal Reflection cell (CIR) with a ZnSe crystal (Figure 5.4B).

In this case, H_2O and D_2O solutions of Gly have been prepared at concentration 0.5 M and at different pH values. In particular by simply dissolving Glycine powder in H_2O (or D_2O) a solution at pH 5.5 has been obtained, while pH 13.0 and 1.0 have been prepared by adding to the glycine solution few drops of NaOH solution and HCl, respectively.

In addition, the adsorbed molecules have been analyzed through Electrospray Ionization Mass Spectrometry (ESI-MS) in a LTQ Obritrap instrument, following the experimental protocol here reported: (i) the TiO_2 pellet, after glycine adsorption, has been put in contact with 0.5 mL of H_2O (ii) sonicated for 20 min (iii) the suspended powder has been centrifuged at 10000 rpm for 10 minutes (iv) the supernatant has been separated and centrifuged a second time at 10000 rpm (v) after the addition of formic acid (with sample and formic acid in ratio 1:1), the supernatant has been analyzed by MS (the mass reported in the spectra will be one unit higher than for the neutral molecule because of the use of formic acid will provide protonated molecules).

5.3. The selected amino acid: glycine

5.3.1. IR study of glycine crystalline forms

Polymorphism, ability of a solid material to exhibit more than one crystal form, has been intensively studied, because the presence of different polymorphs can produce differences in mechanical, thermal and physical properties, such as melting point, solubility and furthermore, in the case of biomolecules, modification of the bioavailability and absorption processes.[11]

Polymorphism occurs also for amino acids, resulting from a different packing arrangement of zwitterions.

Glycine exists in α-, β- and γ- forms, the first two characterized by monoclinic crystals, while the last by hexagonal ones. The γ-glycine is formed from aqueous acetic acid or ammonia solution; the glycine α-form is obtained by spontaneous nucleation from pure aqueous solution.[12,13] The β-form results from the condensation in dry condition of glycine vapors resulting from the sublimation of the γ- and α-forms.[11] γ-glycine can be transformed in the α-form by heating at 443 K, while the β-form is converted in the α-form by hydration (exposure to moisture) or grounding.

On the basis of these considerations, the transformations which involve the glycine crystalline structures are described schematically in Figure 5.5.

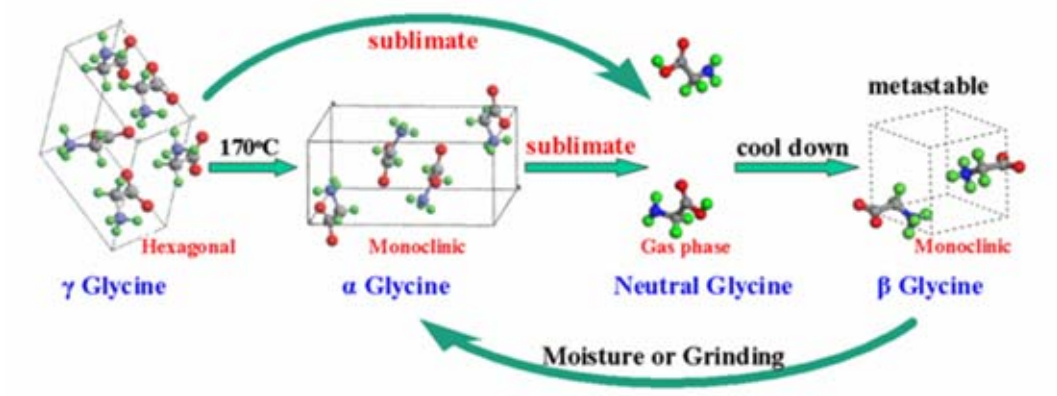

Figure 5.5. Glycine transformations during sublimation process.[11]

In the present study the glycine used for the experiments was provided by Sigma-Aldrich, and was found to be in the γ-form, by XRD measurements. This work was based on the adsorption of glycine from the vapor phase and then, the possibility of formation of glycine crystals in the β-form, by simple condensation on the sample, and/or in the α-form, by subsequent exposure to water vapor, was not excluded *a priori*.

Then, it appeared useful to consider, for the sake of comparison, the IR spectra of

the three crystal forms. The spectrum of γ-glycine was collected by using the product received from Sigma. Conversely, those of α- and β-forms were derived from the literature.[11,14] Unfortunately, the data found reported only a limited range of spectra in the mid-IR region, namely the 1800-1300 cm^{-1} range.

Moreover, a disagreement between the spectra of α-form reported by Liu et al.[11] and Lambert et al.[14] was found. Not enough experimental details have been reported in such papers, and then it is difficult to understand the origin of such disagreement. Then, both spectra have been considered for this form and were reported in Figure 5.6.

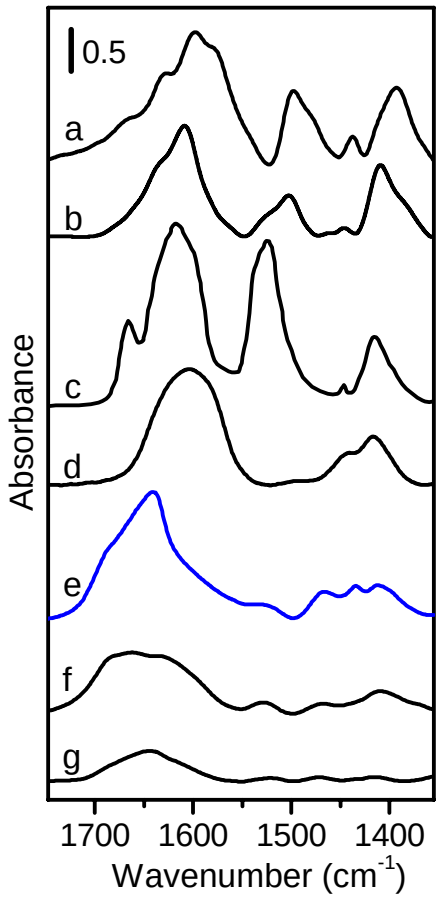

Figure 5.6. IR spectra of glycine: (a) α form, (b) β form, (c) γ form and adsorbed from the vapor phase on (d) HA; (e) TiO_2 P25-Degussa; (f) TiO_2 Merck; (g) SiO_2 Aerosil OX-50 Degussa. Spectra d-g were recorded after a total time of contact of the samples with Gly vapor, adopting in all cases the stepwise procedure described in Section 5.2. Before IR measurement, the samples underwent several D_2O adsorption/desorption cycles. Spectra of adsorbed Gly are reported having subtracted the spectrum of the bare inorganic powders as background. (The results obtained for glycine adsorbed on different surfaces will be described in details in Section 5.4.)

None of the spectra resulting from the adsorption of Gly on the series of materials indicated above resulted similar to those of the crystal forms of the amino acid. Furthermore, different spectral profiles were obtained for Gly adsorbed on different materials, indicating the actual occurrence of molecules-surface

interactions. It is of interest to notice that just traces of adsorbed Gly were found for SiO_2, typically exposing apolar siloxane bridges and poorly acidic silanol groups, clearly indicating that, in the adopted conditions, the fixation of Gly molecules from the vapor phase requires a proper surface reactivity.

5.3.2. IR spectra of glycine in aqueous solution

In addition to the IR spectra of glycine in the three crystal forms, it appeared interesting to collect also the IR spectra of glycine in aqueous solutions, as possible references for the IR features of amino acid molecules considered in this study.

A solution of glycine 0.5 M was then prepared by dissolving crystals of the γ-form. As the pH of the solution was 5.5, the dissolved molecules retained their zwitterionic form, as a result of the pK_1 and pK_2 values.

Noticeably, the possibility to change the pH by addition of small amounts of strong acids (HCl) or bases (NaOH) resulted in the possibility to modify the state of glycine molecules, that can be converted in the completely protonated form $NH_3^+–CH_2–COOH$ at the low pH (in the present case 1.0), or in the completely deprotonated form $NH_2–CH_2–COO^-$ at high pH values (in this case 13.0) (see Figure 5.7).

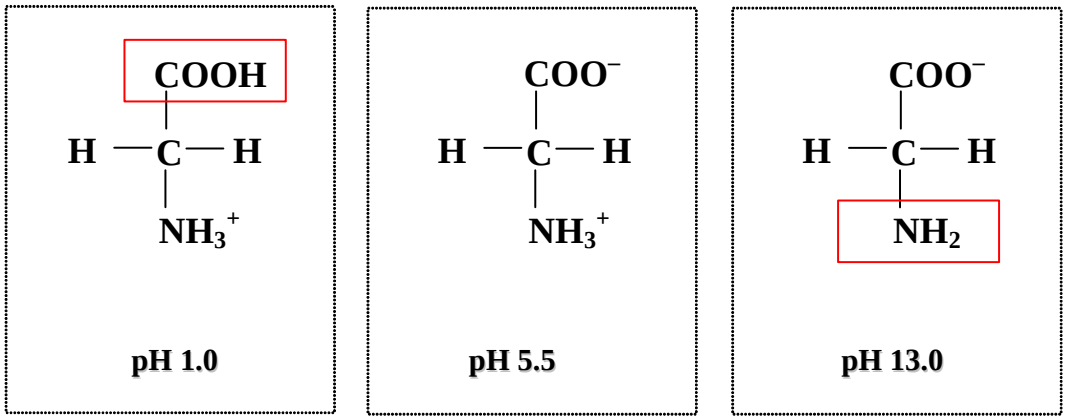

Figure 5.7. Lewis structure of glycine at: (a) pH 1.0, (b) pH 5.5, (c) pH 13.0 highlighting the protonation state of functional groups.

In this way, a more rich set of reference data was obtained, containing the vibrational feature of –COOH, $–COO^-$, $-NH_3^+$ and $-NH_2$ functional groups, as the interaction of $NH_2–CH_2–COOH$ neutral glycine molecules, obtained by sublimation, with the surface of the materials considered in this work could give origin to various kind of species.

Additionally the same spectra were collected for the solutions prepared in D_2O: this allows to downshift the signals related to amino group and, therefore, to simplify the pattern and more easily assign all the vibrational bands.

For each solution an IR spectrum was collected in the ATR mode, by using a CIR cell for liquid samples, and the spectrum of water was subtracted as background.

The resulting spectra of glycine ions and zwitterions are shown in Figure 5.8 and the relative assignment are reported in Table 5.1.

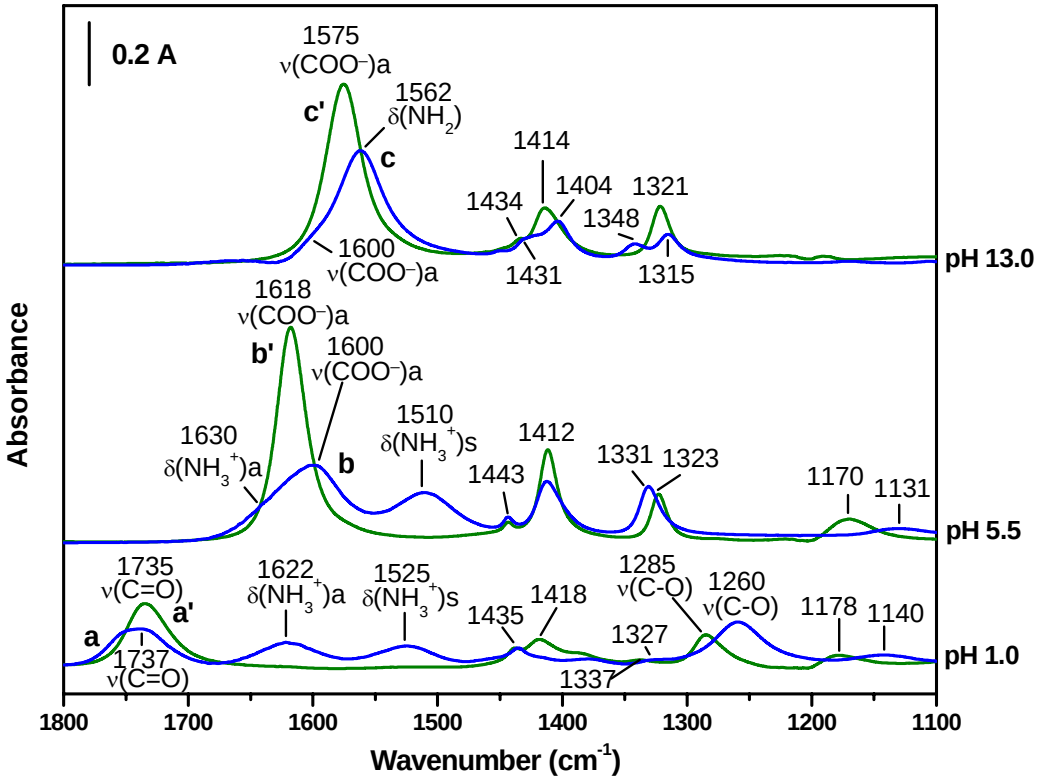

Figure 5.8. IR spectra (collected in the ATR mode, by using a cylindrical internal reflection element) of 0.5 M Gly solutions in H_2O (lines: a,b,c) and in D_2O (lines: a',b',c') at different pH (pD): a,a') 1.0; b,b') 5.5. c ,c') 13.0.

IR bands assignment in 1800-1100 cm^{-1} range for Glycine-1-^{12}C in H_2O and D_2O solutions at different pH.						
Assignment *	**Wavenumber (cm^{-1})**					
	pH 1.0		**pH 5.5**		**pH 13.0**	
	H_2O	**D_2O**	**H_2O**	**D_2O**	**H_2O**	**D_2O**
ν C=O	1737	1735	-	-	-	-
δ NH_3^+	1622		1630		-	
$\nu_{asym}COO^-$	-	-	1600	1618	1600	1575
δ NH_2	-	-	-	-	1562	
δ NH_3^+	1525		1510		-	
δ CH_2	1435	1435	1443	1443	1431	1434
n.a.		1418				
$\nu_{sym}COO^-$	-	-	1412	1412	1404	1414
n.a.					1348	
ω CH_2	1327	1337	1331	1323	1315	1321
ν C–O	1260	1285	-	-	-	-
ρ NH_3^+	1140		1131		-	
δ ND_3^+		1178		1170		-
* ν, stretching mode; δ, bending mode; ω, wagging mode; ρ, rocking mode. a, antisymmetric vibration; s, symmetric vibration; n.a., not assigned. References for assignment:[10,15-19]						

Table 5.1. Assignment of the bands present in the spectra of Gly in H_2O or D_2O solutions (0.5 M) at different pH (pD), displayed in Figure 5.9.

It is noteworthy to observe that deuteration of Gly molecules resulted also in significant changes in the intensity of several bands. The extent of such behavior is particularly relevant for the band that, in terms of group frequencies, is assigned to the antisymmetric stretching mode of the carboxylated moiety [labeled as

$\nu(COO^-)$a]. When $-NH_3^+$ and $-NH_2$ groups are present (curves b and c, respectively), their deformation absorptions are quite close in frequency to the $\nu(COO^-)$a band. Hence, the occurrence of changes in the relative intensity of the signals due to the carboxylate and amino (protonated or not) groups appeared related to their relevant separation (hundreds of cm^{-1}) in frequency after deuteration. By considering that the signals present in a IR absorption spectrum are actually due to the excitation of normal modes, involving all atoms present in a molecule, the described behavior can be interpreted as the result of a decoupling between zeroth-order states involving the carboxylic and amino moieties.[20] A similar explanation was recently proposed for the strong isotope effects observed in the infrared spectrum of the protonated water dimer $H(H_2O)_2^+$ (also known as the Zundel cation).[21]

5.4. Glycine adsorption from the vapor phase on TiO_2 P25: FTIR and Mass Spectrometry evidence of oligomerization

In Section 5.2 has been described the procedure used to perform the adsorption of glycine from the vapor phase. In particular the TiO_2 pellet has been pretreated in oxygen at 723 K, in order to completely remove species present on the surface like carbonates, bicarbonates, and this results also in a complete dehydration and significant level of dehydroxylation (as described in Chapter 3). After the activation at 723 K water vapor was sent on the sample surface, in order to obtain a rehydration of the surface. At this point, the ideal working condition should provide the possibility to perform the sublimation on a pellet of titania just outgassed at room temperature, to study some competition between glycine and water pre-adsorbed on the surface. However as the sublimation is carried out at 433 K, it would result in a simultaneous dehydration of the titania surface. To have an initial dehydration condition similar to that experienced by glycine adsorbed from the vapor phase during sublimation, it was then decided to outgas the sample at 433 K for 40 minutes after the rehydration.

After such a treatment, the sample was then moved close to the amino acid pellet

and that part of the cell was heated at 433 K, temperature representing the best compromise between the sublimation rate and the possible desorption of glycine molecules already adsorbed on surface sample; then, sublimation steps lasting ca. 1 hour each were performed, collecting an IR spectrum after each step (Figure 5.9).

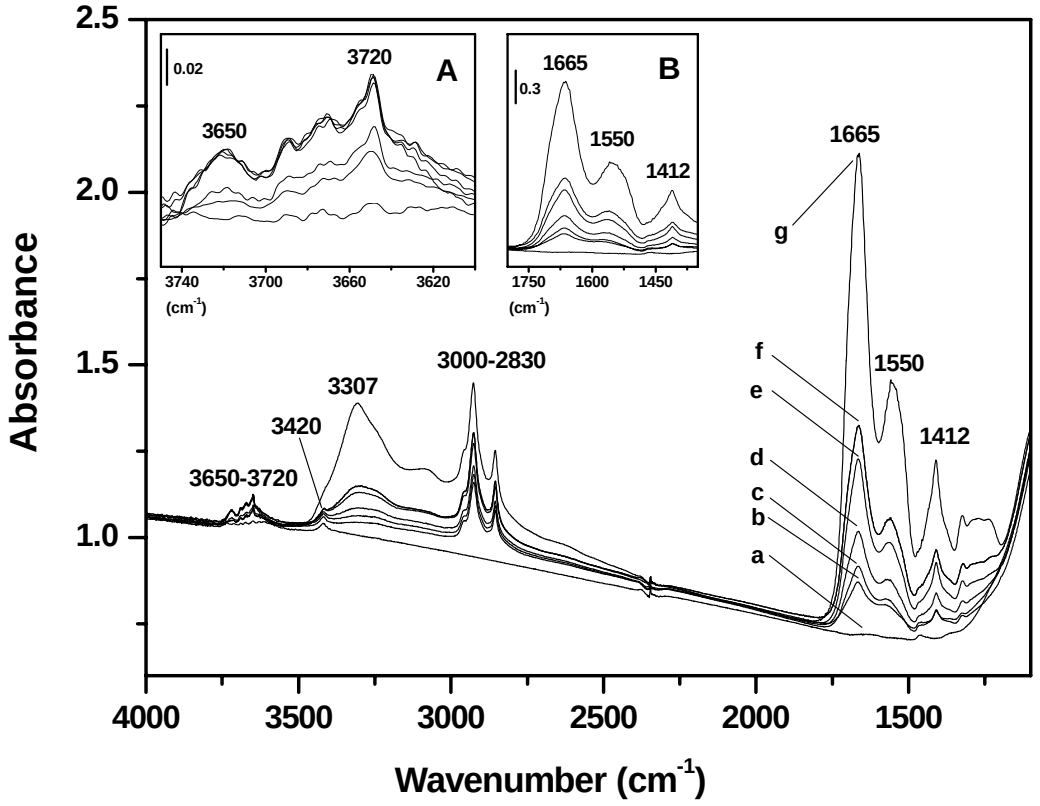

Figure 5.9. IR spectra of TiO_2 P25 during the sublimation of glycine: (a) surface after dehydration at 433 K; (b) one hour of sublimation; (c) two hours of sublimation; (d) three hours and 30 minutes of sublimation; (e) four hours of sublimation; (f) five hours of sublimation; (g) five hours and 45 minutes. Inset A: zoom in 3760 – 3600 cm^{-1} range. Inset B: zoom of the 1800 – 1450 cm^{-1} range.

During the sublimation a number of bands grow in the region between 1700-1400 cm^{-1} due to the functional groups of glycine (carboxylic and amino group) in interaction with the surface. Also in the region at high frequencies, modification occurred during the sublimation steps: an increase in intensity of a broad band at 3307 cm^{-1}, likely due to NH stretching modes of the amino acid and, contemporary, a decrease in intensity of signals of hydroxy groups present on the surface, indicating that some OH were progressively involved in the amino acid adsorption. The rising signals in the range 3000-2830 cm^{-1} are due to the stretching modes of CH_2 of adsorbed glycine molecules.

An important task at this point was to compare the shape of bands from the first to the last sublimation step, after a normalization of all spectra at their maximum in the 1700-1300 cm^{-1} region (Figure 5.10).

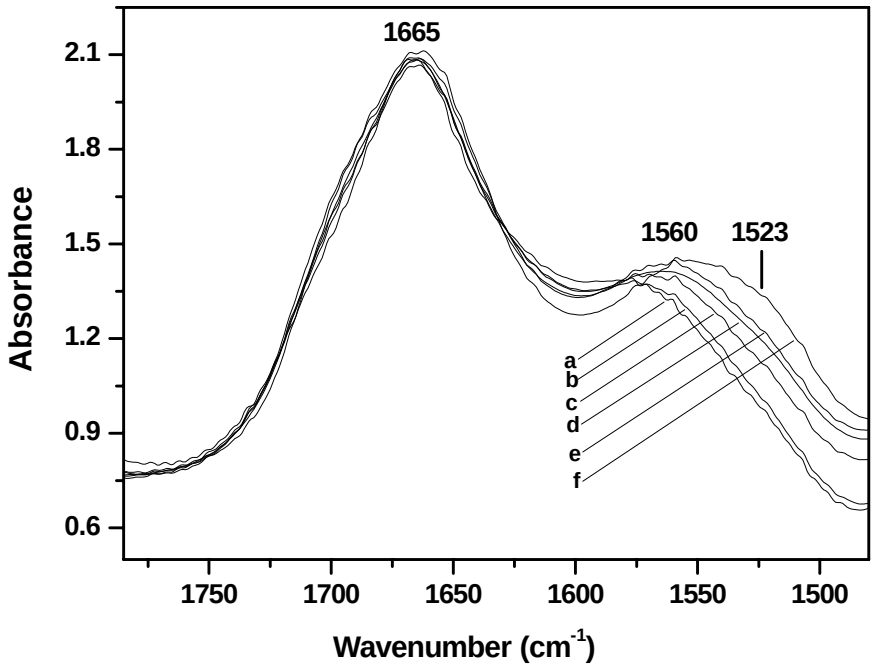

Figure 5.10. IR spectra of glycine sublimation steps on TiO_2 P25 normalized in intensity (a) one hour of sublimation; (b) two hours of sublimation; (c) three hours and 30 minutes of sublimation; (d) four hours of sublimation; (e) five hours of sublimation; (f) five hours and 45 minutes.

As a first point, it can be observed that the overall shape of the spectral profile remains quite similar by increasing the Gly coverage (curves a-f), indicating that most amino acid molecules experience a similar interaction with the surface.
However, a significant modification occurred, that is the progressive downshift of the component at 1560 cm^{-1}, also slightly increasing in intensity, accompanied by the growth of the shoulder at 1523 cm^{-1}, indicating that some new species are formed on the surface by increasing the amount of glycine on the surface.

The same measurements were performed without rehydrating the TiO_2 sample after the activation at 723 K and essentially the same results were obtained. Therefore, it can be concluded that the surface hydration level attained after rehydration and subsequent outgassing at 433 K is rather limited, and that the amount of water molecules present on the surface does not affect the adsorption mechanism of Gly in a significant extent.

5.4.1. Evaluation of the coverage of the TiO_2 surface by glycine

In a study of molecules adsorbed on a surface, it is important to have the possibility to establish when all adsorbing sites have been occupied, and molecules start to form overlayers. Typically, when the investigation method is IR spectroscopy of molecules adsorbed from a gas or vapor phase, the occurrence of molecules-molecules interactions (along a direction normal to the surface) in addition to surface-molecules interactions, can be evaluated by the appearance of new IR bands similar to those exhibited by such molecules in the liquid state. Furthermore, molecules are usually adsorbed on the sample from gas or vapor phases that are stable at the temperature of the experiment, and this allows a quite fine control of the dosage of molecules on surfaces and, in the case of reversible adsorption, also of a controlled desorption. Such a fine control of the amounts of adsorbed species is significantly more difficult by adsorbing molecules from a vapor phase resulting from a sublimation. Moreover, there is the possibility not only to form overlayers, but also to have a simple condensation of “solid-like”

phases, and in the case of glycine several crystalline polymorphs, as well as other kinds of not crystalline structures could be formed, even at the same time. As a consequence, the formation of overlayers or of “solid-like” structures might be accompanied by the appearance of possibly quite complex IR features, that might be not easily/immediately assigned to actual overlayers, instead to molecules adsorbed on different surface sites, assuming different structures.

To overcome this difficulty, the surface coverage, was evaluated step by step through the use of a probe molecule, such as CO_2. In particular, the method used was based on the adsorption of a molecule, CO_2, that can interact with all surface sites of titania at room temperature, giving origin to adsorbed species that can be completely removed by the surface at mild temperature. On such basis, a stepwise procedure was adopted in performing the experiment, by alternating adsorption/desorption of CO_2 with increasing amount of glycine coverage by sublimation.

In Figure 5.11, curve a, the infrared spectrum of CO_2 adsorbed on TiO_2 P25 exhibiting an intense peak at 2351 cm^{-1}, accompanied by a weak complex pattern of signals in the 1750-1200 cm^{-1} range can be observed.

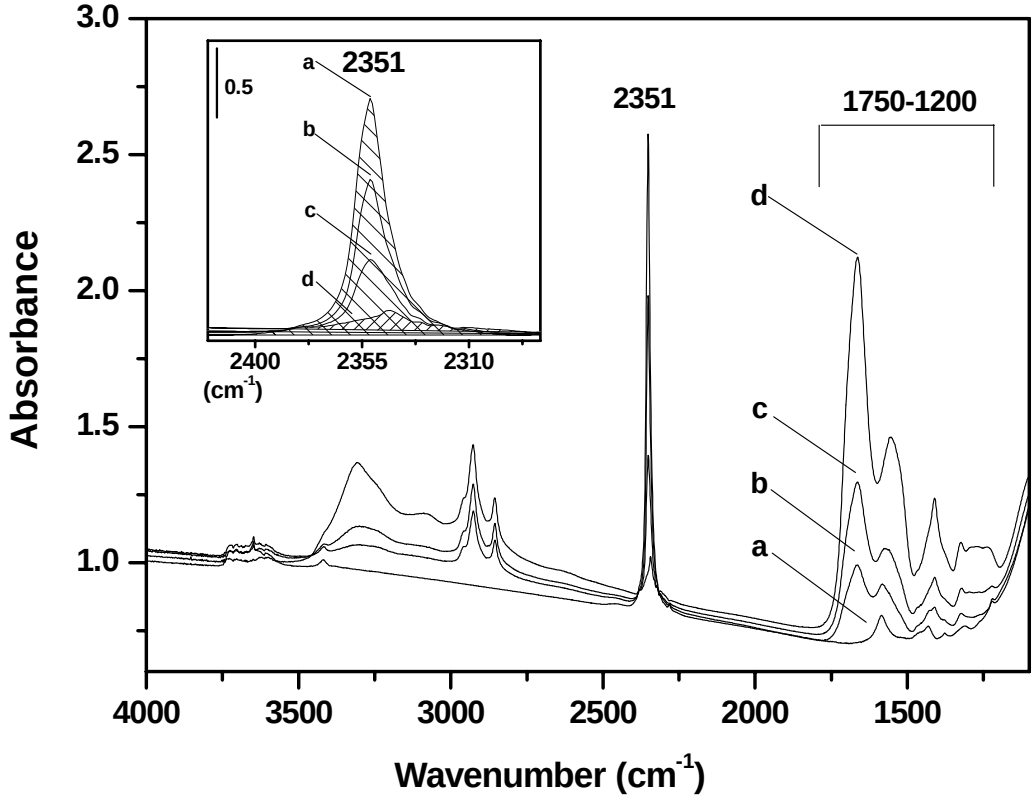

Figure 5.11. IR spectra of TiO_2 P25 in contact with 40 Torr of CO_2 after some steps of glycine sublimation: (a) surface after dehydration at 433 K; (b) after three hours and 30 minutes of sublimation; (c) after five hours of sublimation; (d) after five hours and 45 minutes of sublimation. Inset: zoom of the 2420–2280 cm^{-1} range.

The main band at 2351 cm^{-1} is due to the stretching mode of CO_2 linearly adsorbed on Ti^{4+} ions, while the complex weaker pattern at lower frequencies is mainly due to various types of carbonate-like species, namely mono- and bidentate carbonate groups, produced by nucleophilic attack of surface O^{2-} sites to CO_2 molecules which, in a first step of interaction, were adsorbed linearly on neighbor cations. Furthermore, some other components in that range are due to bicarbonates species, which should have been produced by reaction of CO_2 with some basic OH groups.[22] The presence of bands due to carbonates and

bicarbonates species witnesses the presence of Ti^{4+}-O^{2-}/Ti^{4+}-OH^- pairs where the anionic moiety is basic enough to react with CO_2, indicating that Lewis acid-base couple are actually exposed on the surface planes of TiO_2 P25. However, these couples correspond only to a fraction of surface sites, as CO_2 molecules are largely adsorbed in linear form also, indicating that the main fraction of O^{2-} sites present on the surface are unable to carry out a nucleophilic attack to CO_2 molecules.[22]

For this reason, in order to monitor the degree of coverage of the surface by glycine molecules, is useful to take into account the band of linear adsorbed CO_2, instead of those due to carbonates and bicarbonates species. Furthermore, these latter species, have an anionic character, and then their absorption coefficient is expected to be significantly higher than for neutral molecules as linearly adsorbed CO_2. As a consequence, the actual amount of carbonate/bicarbonate-like species should be even lower than what indicated by the intensity ratio between the peak due to linearly adsorbed CO_2 at 2351 cm^{-1} and the pattern in the 1700-1200 cm^{-1} range.

As for the experimental procedure, 40 Torr of CO_2 were dosed in the cell and left in contact with the sample for 10 minutes, and then the IR spectrum was collected. Subsequently, CO_2 was removed by outgassing for 20 minutes, while the other species still adsorbed on the surface, such as carbonates and bicarbonates, were removed during the following sublimation step at 433 K. In the inset of Figure 5.11 the results are shown, where it is possible to observe the decrease in intensity of the adsorbed linear CO_2 with the progressive occupation of the surface sites by adsorbed glycine. The curve (a) represents the initial amount of linear CO_2 in interaction with the clean surface before sublimation, after treatment at 433 K, the curves (b) and (c) represent some intermediate steps, and the curve (d) is the spectrum obtained after the last step of sublimation and contact with CO_2. In case of curve (c), the signal due to the presence of linearly adsorbed CO_2 exhibits an intensity that is ca. 35% of the initial one, indicating that ca. the 65% of the surface is occupied by glycine molecules.

After the last step of sublimation, the shape of the band due to CO_2 linearly adsorbed changes (Figure 5.11, curve d): in this case the CO_2 molecules are interacting with the adsorbed species and there are no free sites on titania surface. From the spectra reported in Figure 5.10 it can be noticed that for the last two steps of sublimation (curves e and f), the only change is the increase in intensity of the signal at 1523 cm^{-1}, present since the first sublimation step; therefore, it is not possible to exclude that some multilayers of adsorbed glycine are formed from the beginning of the sublimation procedure, but it can be excluded the presence of "solid-like" structures resulting from a physical deposition of Gly, even when all sites exposed at the TiO_2 surface are occupied.

5.4.2. Comparison between glycine adsorbed on HA and TiO_2 P25

The assignment of glycine adsorption bands reported in Figure 5.9 results difficult for the complexity of the vibrational profile. Therefore an helpful tool is the comparison of the obtained IR spectra with those reported for Gly adsorbed on hydoxyapatite (HA). Indeed, the same experimental method has been used to adsorb Gly from the vapor phase on HA, and the IR study combined with a theoretical one[10] allowed to assign the bands present in the spectra.

Furthermore, in order to simplify the assignment, it is possible to perform an H/D isotopic exchange by contacting the sample with deuterated water: in this way the contribution of amino group and water deformation can be removed, because downshifted in 1190-1160 cm^{-1} range.[18] To distinguish between the effects of rehydration ad those of H/D exchange, the surface was first hydrated by contact with H_2O vapor pressure for 30 min and then outgassed for 30 min. Subsequently, five cycles of isotopic exchange were carried out by addition/removal of D_2O vapor pressure (until the attainment of invariance between the spectra collected for two consecutive exchange with D_2O).

Figure 5.12 shows the spectra of Gly adsorbed on TiO_2 P25 and HA, before and after deuteration.

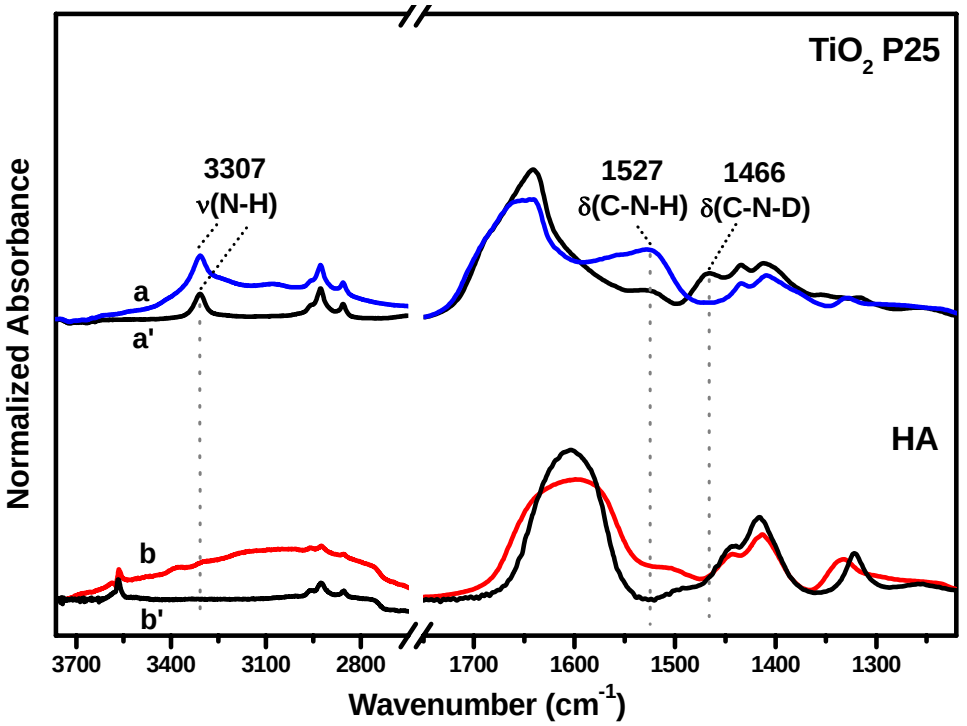

Figure 5.12. Comparison between IR spectra of Glycine adsorbed on: (a) TiO_2 P25 after hydration by contact with H_2O vapor pressure for 30 min and following outgassing for other 30 min; (a') TiO_2 P25 after five cycles of D_2O exchange; (b) HA after hydration by contact with H_2O vapor pressure for 30 min and following outgassing for other 30 min; (b') HA after five cycles of D_2O exchange.

After glycine adsorption from the vapor phase, both materials (TiO_2 P25 and HA) show a main absorption in 1750-1500 cm^{-1} range, accompanied by a pattern of weaker signals in 1500-1350 cm^{-1} range.

In the case of TiO_2 P25, the main differences with respect to HA are: (i) a narrow band at 3307 cm^{-1} that resisted the H/D exchange; (ii) the shift at higher frequency of most part of the νC=O pattern in the 1700-1600 cm^{-1} range; (iii) the presence of a group of signals in 1600-1500 cm^{-1} region that disappears after deuteration accompanied by the appearance of a third band contributing to the pattern in the 1500-1350 cm^{-1} range, namely at 1466 cm^{-1}.

In order to distinguish the possible contribution of different components to the observed spectra after H/D exchange, the experimental spectrum of Gly adsorbed on TiO_2 P25 was deconvoluted by using a fitting procedure, and the obtained result are shown in Figure 5.13.

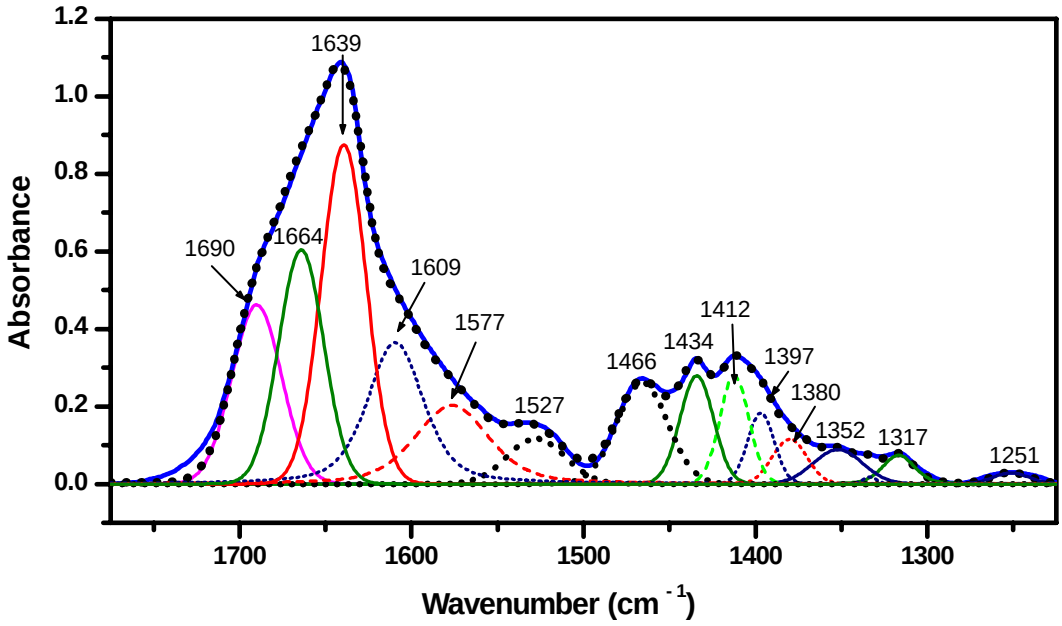

Figure 5.13. Deconvolution of the IR spectrum of deuterated Gly adsorbed on TiO_2 P25 after totally 5 hours and 45 minutes of sublimation. The dotted line overimposed to the experimental profile is the result of components obtained by fitting procedure.

Some different set of components was attempted, but none of them allows a better fit with a lower number of components, especially for the main band in the 1750-1500 cm^{-1} range. In each trial, however, the position of bands was almost the same, witnessing their reliability, whereas the relative intensity assigned to the various components was not unequivocal, because different combinations resulted in very similar overall profiles. On the basis of the results of the fitting, and taking into account the experimental and calculated spectra of Gly on HA, it was then possible to propose an assignment for most part of the components.

Furthermore, IR spectra of glycine hexamers derived from the literature[23] (Figure 5.14) were also taken in consideration. The hexaglycine has been chosen because is the longest glycine oligomer available in a pure form in commerce.

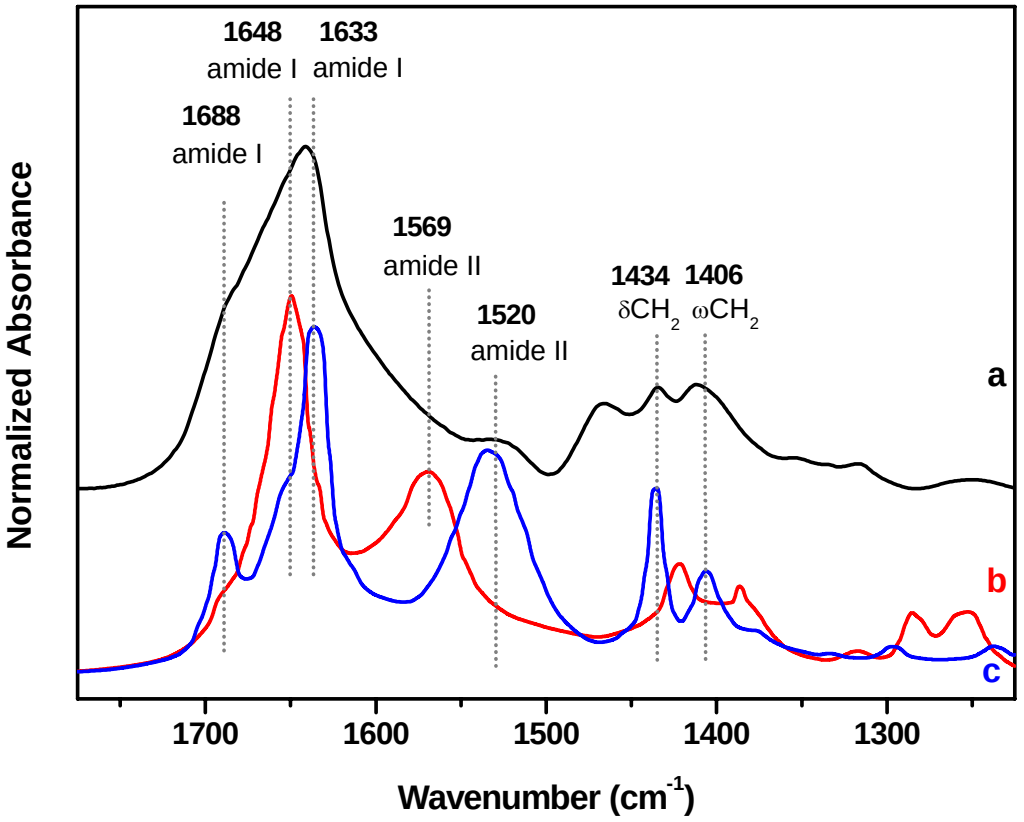

Figure 5.14. IR spectra of (a) Gly adsorbed on TiO_2 P25; (b) PGII and (c) PGI type of hexaglycine.[23] Amide I: stretching C=O (νC=O) of amide group; amide II: coupling between the C-N stretching mode and C-N-H in-plane deformation mode of amide group; δCH_2: bending mode of CH_2 group; ωCH_2: wagging mode of CH_2 group.

In Figure 5.14 the spectrum of Gly adsorbed on TiO_2 P25 is compared with those of glycine hexamers of PGI and PGII types, where PGI refers to planar (β) zig zag conformation and PGII to helical conformation.[23]

Some components due to species formed on TiO_2 (Figure 5.14, curve a) are quite similar in position to those spectra of hexaglycine oligomers (curves b and c). In particular, beside the almost coincidence of the signal related to $–CH_2$ deformation modes, in the 1700-1600 cm^{-1} pattern they seem to be actually present subbands due to the νC=O mode of amide species of oligomers. The presence of two νC=O signals in the case of the PGI structure is due to the through space coupling of oscillators typical of β-sheets of polyamide structures.[24]
Coming back to the different components obtained from the fitting procedure of spectrum shown in Figure 5.13, and taking in consideration the observations derived from the analysis of glycine oligomers spectra, it is possible to propose the assignment of some of those signals.
Both the presence in the original spectra of some extra components with respect to the Gly/HA system, and the location of related partners after deuteration, suggest the possibility that glycine molecules reacted when in contact with the TiO_2 surface, giving origin to an amide bond. In particular, this hypothesis results from the following assignments:

- The quite intense signal that before deuteration appeared at ca. 1527 cm^{-1} is (Figure 5.12, curve a) compatible with the so called vibrational mode of an Amide II, resulting from the coupling between the C-N stretching mode and C-N-H in-plane deformation mode of an amide group.[25] This attribution is supported by its behavior observed with H/D exchange, that results in a shift of about 60 cm^{-1}, responsible for the band at 1466 cm^{-1}. The observed shift is in agreement with literature data,[25] considering that C-N-H(/D) deformation is only one of the modes contributing to the Amide II absorption, and this results in a limited H/D exchange. Moreover, by observing the fit result (Figure 5.13), it can clearly be seen that the component at 1527 cm^{-1} did not disappear completely after D_2O exchange, indicating that probably not all species forming amide bond are reached by D_2O molecules.

- The same incomplete exchange it is observed for the band at 3307 cm^{-1} (Figure 5.12, curve a), that is attributed to the N-H stretching mode of an amide group.[25] This particular behavior will be discussed in the Section 5.4.4.
- The components, with maximum at 1690, 1664 and 1639 cm^{-1} (Figure 5.13), could be attributed to the carbonyl stretching mode of amide groups (amide I);[25] in particular, on the basis of the spectra reported in Figure 5.14, the signal at 1664 cm^{-1} can be assigned to the presence of glycine oligomers in helical conformation, while the other two are related to oligomers in β conformation.
- Depending on the length of glycine oligomers, also some vibrational signals due to carboxylated stretching are observed, in particular for small polyglycines (till five terms).[23] The out-of-phase and in-phase stretching of COO^- groups can contribute to the bands at 1609 and 1397 cm^{-1}, respectively (Figure 5.13).
- Finally, the peak at 1434 cm^{-1} is assigned to CH_2 bending,[25] while the wagging mode can contribute to band at 1397 cm^{-1}.[23]

Assignment *	*Wavenumber (cm^{-1})*	*Remarks*
νC=O	1690	Amide I, β conformation
νC=O	1664	Amide I, helical confromation
νC=O	1639	Amide I, β conformation
$\nu_{out}COO^-$	1609	present in glycine monomers and small oligomers
νC–N + δC–N–H	1527	Amide II not deuterated
νC–N + δC–N–D	1466	Amide II deuterated
δCH_2	1434	Scissoring mode
$\nu_{in}COO^-$	1397	present in glycine monomers and small oligomers
ωCH_2	1397	Wagging mode
ν, stretching mode; δ, bending mode; ω, wagging mode. out, out-of-phase vibration; in, in-phase vibration		

Table 5.2. Proposed assignment for the components obtained from the fitting procedure (Figure 5.13).

Hence the assignment of the IR bands of glycine in interaction with TiO_2 P25 surface, allowed to put in evidence the presence of signals due to amide groups. It is worthwhile to notice that the condensation reaction between glycine molecules resulting in peptide bond formation, is certainly promoted by titania surface. Indeed, such species were not formed by adsorbing Gly in the same conditions on the HA surface[10] (Figure 5.12, curves b and b').

In order to confirm the specific role of titania surface in promoting the glycine reactivity and in order to estimate the length of the molecules derived from the reaction among Gly units, a Mass Spectrometry analysis has been performed for both the systems Gly/HA and Gly/TiO_2 P25 and the spectra are reported in Figure 5.14.

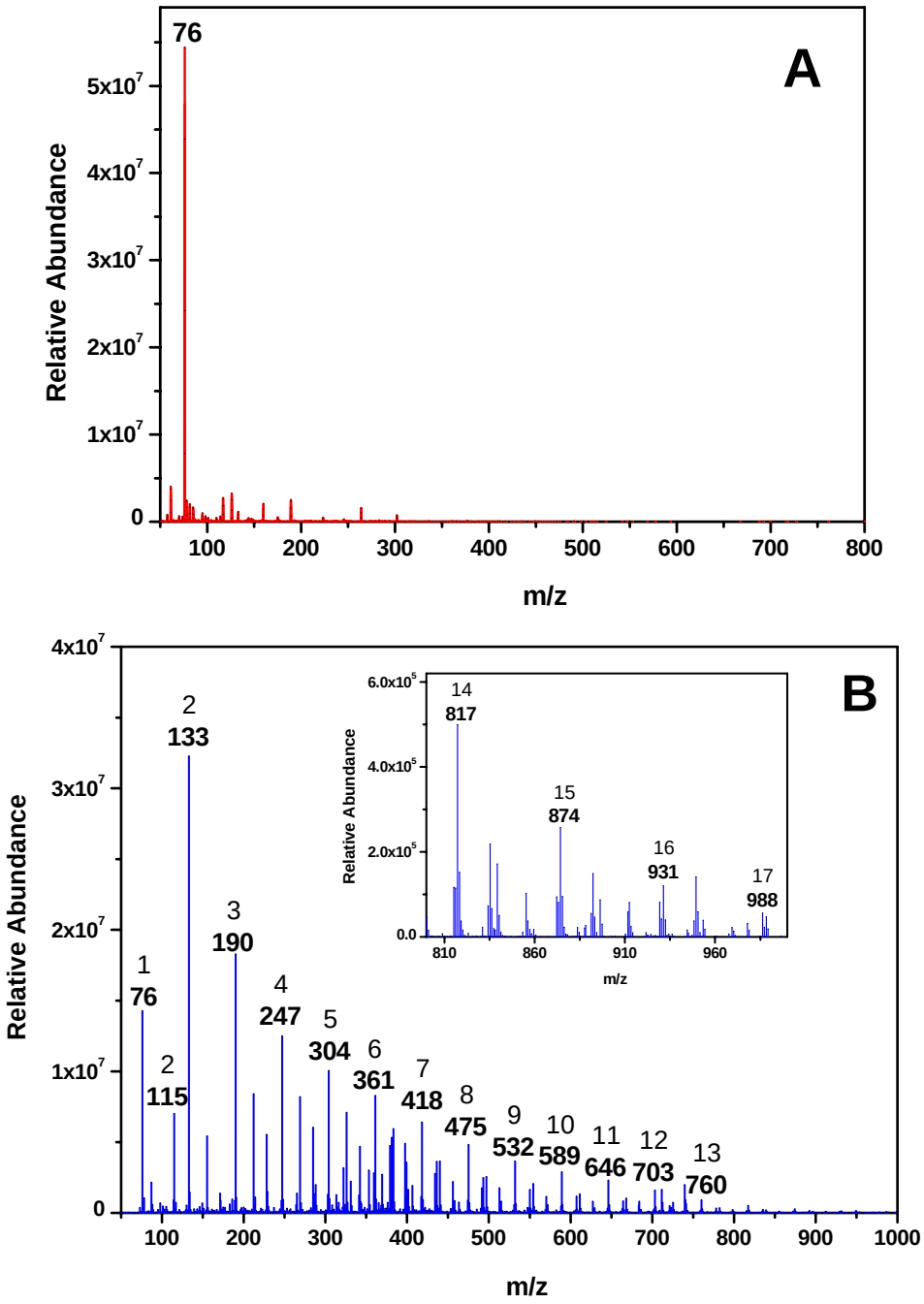

Figure 5.15. Mass spectra of surface products obtained after glycine sublimation on HA (Panel A) and on TiO_2 P25 (Panel B and inset with zoomed view of range 800-1000 m/z range). In both cases, the signals of species present in the water solvent has been subtracted as background.

As reported in Figure 5.15A, in the case of glycine adsorbed on HA, only one main signal at 76 m/z is present, assigned to protonated glycine in monomeric form (protonation derived from the preparation of the sample in formic acid, as described in Section 5.2). It is important to highlight that after the washing procedure used to remove the adsorbed species from the HA (or TiO_2) surface, only the 10% of adsorbed species remains on the surface, as shown in Figure 5.16.

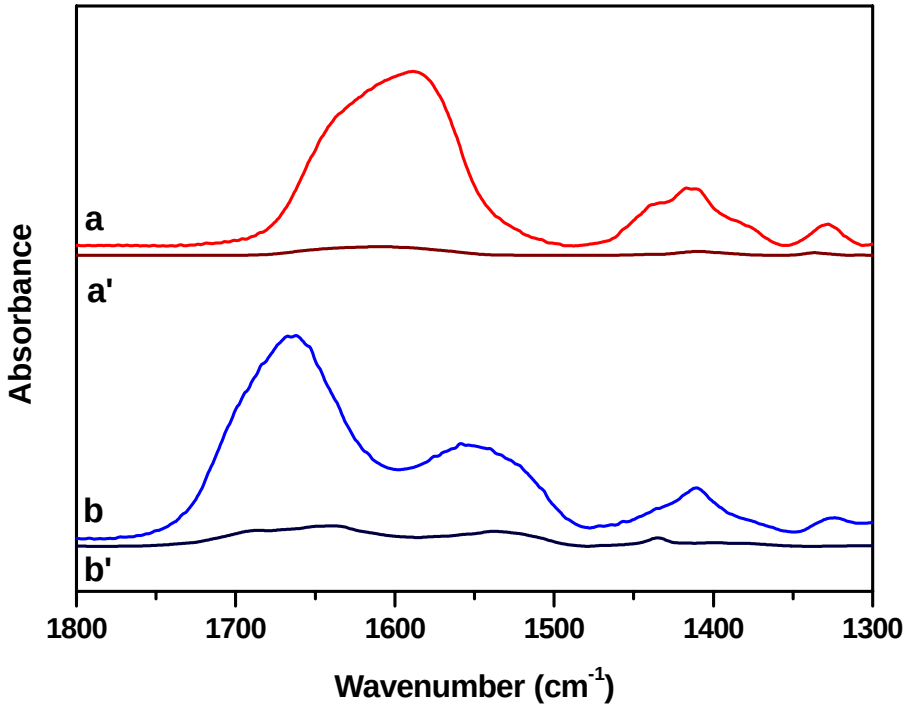

Figure 5.16. IR spectra of (a) Gly adsorbed on HA and (a') after washing procedure; (b) Gly adsorbed on TiO_2 P25 and (b') after washing procedure.

This result obtained with mass spectrometry, confirms the absence of the formation of any amide species by adsorption on Gly on HA, as proposed on the basis of the IR and ab initio investigations.[10] Conversely, in case of glycine

adsorbed on TiO_2 P25 it is possible to observe the presence of small oligomers till 17 units, that confirms the specific role of this material in promoting the peptide bond formation among glycine molecules.

The results obtained with mass spectrometry confirm that not only the oligomerization occurs when glycine molecules are adsorbed on titania, conversely to what reported in literature,[26] but also that the polymerization doesn't end with the cyclic dimer (diketopiperazine),[14] indeed, in the present study, oligomers with 17 units are found.

[The same preparation procedure for mass spectrometry analysis has been used for a sample of commercial hexaglycine (by Sigma-Aldrich), and only the signal corresponding to the mass of hexaglycine was found. It can be then concluded that the analytical method doesn't affect (for example by hydrolysis) the structure of the analyzed oligomers.]

As additional evidence for the formation of the oligomers, the same experimental procedure was followed for the adsorption of isotopic Glycine-1-^{13}C, isotopically labeled with ^{13}C at the carboxylic group (hereafter ^{13}Gly).
The mass spectrum is reported in Figure 5.17, and the expected masses for ^{12}Gly and ^{13}Gly adsorbed on titania, are listed in Table 5.3.

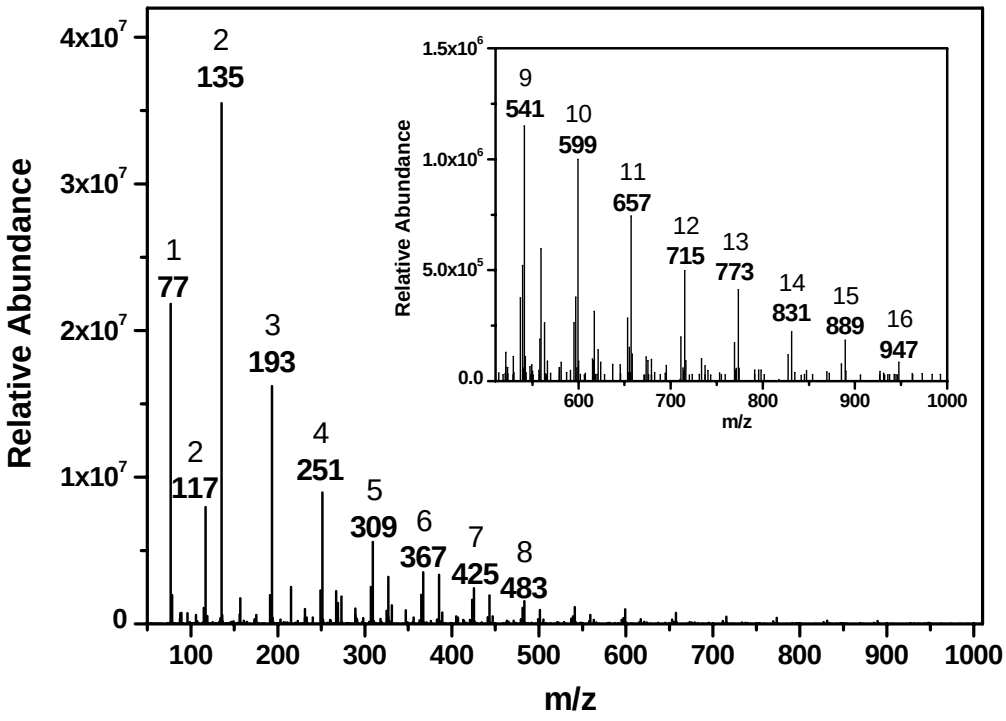

Figure 5.17. Mass Spectra of surface products obtained after ^{13}Gly sublimation on TiO_2 P25. Inset: zoomed view of range 510-1000 m/z. (Signals of species present in the water solvent has been subtracted as background).

Expected masses in electro-spray mass spectrometry																		
	Number of glycine units																	
Glycine isotopes	1	2 (DKP)	2 (Gly-Gly)	3	4	5	6	7	8	9	10	11	12	13	14	15	16	17
Glycine -1-12C	76	115	133	190	247	304	361	418	475	532	589	646	703	760	817	874	931	988
Glycine -1-13C	77	117	135	193	251	309	367	425	483	541	599	657	715	773	831	889	947	1005

Table 5.3. Expected masses for ^{12}Gly and ^{13}Gly oligomers.

A full coincidence between expected mass values for –(^{13}Gly)n- (n=1-16) oligomers and the experimental one was obtained (Table 5.3), clearly confirming

the formation of the oligomers.

5.4.3. Evidence of successive feeding of monomers

Finally another experiment has been carried out in order to understand if the longest chains are immediately formed on the surface or if they are the product of a successive addition of glycine terms. Therefore, a glycine adsorption from the vapor phase has been performed in two sublimation steps: during the first one, ^{12}Gly has been adsorbed on the surface and the sublimation has been stopped when a coverage of titania surface of ca. 35% was reached (established by CO_2 adsorption, following the procedure reported in section 5.4.1). During the second step ^{13}Gly has been adsorbed till final 70% of the maximum coverage. A mass spectrometry analysis was then performed and the resulting spectra and the assignment are reported in Figure 5.18 and Table 5.4, respectively.

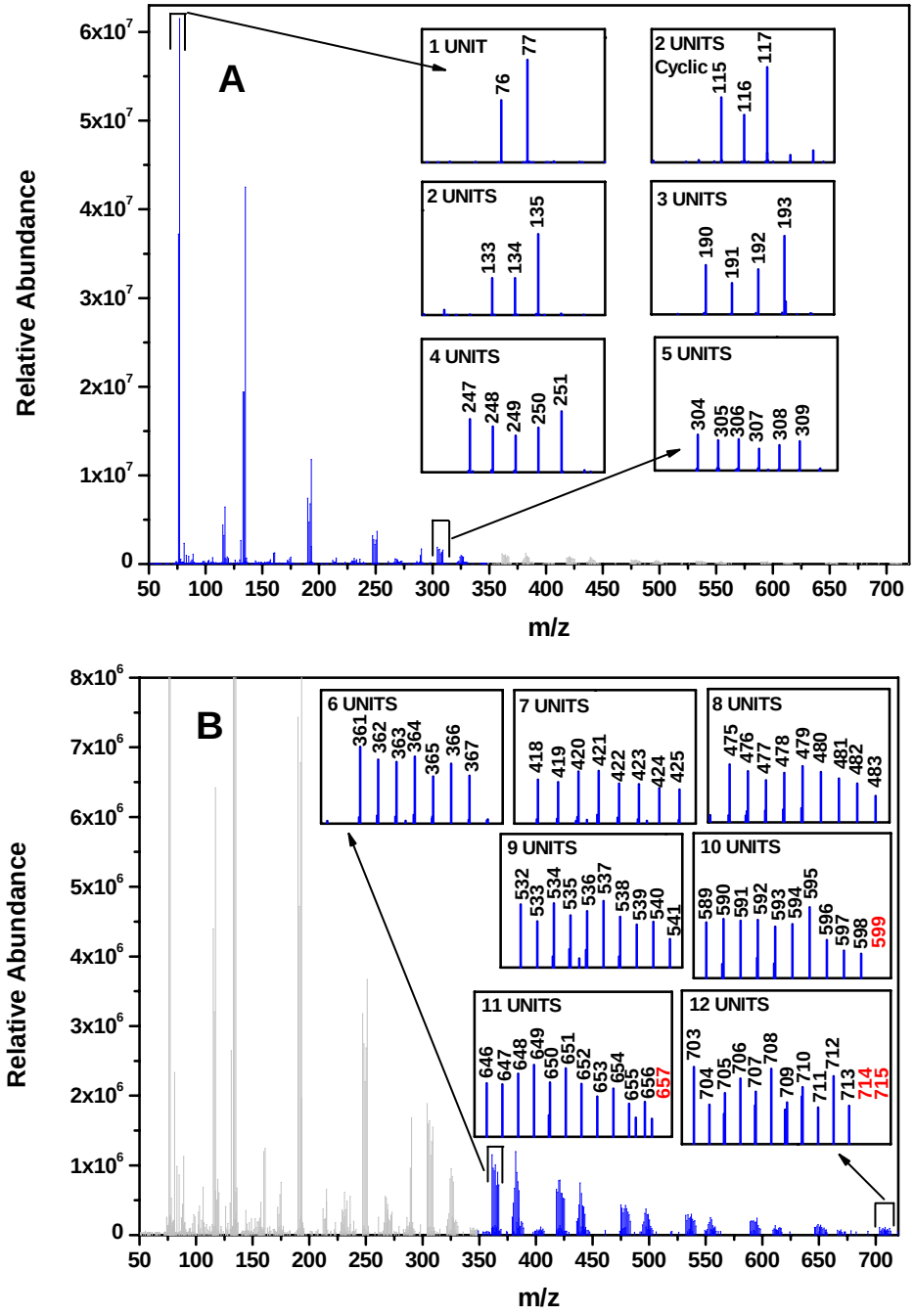

Figure 5.18. Mass spectra of surface products obtained after ^{12}Gly and ^{13}Gly sublimation on TiO_2 P25. Panel A: range 50-350 m/z; Panel B: range 350-750 m/z. (Spectra subtracted of the water signals).

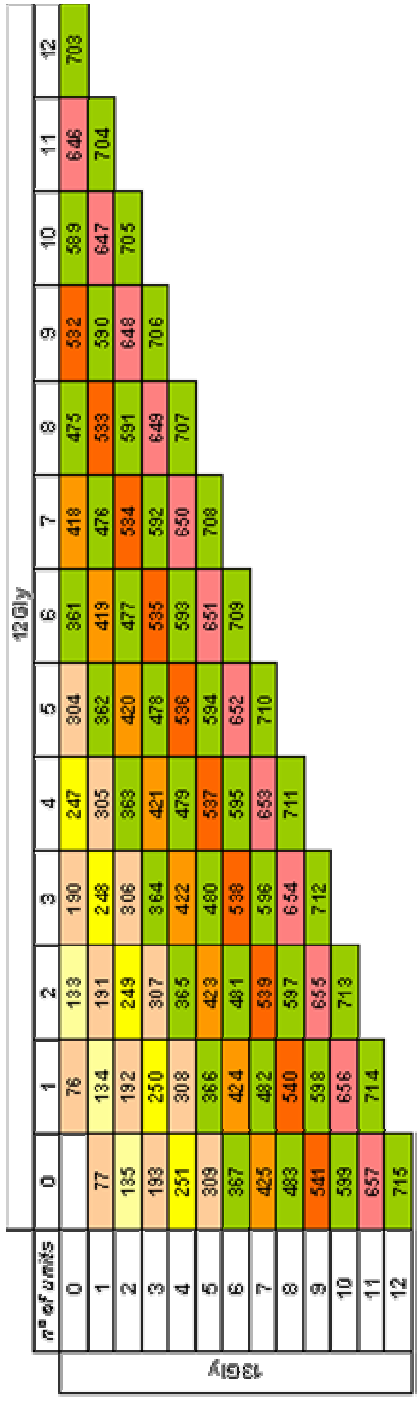

Table 5.4. Mass assignment for oligomers containing mixed terms of ^{12}Gly and ^{13}Gly.

In Figure 5.18 the mass spectra of ^{12}Gly-^{13}Gly adsorbed on TiO_2 P25 are reported and the detailed assignment of each mass can be found in Table 5.4. From the analysis of these results can be deduced that after the first sublimation step with ^{12}Gly, when the coverage of the TiO_2 surface is not complete, the chains till 12 units are formed, containing only units of ^{12}Gly (masses reported in first row of Table 5.4). After the second step of sublimation, when subsequently ^{13}Gly is adsorbed, chains containing only ^{13}Gly units are formed (masses reported in first column of Table 5.4), but only till 9 terms; indeed the 10, 11, 12 oligomers containing exclusively ^{13}Gly terms (in red in Figure 5.18B), are not present, probably because during this second step the temperature and the time of sublimation suitable for longest chains formation were not reached.

However, a relevant source of information is represented by the presence, besides the signals of pure ^{12}Gly and ^{13}Gly-mers, of the masses due to mixed species containing in the same chain both ^{12}Gly and ^{13}Gly, and this allows to conclude that (i) chains with different lengths are contemporary formed on the surface; (ii) the oligomers are the result of a successive “feeding” process, i.e. a chain growth due to a step by step addition of glycine units, as reported in literature by Ferris and co-workers[27] for chemically pre-activated amino acid molecules that formed “long” oligopeptides when adsorbed on various kinds of minerals.

5.4.4. Effect of water on the adsorbed molecules: self-aggregation

The collection of results obtained by IR and mass spectrometry investigations provided the evidence for the formation of oligomers long up to 17 glycine units, that is a result with a relevant aspect of novelty. However, another significant insight was obtained by analyzing in more detail the effects of exposure to H_2O and D_2O vapor on the spectral pattern of the mixture of Gly oligomers formed on the TiO_2 surface (partially presented in section 5.4.2). As a first point, the results of the exposure to H_2O vapor will be considered (Figure 5.19).

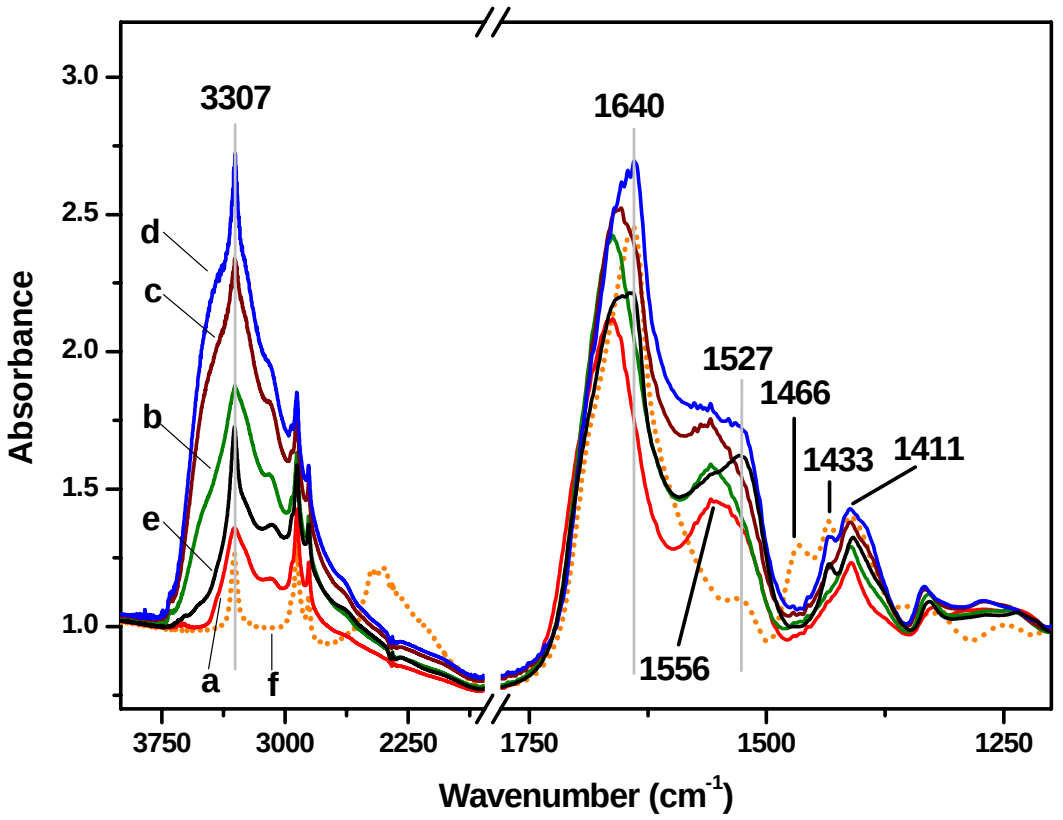

Figure 5.19. IR spectra of the last step of glycine sublimation on (a) TiO_2 P25 (red); (b) immediately after contact with water vapor pressure (green); (c) 10 minutes of contact with water vapor pressure (dark red); (d) 15 minutes of contact with water vapor pressure (blue); (e) 30 minutes outgassing of H_2O at r.t. (black); (f) H/D exchange and then outgassing of D_2O (dotted orange).

As reported in Figure 5.19, immediately after dosing the H_2O vapor pressure (curve b), the expected broad signal due to water νOH modes, spread over the 3700-3500 cm^{-1} range, and the partner signal due to the δH_2O mode, appearing as a subband at ca. 1625 cm^{-1}, of the complex pattern in the 1750-1500 cm^{-1} region, appeared.

By increasing the time of contact (curves c, d), a distinct narrow band progressively grew at 3307 cm^{-1} and simultaneously a narrowing νC=O band,

accompanied by an increase in intensity and a shift at 1640 cm^{-1}, occurred. The subsequent outgassing of H_2O at b.t. (curve e) resulted in a strong decrease in intensity of the νOH and δH_2O components, monitoring the removal of water molecules adsorbed in form of liquid-like multi layers. Conversely, the new peak at 3307 cm^{-1} appeared essentially unaffected, and in the region at ν > 1350 cm^{-1} new subbands can be observed at 1640, 1527 cm^{-1}.

Then, D_2O vapor was admitted in the cell, and adsorption/desorption cycles were reported until invariance of the spectra (curve f). In the high frequency range, only the narrow band at 3307 cm^{-1} was still present, whilst the rest of the pattern appeared downshifted in the 2750-2000 cm^{-1} region.

At lower wavenumbers, the narrow component at 1640 cm^{-1} exhibited an increase in intensity, while the complex absorption with maximum at 1527 cm^{-1} underwent a significant decrease in intensity, in favor of a new, weaker component at 1466 cm^{-1}. This behavior monitors the conversion of amide N-H moieties (C-N-H bending + C-NH stretching: band at 1527 cm^{-1}) in N-D ones (C-N-D bending + C-ND stretching: band at 1466 cm^{-1}). As a related effect, the decoupling with the C=O stretching by passing from the N-H to the N-D groups was responsible for the increase in intensity of the νC=O signal and the decrease in intensity of the (C-N-D bending + C-ND stretching) band.

Noticeably, a peculiar information is contained in the part of the spectrum that remained unaffected by the H/D exchange, namely the narrow peak at 3307 cm^{-1} and the weak component at 1527 cm^{-1}, indicating that a fraction of the amide N-H groups resisted to the isotopic exchange.

By considering that polyglicines are known to exhibit an hydrophobic character,[28] and taking into account the spectral evolution observed during the time of contact with physisorbed H_2O (Figure 5.19), such a behavior can be rationalized in terms of a self-aggregation of the “long” glycine oligomers on the hydrated TiO_2 surface. This process started to occur only when liquid-like water layers were formed, allowing the mobility of the oligomers on the TiO_2 surface.

The resistance of some amide N-H species to the H/D exchange, indicated the

formation of 3D self-aggregates of oligoglycine, with core not accessible to the solvent molecules.

Furthermore, the narrowness of the N-H IR bands still present after H/D exchange appeared quite similar to the band shape typical of polyglicine polymorphs of type I and II,[23,29,30] then supporting that aggregates with a quite well ordered structure were formed.

At the best of our knowledge, this is the first case of formation of oligopeptides with a significant chain length by activation of single amino acid molecules by a surface, followed by a self-aggregation of the oligomers after subsequent hydration of the system.

Conclusions and perspectives

The first evidence of formation of oligomers up to 17 terms on TiO_2 surface has been reported. Additionally, the polyglycines self-aggregation, as consequence of hydration, and their removal from the surface as effect of washing, have been observed.

Despite this investigation has been carried out in order to develop a model system to study the biomaterial-biomolecule interactions, the results obtained concerning the capability of TiO_2 P25 to promote the formation of oligoglycines, are also interesting for the study of origin of biopolymers in prebiotic conditions.

Indeed, one of the hypothesis suggested from Bernal,[31] proposes that amino acids polymerization occurred on the surface of oxide minerals and not in solution. In particular, the main problems concerning the polymerization in solution are (i) thermodynamically unfavorable peptide bond formation in water and (ii) low concentration of amino acids in primordial oceans.[32] Therefore, taking into account that the peptide bond formation occurs via a condensation reaction, the mineral surfaces could have been fundamental both for the accumulation of the amino acids and for promoting the polymerization in dry conditions, thanks to the exposure to the sun and, as a consequence, shifting the equilibrium towards the condensation of amino acids.[32]

Moreover, in the presolar stardust in meteorites has been identified the presence of titanium dioxide.[33] Hence, the results obtained for glycine polymerization on titania, can be useful for modeling the synthesis of biopolymers in prebiotic conditions and future experiments could be carried on in order to elucidate the reaction mechanism and, additionally, to perform the same investigation on other mineral surfaces.

References

(1) Linsebigler, A. L.; Lu, G. Q.; Yates, J. T. *Chemical Reviews* **1995**, *95*, 735.

(2) Grätzel, M. *Journal of Photochemistry and Photobiology C-Photochemistry Reviews* **2003**, *4*, 145.

(3) Wong, J. Y.; Bronzino, J. D. *Biomaterials*; Broken Sound Parkway, NW, Boca Raton, FL: CRC Press, 2007.

(4) Gray, J. J. *Current Opinion in Structural Biology* **2004**, *14*, 110.

(5) Costa, D.; Lomenech, C.; Bery, G.; Stievano, L.; Lambert, J. F. *Chemphyschem* **2005**, *6*, 1061.

(6) Barteau, M. A.; Qiu, T. Z. *Journal of Colloid and Interface Science* **2006**, *303*, 229.

(7) Szieberth, D.; Ferrari, A. M.; Dong, X. *Physical Chemistry Chemical Physics* **2010**, *12*, 11033.

(8) *Nomenclature and symbolism for amino acids and peptides (IUPAC-IUB Recommendations 1983)*, 1984; Vol. 56.

(9) Stepanian, S. G.; Reva, I. D.; Radchenko, E. D.; Adamowicz, L. *Journal of Physical Chemistry A* **1998**, *102*, 1041.

(10) Rimola, A.; Sakhno, Y.; Bertinetti, L.; Lelli, M.; Martra, G.; Ugliengo, P. *The Journal of Physical Chemistry Letters* **2011**, *2*, 1390.

(11) Liu, Z.; Zhong, L.; Ying, P.; Feng, Z.; Li, C. *Biophysical Chemistry* **2008**, *132*, 18.

(12) Iitaka, Y. *Acta Crystallographica* **1961**, *14*, 1.

(13) Albrecht, G.; Corey, R. B. *Journal of the American Chemical Society* **1939**, *61*, 1087.

(14) Meng, M.; Stievano, L.; Lambert, J. F. *Langmuir* **2004**, *20*, 914.

(15) Rosado, M. T.; Duarte, M. L. T. S.; Fausto, R. *Vibrational Spectroscopy* **1998**, *16*, 35.

(16) Fischer, G.; Cao, X. L.; Cox, N.; Francis, M. *Chemical Physics* **2005**, *313*, 39.

(17) Bellamy, L. J. *Carboxylic Acids, in The Infra-red Spectra of Complex Molecules*; Chapman and Hall: London, 1975.

(18) Suzuki, S.; Shimanouchi, T.; Tsuboi, M. *Spectrochimica Acta* **1963**, *19*, 1195.

(19) Kim, M. K.; Martell, A. E. *Journal of the American Chemical Society* **1963**, *85*, 3080.

(20) Gussoni, M.; Castiglioni, C.; Zerbi, G. Vibrational Intensities: Interpretation and Use for Diagnostic Purposes. In *Hanbook of Vibrational Spectroscopy*; J.M. Chalmers and P.R. Griffiths Eds., Wiley: Chichester, 2002; Vol. 3; pp 2040.

(21) Meyer, H. D.; Vendrell, O.; Gatti, F. *Angewandte Chemie-International Edition* **2009**, *48*, 352.

(22) Martra, G. *Applied Catalysis A-General* **2000**, *200*, 275.

(23) Taga, K.; Sowa, M. G.; Wang, J.; Etori, H.; Yoshida, T.; Okabayashi, H.; Mantsch, H. H. *Vibrational Spectroscopy* **1997**, *14*, 143.

(24) Barth, A. *Biochimica Et Biophysica Acta-Bioenergetics* **2007**, *1767*, 1073.

(25) Chalmers, J. M.; Griffiths, P. R. *Handbook of Vibrational spectroscopy*; Wiley: London, 2002; Vol. 3.

(26) Lambert, J. F.; Stievano, L.; Lopes, I.; Gharsallah, M.; Piao, L. Y. *Planetary and Space Science* **2009**, *57*, 460.

(27) Ferris, J. P.; Hill, A. R.; Liu, R. H.; Orgel, L. E. *Nature* **1996**, *381*, 59.

(28) Lu, J.; Wang, X. J.; Yang, X.; Ching, C. B. *Journal of Chemical and Engineering Data* **2006**, *51*, 1593.

(29) Gorokhova, I. V.; Chinarev, A. A.; Tuzikov, A. B.; Tsygankova, S. V.; Bovin, N. V. *Russian Journal of Bioorganic Chemistry* **2006**, *32*, 420.

(30) Crick, F. H. C.; Rich, A. *Nature* **1955**, *176*, 780.

(31) Bernal, J. D. *The Proceedings of the Pysical Society* **1949**, *62*, 597.

(32) Lambert, J. F. *Origins of Life and Evolution of Biospheres* **2008**, *38*, 211.

(33) Nittler, L. R. *Earth and Planetary Science Letters* **2003**, *209*, 259.

Chapter 6

Electronic properties of B and F co-doped rutile TiO_2

6.1. Introduction

In this last chapter, results dealing with the study of the electronic properties of TiO_2 rutile will be reported. In particular, this work was a part of a research aimed to the development of visible-light-active and stable TiO_2-based photocatalysts for environmental/energy applications to which many works have been devoted.[1-3] In this regard, F- [4-6] and more recently B-doped TiO_2 [7-9] are receiving increasing attention. In particular B,F co-doped TiO_2 materials have shown an improvement of Vis light absorption that, as a consequence, enhances the methylene blue (MB) degradation rates under visible (Vis) irradiation compared to undoped or single-doped materials.[10] This enhancement was related to an improved absorption of visible light.[10] B,F co-doped TiO_2 nanotubes showed high photoelectrocatalytic conversion of methyl orange (MO).[11] In this case, the excellent performances were associated to the predominant presence of the highly reactive anatase structure[11] and to the high system surface area. Nevertheless, no clear and unambiguous explanation of these challenging performances is available in the literature up to date. B,F-doped TiO_2 powders have been synthesized and for the first time the nature of active centers responsible for the catalytic activity of rutile TiO_2 has been elucidated, even when a very low surface area is present.

Since during TiO_2 synthesis the presence of B or F dopants induces the low-temperature formation of a mixture of anatase, rutile, brookite polymorphs, the

attention was focused on high-temperature-treated materials, containing the pure rutile phase and possessing a negligible surface area. This work demonstrates that a suitable synthetic design can transform even a “stone” with insignificant surface area into a very efficient photocatalyst. Specifically, herein it has been show the existence of a critical synergic interaction between B and F codopants in rutile titania that weakly enhances Vis-light absorption but, notably, generates active photocatalytic sites.

6.2. Materials and methods

Pure and B-doped TiO_2 photocatalysts were prepared by a sol-gel method.[8] 17 g of $Ti(OBu)_4$ were dissolved in 40 mL of anhydrous ethanol under Ar atmosphere (Solution I). 2.8 mL of concentrated HNO_3 were mixed with a solution of 35 mL anhydrous ethanol and 5 mL water (Solution II). Solution I was drop-wise added to solution II, under argon atmosphere and vigorous stirring. Approximately 0.6 g of H_3BO_3 were dissolved in 10 mL of water and rapidly added dropwise to the resulting solution. The solution was continuously stirred till the formation of TiO_2 gel. After 24 h aging at room temperature, the as-prepared TiO_2 gel was dried at 120°C for 12 h. The obtained solid was ground and calcined at 450°C for 6 h at heating rate of 1.5°C/min and subsequently at 900°C for 2 h at heating rate of 3°C/min. Undoped TiO_2 was synthesized by the same procedure, but without the addition of H_3BO_3. Fluorination treatments were performed by suspending TiO_2 in diluted HF (TiO_2 concentration = 20 mg/mL; total fluoride concentration = 10 mM; HF/TiO_2 ratio = 0.024) at pH 3.0, stirring for 8 h at room temperature in the dark.[12] The solid was recovered by centrifugation at 3500 rpm for 20 min and washed with water one time. Then the fluorinated powders were dried for 8 h at 80°C.

All the samples resulted in the rutile phase from the X-Ray Diffraction (XRD) analysis.

UV-Vis spectra of the materials in air were collected by using a Cary 5000 Varian instrument, equipped with an integrating sphere Spectralon®, operating in Diffuse Reflectance mode.

The specific surface area (SSA_{BET}) of the different materials is reported in Table 6.1.

Sample	SSA_{BET} [m^2g^{-1}]
TiO_2	0.34
F-TiO_2	0.53
B-TiO_2	0.65
B,F-TiO_2	1.74

Table 6.1. Specific Surface Area of the four samples.

6.3. Effect of dopants on electronic properties

The study of electronic properties of powders, as in the present case, can be carried on through the use of Diffuse Reflectance (DR) spectroscopy.

In Figure 6.1 the DR-UV-Vis spectra of the samples, collected in reflectance mode (R), are reported and compared with TiO_2 P25.

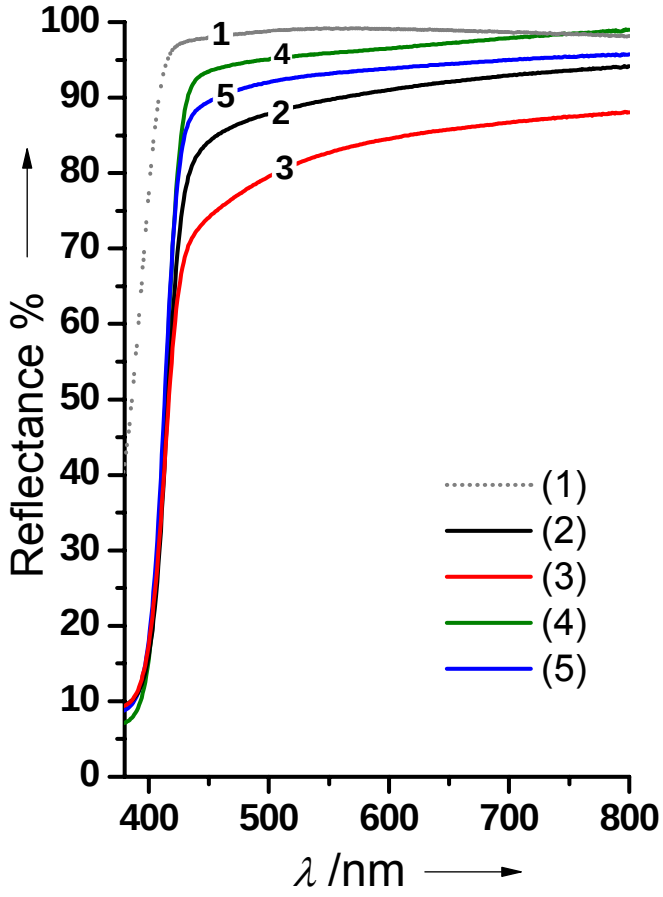

Figure 6.1. DR UV-Vis spectra of: TiO_2 P25 (1), TiO_2 (2), F-TiO_2 (3), B-TiO_2 (4), B,F-TiO_2 (5) collected in reflectance mode.

Because of the dependence of reflectance on the concentration,[13] the weaker absorptions result intensified in respect with the more intense ones; hence the collection of spectra in reflectance mode, allows to observe the structureless absorption spread over the whole visible region exhibited by all materials. Such spectral feature was not reported in a previous work on similar systems,[14] probably because the data were reported already elaborated with the Kubelka-Munk function and plotted with a scale proper to observe the maximum of the very intense interband absorption, and this resulted in a strong depression of the weak absorption in the Vis range. Conversely, an absorption in this range was present

in the Absorbance spectra of titania materials studied by Yu et al.,[4] but the lack of experimental details and the presence of a visible absorption even for TiO_2 P25 prevent a significant comparison.

Here the spectrum of Degussa TiO_2 P25 has been inserted as representative of titania powders free from significant absorption in the Vis region (Reflectance % very close to 100% in the 430-800 nm). As this material is a mixture of anatase and rutile phases (average: 80:20 in volume) the strong decrease in reflectance due to the inter-band transition (with onset at ≈ 410 nm) occurs at shorter wavelength with respect to rutile.

The continuous, featureless absorption throughout the whole Vis region observed in Figure 6.1, with the intensity increasing in the order F-TiO_2 >> TiO_2 > B,F-TiO_2 > B-TiO_2, indicates that it should be due to transitions involving populated defect sites in the band gap, from which electrons can be promoted to the conduction band. The extension down to the limit of the visible suggests a position in energy at least 1.5 eV below the band gap.

These defect states can be associated to the presence of Ti^{3+} species, formed by oxygen loss during the calcination at high temperature,[15] the presence of which was confirmed by EPR. Fluorinated materials exhibited stronger visible absorption properties compared to the corresponding parent titania materials, as expected for substitutional fluoride species.[16]

DR-UV-Vis can be used to investigate the absorptions in the UV-Vis (and NIR) range, in particular provides information on the absorption edge of metal oxides, the interband electron transition that falls in the UV-Vis range. The band-gap energy is therefore used to study the electronic properties of materials used in photocatalytic applications. To calculate the band-gap energy, the spectra of Figure 6.1, have been elaborated with the Kubelka-Munk function:

$$K/S = F(R_\infty) = (1-R_\infty)^2 / (2R_\infty) \qquad (6.1)$$

where K is the absorption, S is the scattering, R_∞ is a layer of infinite thickness and $F(R_\infty)$ is the Schuster – Kubelka – Munk (SKM) function.[17]
In the present case the band-gap energy has been estimated and the change in E_g due to presence of dopants has been monitored and compared with the results obtained for TiO_2 Degussa P25.

It is worth noting that in semiconductor oxides where the fundamental absorption edge is due to allowed transitions between indirect valleys, such as TiO_2, the interactions with phonons (absorption or emission), must be taken into account.[18,19]

Hence, two adsorption coefficients must be considered, one (α_a) for the process with phonon absorption:

$$\alpha_a(h\nu) = A(h\nu - E_g + E_p)^2[\exp(E_p kT) - 1]^{-1} \quad (6.2)$$

and a second one (α_e) for the process with phonon emission:

$$\alpha_e(h\nu) = A(h\nu - E_g - E_p)^2[1 - \exp(-E_p kT)]^{-1} \quad (6.3)$$

where E_g is the energy and E_p is the phonon energy and the terms in square brackets contain the dependence on the number of phonons of energy E_p.

When $h\nu > E_g + E_p$ both phonon and emission absorption are possible, then absorption coefficient is:

$$\alpha(h\nu) = \alpha_a(h\nu) + \alpha_e(h\nu) \quad (6.4)$$

In Figure 6.2 the DR-UV-Vis spectra, elaborated with Kubelka-Munk function for the calculation of band-gap energy, are reported.

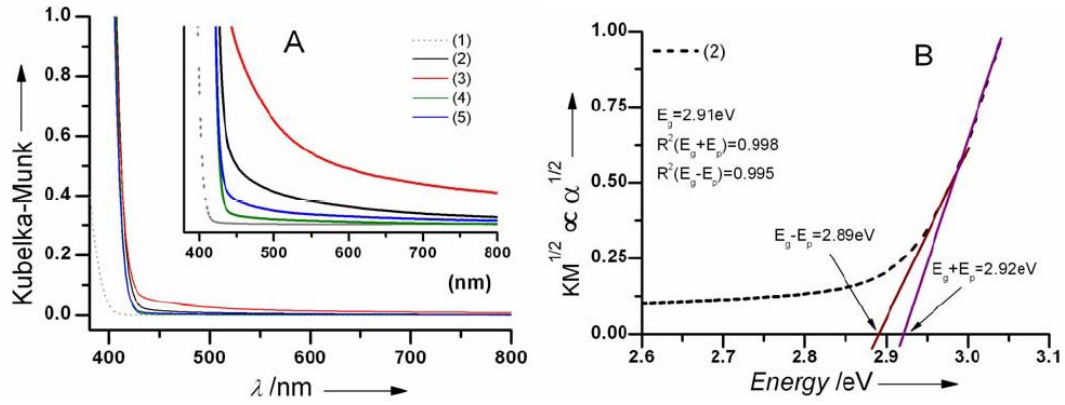

Figure 6.2. Panel A: Diffuse Reflectance (DR) UV-Vis spectra (processed by using the Kubelka- Munk function) of: TiO_2 P25 (1), TiO_2 (2), F-TiO_2 (3), B-TiO_2 (4), B,F-TiO_2 (5). Panel B: plot of the square root of the absorption coefficient $\alpha(h\nu)$ *vs.* transition energy (eV). The Y axis is limited to 1.0, that represents the limit for a correct application of the Kubelka-Munk function. The resulting energy gap (E_g) values are reported in the following Table 6.2.

Material	**E_g+E_p (eV)**	**Optical absorption (nm)**	**E_g-E_p (eV)**	**Optical absorption (nm)**	**E_g (eV)**
TiO_2	2.92	425	2.89	429	2.91
F-TiO_2	2.91	426	2.87	432	2.89
B-TiO_2	2.95	420	2.92	425	2.93
B,F-TiO_2	2.95	420	2.93	423	2.94

Table 6.2. Energy gap (E_g) values and corresponding optical absorptions of the various specimens evaluated from the above optical spectra by using the method displayed in Figure 6.1B.

Diffuse reflectance (DR) UV/Vis analysis enables to estimate a band-gap energy of 2.91 eV for the bare TiO_2, with minor changes occurring for the doped samples. The value obtained was lower than the value expected for defect free TiO_2 rutile.[20]

Conclusions

The data reported above indicated that doping and co-doping TiO_2 rutile with F and B resulted in the appearance of electronic defects that imparts to the material the capability to absorb visible light, and in a narrowing of the band gap. In particular, this kind of spectroscopic data provided evidence also for the mutual interaction between F and B induced defects in the co-doped material. Such finding was in agreement with the results obtained by employing other techniques like EPR and XPS.[21] Moreover, the combination with the results of photocatalytic tests allowed to propose the occurrence of a synergy between the two types of defects in inducing a relevant photocatalytic activity of the material under irradiation with visible light.

References

(1) Bach, U.; Lupo, D.; Comte, P.; Moser, J. E.; Weissörtel, F.; Salbeck, J.; Spreitzer, H.; Grätzel, M. *Nature* **1998**, *395*, 583.

(2) Irie, H.; Watanabe, Y.; Hashimoto, K. *Chemistry Letters* **2003**, *32*, 772.

(3) Liu, G.; Zhao, Y. N.; Sun, C. H.; Li, F.; Lu, G. Q.; Cheng, H. M. *Angewandte Chemie-International Edition* **2008**, *47*, 4516; *Angewandte Chemie* **2008**,*120*, 4592.

(4) Yu, J. C.; Yu, J.; Ho, W.; Jiang, Z.; Zhang, L. *Chem. Mater.* **2002**, *14*, 3808–3816.

(5) Minero, C.; Mariella, G.; Maurino, V.; Pelizzetti, E. *Langmuir* **2000**, *16*, 2632.

(6) Minero, C.; Mariella, G.; Maurino, V.; Vione, D.; Pelizzetti, E. *Langmuir* **2000**, *16*, 8964.

(7) Chen, D.; Yang, D.; Wang, Q.; Jiang, Z. Y. *Industrial & Engineering Chemistry Research* **2006**, *45*, 4110.

(8) Bettinelli, M.; Dallacasa, V.; Falcomer, D.; Fornasiero, P.; Gombac, V.; Montini, T.; Romanò, L.; Speghini, A. *Journal of Hazardous Materials* **2007**, *146*, 529.

(9) In, S.; Orlov, A.; Berg, R.; García, F.; Pedrosa-Jimenez, S.; Tikhov, M. S.; Wright, D. S.; Lambert, R. M. *Journal of the American Chemical Society* **2007**, *129*, 13790.

(10) Reyes-Garcia, E. A.; Sun, Y. P.; Raftery, D. *Journal of Physical Chemistry C* **2007**, *111*, 17146.

(11) Su, Y. L.; Zhang, X. W.; Han, S.; Chen, X. Q.; Lei, L. C. *Electrochemistry Communications* **2007**, *9*, 2291.

(12) Minella, M.; Faga, M. G.; Maurino, V.; Minero, C.; Pelizzetti, E.; Coluccia, S.; Martra, G. *Langmuir* **2010**, *26*, 2521.

(13) Saferstein, R. *Forensic Science Handbook* Prentice Hall: Upper Saddle River, New Jersey, 1993; Vol. III.

(14) Czoska, A. M.; Livraghi, S.; Chiesa, M.; Giamello, E.; Agnoli, S.; Granozzi, G.; Finazzi, E.; Di Valentin, C.; Pacchioni, G. *Journal of Physical Chemistry C* **2008**, *112*, 8951.

(15) Bak, T.; Nowotny, J.; Rekas, M.; Sorrell, C. C. *Journal of Physics and Chemistry of Solids* **2003**, *64*, 1043.

(16) Di Valentin, C.; Finazzi, E.; Pacchioni, G.; Selloni, A.; Livraghi, S.; Czoska, A. M.; Paganini, M. C.; Giamello, E. *Chemistry of Materials* **2008**, *20*, 3706.

(17) Jackson, S. D.; Hargreaves, J. S. J. *Metal Oxide Catalysis*; WILEY-VCH Verlag GmbH & Co. KGaA, Weinheim, 2009.

(18) Carp, O.; Huisman, C. L.; Reller, A. *Progress in Solid State Chemistry* **2004**, *32*, 33.

(19) Serpone, N.; Lawless, D.; Khairutdinov, R. *Journal of Physical Chemistry* **1995**, *99*, 16646.

(20) Hossain, F. M.; Sheppard, L.; Nowotny, J.; Murch, G. E. *Journal of Physics and Chemistry of Solids* **2008**, *69*, 1820.

(21) Fittipaldi, M.; Gombac, V.; Gasparotto, A.; Deiana, C.; Adami, G.; Barreca, D.; Montini, T.; Martra, G.; Gatteschi, D.; Fornasiero, P. *Chemphyschem* **2011**, *12*, 2221.

General conclusions

The IR spectroscopic study of TiO_2 surface, combined with the theoretical investigation of the anatase facets, allowed to obtain new insights on the surface structure of sites exposed at the surface.

In particular, OH families resulting from dissociation of water on cationic sites with higher Lewis acidity with respect to Ti^{4+}_{5c} exposed at the most abundant faces of the “landmark” TiO_2 P25, were identified.

The IR study of CO adsorbed on TiO_2 anatase nanoparticles with defined surfaces and its combination with theoretical modeling resulted in:

(i) the recognition of the signal due to CO adsorbed on Ti^{4+} sites exposed at (101) faces, that are the most stable, and then are expected to be the most abundant for TiO_2 nanoparticles also produced by other methods. Actually, on such a basis it is now possible to propose that Ti^{4+} (101) type sites are the most abundant also on TiO_2 P25, that is produced by pyrolysis;

(ii) the validation of theoretical models on extended slabs and derived steps and the elucidation of the role of the disorder among adsorbed CO molecules in determining their frequencies;

(iii) the suggestion that on a semiconductor oxide like TiO_2, the increase of the Lewis acid strength of a surface cation can be related not only to its increase in coordinative unsaturation, but also to its location near an edge;

(iv) the first spectroscopic evidence of combination between stretching and frustrated translational mode of adsorbed CO, enriching the spectroscopic information on the use of CO as probe molecule.

The interest in the investigation at molecular level of interaction among surface and adsorbed biomolecules, led to the IR study of the TiO_2-glycine interface. Thus resulted in the first observation of the formation of long glycine oligomers (up to 17 terms) under the vapor-solid interaction regime and the subsequent self-assembling by contact with water. This could represent a possible contribution to the elucidation of the reactive events resulting in the formation of biopolymers, on mineral surfaces, in pre-biotic conditions.

A significant part of this work concerned the development of experimental set-up for the study of surface interaction at molecular level.
Regarding the study of surface OH groups on more acidic sites of TiO_2 P25, the choice of the proper pre-outgassing conditions allowed to evidence the bands of the complex OH vibrational pattern, related to the sites where the water is dissociatively adsorbed.
Concerning the theoretical modeling of surface local structure of sites, it has been put in evidence that the simulation of vibrational spectrum of adsorbed CO must be performed taking in consideration the disordered conditions of the experimental system.
Finally, the selective study of TiO_2-glycine interaction required the development of investigation methodology for the in-situ IR spectroscopy.

In conclusion, the investigation methods used in this work, provided a collection of new data for the characterization of TiO_2 surface structure and reactivity.
The future study of other materials or other adsorbed molecules with the combination of modeling, would provide further information on the surface local structure of sites, including the defective ones, whose investigation has been already started.
Thus would result in the elucidation of role of the specific surface sites in the surface chemistry, allowing to improve the performances in the use of the titanium dioxide.